Rheological Responses under Elongational Flow for Polyolefin Melts

JIRAPORN SEEMORK

Japan Advanced Institute of Science and Technology

Doctoral Dissertation

Rheological Responses under Elongational Flow for Polyolefin Melts

JIRAPORN SEEMORK

Supervisor: **Prof. Dr. Masayuki Yamaguchi**

School of Materials Science

Japan Advanced Institute of Science and Technology

March 2016

Referee-in-chief : **Professor Dr. Masayuki Yamaguchi**
Japan Advanced Institute of Science and Technology

Referees : **Associate Professor Dr. Kazuaki Matsumura**
Japan Advanced Institute of Science and Technology

Associate Professor Dr. Ken-ichi Shinohara
Japan Advanced Institute of Science and Technology

Associate Professor Dr. Toshiaki Taniike
Japan Advanced Institute of Science and Technology

Associate Professor Dr. Kentaro Taki
Kanazawa University

Rheological Responses under Elongational Flow for Polyolefin Melts

Abstract

Various kinds of processing operations are known to be available in polymer industry. Among them, extrusion process is one of the most important operations for shaping a polymer melt into final products. Generally, the shape of a product is determined after passing through a die exit of an extrusion unit, in which elongational flow occurs. Therefore, rheological responses under elongational flow of a melt play a crucial role in polymer processing, because they decide the quality of products. One of the most important rheological responses is the viscosity. However, the data of elongational viscosity has been reported for only specific polymers with high molecular weight because of the difficulty in measurements. In industry, therefore, the drawdown force, defined as force required for uniaxial stretching of a polymer melt, is usually evaluated instead of the elongational viscosity because it has a close relation with elongational viscosity. Besides the elongational viscosity, the drawdown force contains the information on solidification process including crystallization because the drawdown force measurements are performed with non-isothermal condition. From the viewpoint of polymer processing, high level of the drawdown force is often required for good processability. Such situations lead to the confusion to understand the information on the drawdown force. In fact, the effect of the measurement conditions on the drawdown force has not been clarified yet.

Here, I study the measurement of the drawdown force and its enhancement. Firstly, the effect of extrusion condition and material parameters on the drawdown force was investigated. It was found that the drawdown force for polyolefins increases with the die length. This phenomenon is pronounced for the melt having high molecular weight at low extrusion temperature. The mechanism is attributed to the reduction of entanglement coupling density for the melt extruded from a long die, leading to rapid crystallization and thus, enhancement of the drawdown force. Moreover, the sensitivity of the drawdown force to the die length is found to depend on the difference between processing and crystallization temperatures. In addition, the drawdown force of polypropylene is enhanced by blending acrylate polymers having low viscosity, due to prompt solidification of the acrylate polymer dispersion which acts as rigid filler at the extrusion process.

Keywords: Capillary extrusion, Drawdown force, Polyolefin, Elongational flow, Cystallization

Preface

Extrusion process is one of the important steps for shaping a polymer melt into final products. Therefore, rheological responses under elongational flow of a melt, *i.e.*, extensibility and surface roughness, play an important role in polymer processing, because they decide the quality of products. Generally, elongational viscosity is evaluated to predict the processability since it has useful information on processability at processing operation in which a polymer melt with free surface is deformed. However, the measurement is limited due to the difficulty. In industry, drawdown force, defined as force needed to stretch a polymer melt uniaxially, is then evaluated because it has a close relation with elongational viscosity. Since the drawdown force measurements are performed with non-isothermal condition, which is similar to the actual processing condition, it contains the information not only extensional viscosity but also crystallization. Therefore, it is able to predict the processability even though it does not provide the information on the strain-hardening behavior. In particular, high level of the drawdown force is responsible for the marked melt elasticity, which is required for various processing operations. Consequently, the processability can be improved by enhancement of the drawdown force.

In this thesis, the approaches to enhance the drawdown force as well as control the melt fracture for polyolefin melts at capillary extrusion are studied. I hope this contribution will be useful for improvement of processability and further development in industry.

Jiraporn Seemork

Contents

This dissertation was prepared according to the curriculum for the Collaborative Education Program organized by Japan Advanced Institute of Science and Technology and Chulalongkorn University.

Chapter 1

General Introduction

1.1 Introduction

Rheology is the science of deformation and flow.[1,2] Rheological properties are concerned with flow behavior for all types of matter, from liquid to elastic solid materials, especially for molten polymers. Since the rheological properties of a polymer melt play an important role in both academic and industrial fields, they, therefore, have been studied widely in the past decade.[3-10]

One of the most important rheological properties during the flow is viscosity, defined as resistance of a fluid to the flow.[11] The viscosity of a polymer melt depends on molecular weight and temperature. Typically their viscosity drops at high shear rates, known as shear thinning behavior.[12]

For most polymer processing operations, the deformation is an important procedure for various productions. Uniformity of the deformation is usually required at the processing operations since it decides processability and the products quality. Therefore, the deformation

of a polymer melt with free surface, *i.e.*, elongational flow, has been interested and studied widely.[13-18] In particular, elongational viscosity, which has a close relation with processability at actual processing operations such as blow-molding, thermoforming, T-die extrusion, foaming and spinning, is evaluated in both academia and industry. Generally, the elongational viscosity is evaluated using commercial elongational rheometers.[1,19-27] However, the experiment is limited due to difficulty in the measurement especially for low viscosity materials. To overcome this limitation, several methods for indirect measurements of the elongational viscosity have been proposed.[12,13,15,16,28]

Polyolefins have been widely used in numerous applications, such as film, packaging, automotive parts, fiber and electronic parts, because of their outstanding properties. Polyethylene (PE) and polypropylene (PP) are two of the most polymer resins used in the world these days, because these resins can be tailored to achieve wide range of mechanical and chemical properties.[29] Since the most processing operations for polyolefins are based on extensional deformation, their rheological responses under elongational flow, therefore, are important to be investigated.[9,30-33]

In this chapter, I am going to review the following topics; (1) reological response under elongational flow, (2) capillary extrusion, (3) polyolefins, (4) melt elasticity of polyolefins. Finally, the objectives of this research will be explained.

1.2 Rheological response under elongational flow

Generally, flow in rheology can be categorized into two main standard types; shear flow, which is the flow dominated in an extruder, and elongational flow, which is the deformation with free of shear. In the case of shear flow, there are two modes of flow: One is drag flow, which occurs in a liquid between a moving plate and a fixed plate. The other is pressure-driven flow, occurred by a pressure difference in a closed channel.[1,34-36]

Regarding the Cox-Merz rule, the viscosity for most polymer melts obtained from a shear mode has an empirical relationship with the complex viscosity evaluated by an oscillatory measurement.[37] The steady-state shear viscosity η plotted against shear rate relates to the magnitude of the complex viscosity, $|\eta^*|$, plotted against angular frequency, ω, defined as follow:

$$|\eta^*(\omega)|\big|_{\omega\to\dot{\gamma}} = \eta(\dot{\gamma}) \tag{1-1}$$

The steady-state shear viscosity measurements for concentrated polymer solutions and melts carried out by a torsional rheometer may have a problem of edge fracture at low shear rates as around 10 s^{-1}, whereas capillary rheometers are available for the measurements to comparatively higher shear rates. However, flow instabilities limit the overall shear rate range. In such systems, Cox-Merz rule provides valuable estimation of viscosity from small amplitude

oscillatory shear viscosity measurements. The oscillatory shear measurements have the ability to use a smaller sample volume comparing with conventional capillary rheometers and great precision of the measurements.[28,38] Nevertheless, a capillary rheometer is able to investigate the nonlinear elastic properties having close relationship with actual processing especially extrusion, such as extrudate swell and flow instabilities, which cannot be directly measured by torsional rheometers.

1.2.1 Elongational viscosity

Elongational viscosity, defined as the ratio of elongational stress to elongational strain rate, is usually used to characterize the resistance of a fluid to elongational flow.[20,28] Trouton was the first scientist to measure the elongational viscosity of a fluid.[39] For Newtonian fluids, the ratio of axisymmetric uniaxial elongational viscosity to shear viscosity, which is called Trouton ratio, is 3, whereas the ratio of biaxial elongational viscosity to shear viscosity is 6. In the case of planar elongational flow, *i.e.*, elongational flow with a constant width, the ratio of the value in the flow direction to shear viscosity is 4, whereas that of the value in the perpendicular direction to shear viscosity is 2. Because of their long chain molecules, polymers exhibit a stiff resistance to any elongational deformation. Therefore, the elongational viscosity of a polymer is generally quite high. The growth curve of elongational viscosity is calculated from Equation 1-2

$$\eta_E^+(t) = \frac{\sigma_E^+(t)}{\dot{\varepsilon}} \tag{1-2}$$

where $\sigma_E^+(t)$ is the elongational stress as a function of time and $\dot{\varepsilon}$ is the elongational strain rate.

1.2.2 Rheometers

Since the elongational viscosity is a crucial parameter at polymer processing, numerous methods for evaluation of the elongational viscosity have been proposed.[40] The most common way is use of a commercial rheometer, which has been widely reported.[22-25,27] One of the most well-known elongational rheometers is a Meissner-type uniaxial extensional rheometer, which was developed by Meissner in 1969.[22,41] This rheometer consists of rotary clamps having a tension detector (T). A strands will be clamped between the roller gears and floated horizontally on a bath of silicone oil that compensates for the weight of the melt by buoyancy and keeps the sample at the desired test temperature. Then, a melt is homogeneously elongated by rotating of the rotary clamps at a constant strain rate, so called Hencky strain rate.

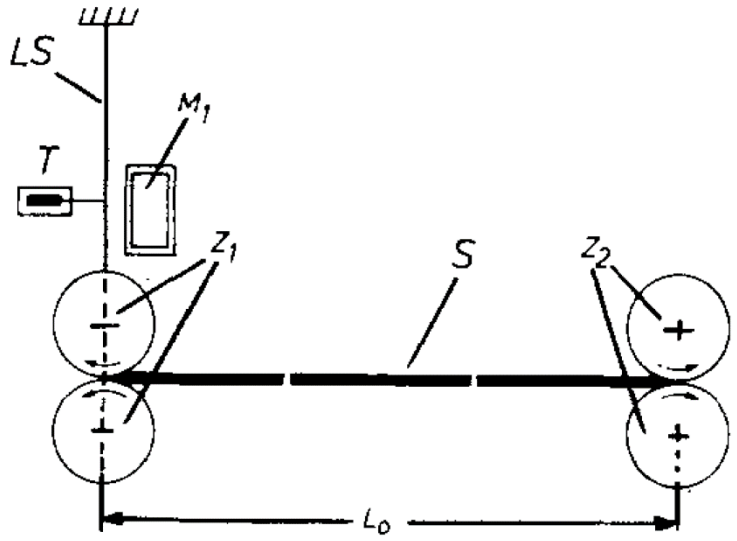

Figure 1-1 Schematic illustration of Meissner-type rheometer[22]

Later, Sentmanat developed Sentmanat Extensional Rheometer (SER), which consists of a dual wind-up drum. This technique allows the ends of a sample to be stretched by means of two counter-rotating drums.[27]

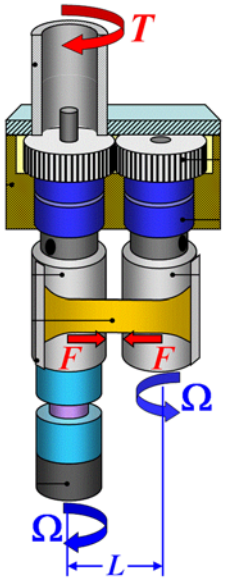

Figure 1-2 Schematic illustration of Sentmanat Extensional Rheometer (SER)[27]

This rheometer composes of a pair of wind-up drums as shown in Figure 1-2. Rotation of the drive shaft results in a rotation of the fixed master drum and an equal rate but opposite rotation of the unfixed drum. These rotations cause the uniaxial stretching of the sample. For a constant drive shaft rotation rate, Ω, the Hencky strain rate $\dot{\varepsilon}_H$ applied to the sample specimen can be expressed as:

$$\dot{\varepsilon}_H = \frac{2\Omega R}{L_0} \tag{1-3}$$

where R is the radius of the equal dimension wind-up drums, and L_0 is the fixed, unsupported

length of the specimen sample being stretched, which is equal to the distance between the pair of drums.

Because of a constant Hencky strain rate, the growth function of uniaxial elongational viscosity, $\eta_E^+(t)$, can be expressed as:

$$\eta_E^+(t) = \frac{F(t)}{\dot{\varepsilon}_H A(t)} \tag{1-4}$$

where F(t) is the instantaneous extensional force at time t exerted by the sample as it resists stretch as determined from the measured torque signal T.

Nevertheless, it is extremely difficult to maintain a purely elongational steady flow at higher elongation rates. Therefore, direct measurement techniques are able to determine elongational viscosity at only relatively low elongation rates (less than 10 s^{-1}). Since in most polymer processing techniques, the elongation rate is typically a high value, this limitation is particularly restrictive for the actual processing. Therefore, the experimental data from various techniques for direct measurements of elongational viscosity is not sufficient for simulation of most polymer processing techniques.

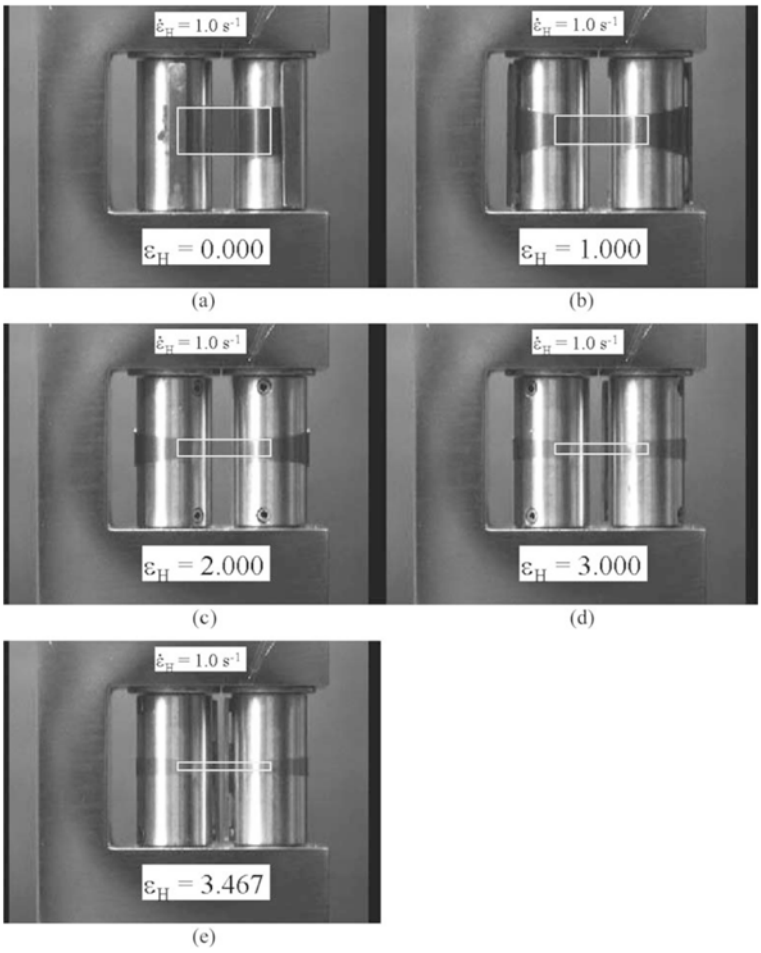

Figure 1-3 Measurement apparatus of Sentmanat Extensional Rheometer (SER). ε_H represents the Hencky strain.[27]

Due to the limitation of direct measurement techniques, the entrance flow method has been used to estimate the elongational viscosity of polymers. Cogswell was the first rheologist who proposed the methods to evaluate elongational viscosity by the entrance flow method using

a capillary rheometer, *i.e.*, a pressure-driven flow rheometer.[42] When pressure drives a fluid through a channel, flow velocity is a maximum at the center. Shear rate and also shear strain will be maximum at the wall and zero in the center of the flow. Thus flow field is not homogeneous for all pressure-driven flows. After passing of the fluid through a channel, *i.e.*, capillary die, a highly elongation-dominated flow, which is referred to an entrance flow, can be conveniently obtained near an abrupt contraction in a channel. A large pressure drop, called entrance loss, is encountered near an abrupt contraction because of the high elongational viscosity of polymers. The value to entrance pressure loss, which depends upon the flow rate in the channel can be used for indirect measurements of elongational viscosity.[12,15,28]

Cogswell investigated the elongational viscosity from the data of pressure drop at the die entrance with some assumptions as follows: (1) there is no slip on funnel surface, (2) the Wiessenberg-Rabinowitsch correction is neglected and (3) shear stress is related to shear rate through a power law.[38]

Later, Binding performed a more accurate analysis of entrance flow based on Cogswell's assumptions using the energy principle.[43] The entrance pressure loss can be obtained from equation 1-5.

$$\Delta P_e = \frac{2C_s(1+m)^2}{3m^2(1+n)^2}\left[\frac{mC_e(3n+1)n^m I_{nm}}{C_s}\right]^{\frac{1}{m+1}} \dot{\gamma}^{\frac{m(n+1)}{m+1}}\left[1-\alpha^{\frac{3m(n+1)}{m+1}}\right] \qquad (1\text{-}5)$$

where C_e and m define the power-law model for elongational viscosity $\left(\eta_e = C_e \dot{\varepsilon}^{m-1}\right)$, $\alpha = r/R$ with R and r being the radii of reservoir and capillary respectively, and I_{nm} is defined as:

$$I_{nm} = \int_0^1 \left| \frac{(3n+1)\rho^{1+\frac{1}{n}}}{n-2} \right|^{m+1} \rho d\rho \tag{1-6}$$

The advantage of the entrance flow method for measuring elongational viscosity is its applicability at high elongation rate and for various types of a material, even for a low viscous melt. The experimental setup is also not difficult since an existing conventional capillary rheometer is applicable. Furthermore, they are very similar to the actual processing operations in industry, of which the crystallization occurs at a non-isothermal process. Nevertheless, the main difficulty in the use of the entrance flow method for measuring elongational viscosity is the complexity of the flow, which, because of the formation of recirculating vortices near an abrupt contraction, is particularly difficult to analyze. As mentioned, the flow is, moreover, nonhomogeneous. Therefore, the effect of various other parameters, such as total strain and normal stress difference may also affect the entrance pressure loss.

1.2.3 Drawdown force

Drawdown force, so called melt strength or melt tension, is defined as the force required

for uniaxial elongation of a polymer melt. It is often evaluated in industry because it has been known that the measurement of the drawdown force at various draw ratios provides the information on elongational viscosity.[44] The drawdown force is measured by stretching a strand extruded downward throughout the die (B) in a capillary rheometer (A) at constant draw ratio by set of rotating wheels (D) as shown in Figure 1-4. Then, the stretching force is measured by a tension detector (C). Moreover, the machine is able to evaluate drawability from the maximum draw ratio, defined as a draw ratio at which the strand is stretched without any rupture. In addition, capillary rheometers are also available to measure the extrudate swell, known as Barus effect. The diameter of the strand extruded from the die is measured on-line using a laser beam emitted from (E) to (F).[32] This technique is useful to determine the non-linear behavior of a polymer melt even for a low viscous material. Moreover, it is well known that most polymer processing operations involve some kinds of extensional flow by converging flow at a die entry or nozzle and also non-isothermal crystallization. In particular, such situation becomes prominent after passing through a die at extrusion. Therefore, the extensional deformation at capillary extrusion possesses the ability to determine the processability of a commercial polymer at actual processing operations.

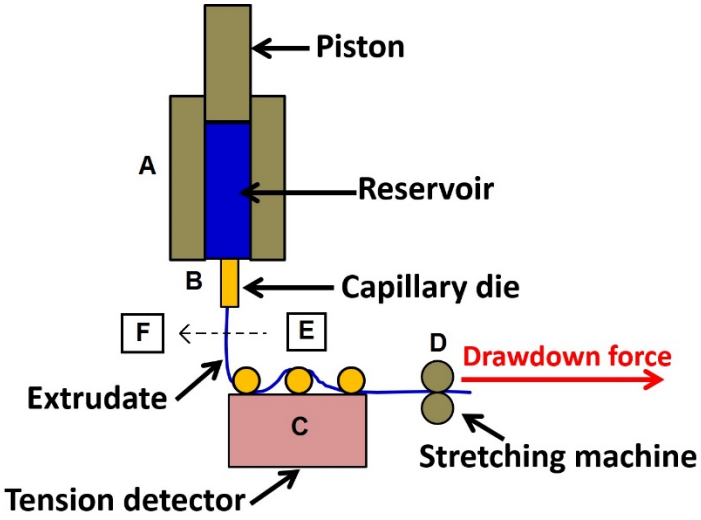

Figure 1-4 Schematic illustration of drawdown force measurement

1.3 Capillary extrusion

1.3.1 Corrections of capillary data

There are three types of the corrections for capillary data. The first one is Mooney analysis, which is to correct the apparent shear rate due to slippage at the wall because the slippage reduces the shear rate near the wall. According to Mooney analysis, shear rate can be corrected by investigation of the apparent shear rate using dies with various radii but with a constant length-to-radius ratio, as written in equation 1-7.

$$\frac{4v_{z,av}}{R} = 4v_{z,slip}\left(\frac{1}{R}\right) + \dot{\gamma}_{a,slip-corrected} \tag{1-7}$$

Capillary flow involves flow through a contraction of a certain angle, where there is a large pressure drop associated with such flow, known as entrance pressure. This pressure is required to calculate the true shear stress.[45] Therefore, the end pressure correction, which was proposed by Bagley in 1957,[46] is needed to correct this effect. The results from this procedure are customarily presented in terms of the Bagley correction or end correction, n_B, defined as;

$$n_B = \frac{\Delta P_{end}}{2\sigma_w} \tag{1-8}$$

where σ_w is the wall shear stress in the die for fully developed flow and ΔP_{end} is the overall pressure drop at the die end.

Then, the true shear stress σ_w can be obtained from equation 1-9.[47]

$$\sigma_w = \frac{\Delta P_{end}}{2\left[\frac{L}{R} + e\right]} \tag{1-9}$$

where *e* is the x-intercept obtained by extrapolation of the curves in Bagley plot.

The last one is the Weissenberg-Rabinowitsch correction, which is the correction for the shear rate due to non-parabolic velocity profile of non-Newtonian fluid. The velocity profile of pressure-driven flow of a Newtonian fluid in a pipe is a parabolic profile. Regarding the Hagen-Poiseuille law, the pressure-drop/flow rate relationship for Newtonian fluids is as follow.[38]

$$Q = \frac{\Delta P \pi R^4}{8 \eta L} \tag{1-10}$$

where Q is the volume flow rate and η is the viscosity.

Thus, for Newtonian fluids, measurements of pressure-drop and flow rate in a capillary tube may be plotted as $4Q/\pi R^3$ (shear rate at the wall for a Newtonian fluid) versus $R\Delta P/2L$ (shear stress at the wall for all fluids), which is a straight line of a slope equal to the inverse of the viscosity. The quantity $4Q/\pi R^3$ is therefore called the apparent shear rate $\dot{\gamma}_a$.

In the case of non-Newtonian fluid, the shear rate will be different from that of a Newtonian fluid. The correct shear rate at the wall $\dot{\gamma}_w$ for a non-Newtonian fluid can be calculated from equation 1-11.

$$\dot{\gamma}_w = \dot{\gamma}_a \left[\frac{3}{4} + \frac{1}{4}\frac{dlnQ}{dln\,\sigma_w}\right] \tag{1-11}$$

1.3.2 Extrudate swell

When a molten polymer flows through a capillary, molecular chains become oriented, uncoiled and disentangled due to the applied shear. As the melt leaves the die, molecular chains tend to recoil and grow in the normal direction, leading to extrudate swell.[48-50] Die swell (extrudate swell) is also called the Barus effect, which is an important parameter for characterizing polymer melt elasticity in an extrusion flow and is related to the quality of the products. Die swell is usually described quantitatively in terms of the swelling ratio (d/D), which is the ratio of extrudate diameter (d) to the die diameter (D). Extrudate swell is affected by the length of capillary die when $\tau_1 >> t_{die}$, where τ_1 is the longest relaxation time and t_{die} is the duration in a capillary die, because the memory of molecular conformation prior to die entrance depends on the length, that is t_{die}. When a die length is long enough to forget the memory, that is $\tau_1 << t_{die}$, swell ratio is described by the primary normal stress difference N_1 at steady state as follows.[44]

$$d/D = 0.13 + \left[1 + \frac{1}{2}\left(\frac{N_1}{2\sigma}\right)^2\right]^{1/6} \tag{1-12}$$

1.3.3 Flow instabilities

Flow instabilities occur during the extrusion and cause distortion on the surface of extrudates, known as melt fracture. From the view point of capillary rheometry, the onset of melt distortion means the end of rheology measurements, *e.g.*, it sets an upper limit on shear stress for the measurement of Barus effect. Moreover, occurrence of the distortions limits the production rate and quality of a product.[33,51-55] Generally, melt fracture at capillary extrusion is categorized into three types.[56,57] The first type occurs when the extrudate begins losing glossy appearance from the presence of small amplitude but high frequency of periodic distortions on the surface. This phenomenon is so called shark-skin failure.[58] Figure 1-5 shows shark-skin failure on the extrudate surface of linear low-density polyethylene (LLDPE).

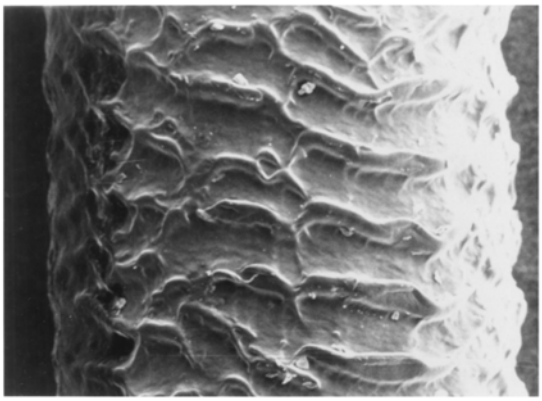

Figure 1-5 Shark-skin failure of LLDPE extrudate[59]

When apparent shear stress is beyond the critical value, slippage of a polymer melt takes place at die wall, resulting in alternating relatively smooth and distorted sections on the surface of an extrudate, known as stick-slip or spurt flow.

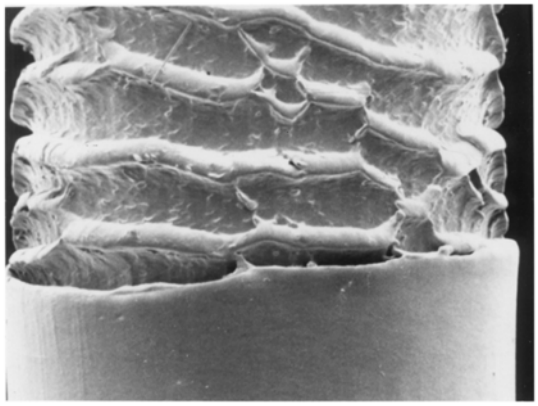

Figure 1-6 Stick-slip or spurt flow of LLDPE extrudate[59]

The last type is gross melt fracture, which is caused by a swirling motion of a melt due to the converging flow at the die entrance, giving rise to volumetric or large amplitude, chaotic distortions.

Figure 1-7 Gross melt fracture of mLLDPE extrudate[60]

There are many researches focus on the mechanism of the shark-skin failure.[54-56,61-64] Cogswell proposed one possible mechanism of the shark-skin failure in 1977.[65] According to him, shark-skin failure occurs due to the surface crack. In other words, cohesive failure at surface takes place by the high level of tensile stress at die exit, resulting in brittle fracture.

Since flow instabilities at capillary extrusion limit processability as well as quality of products, many attempts have been done in order to mitigate flow instabilities. The most common way is to use polymer processing aids (PPAs). Kharchenko et al. (2003)[66], Bigio et al. (2005)[67] and Dubrocq-Baritaud et al. (2005)[68] studied the effect of fluoropolymer-based polymer processing aids for postponing the surface distortion. They found that these additives possess the ability to reduce die pressure and delay the onset of shark-skin by creating the slippage at the die wall. In addition, Kazatchkov et al. (2000)[69] reported that boron nitride powder is also able to postpone the onset shear stress not only for shark-skin failure but also

for gross melt fracture. In 2000, Hong et al. reported that mitigation of the flow instability can be carried out using hyperbranched polymer. The mechanism of this phenomenon is attributed to excessive slip.[70] Later, Kotera and Yamaguchi studied flow instability of ethylene–tetrafluoroethylene copolymer (ETFE) at capillary extrusion. They have found that ETFE exhibits various types of flow instability. Interestingly, quasi-stable flow region, so-called super-extrusion, is detected in the wide range of shear rates between slip-stick and wavy melt fracture regions due to steady slippage, suggesting that ETFE can be processed at a high output rate condition.[71]

1.4 Polyolefins

Polyolefins are among the most widely used polymers because they possess various applications such as film, packaging, automobile and other industries.[29] Polyolefin refers to a class of synthetic resins prepared by the polymerization of olefins. Olefins are hydrocarbons whose molecules contain vinyl functional groups. They are often derived from natural gas or from low-molecular-weight constituents of petroleum, in which their most prominent members are ethylene and propylene. Therefore, the most available polyolefins in industry and market are polyethylene and polypropylene.[72]

1.4.1 Polyethylene

Polyethylene (PE) is one of the oldest commodity plastics and the versatile applications

penetrate deeply in society to support our daily life. PE was first produced by British company. Preparation required temperatures up to 200 °C and pressures up to 2000 atm. In 1952, Karl Ziegler was successful to prepare a high molecular weight polyethylene at room temperature. The structure of PE is represented as a simple alkane formula C_nH_{2n+2} consists of covalently linked carbon atoms with pendant hydrogen atoms. However, PE provides a wide range of mechanical properties due to variations in polymer chain structure. PE is generally classified by the density, although the catalyst and polymerization conditions also affect the properties. As the packing of crystalline regions is better than that of noncrystalline regions, the overall density of a polyethylene resin will increase as the degree of crystallinity rises. Generally, the higher the concentration of branches, the lower the density of a solid.[73]

In addition, copolymers of ethylene and α-olefin are also generally regarded as PE, as well as linear low-density polyethylene (LLDPE) or very low-density polyethylene (VLDPE) when the density range is within LDPE or lower than LDPE, respectively. Further, copolymers of ethylene and non-olefin monomer, in which the functional group consists of carbon, oxygen and hydrogen, are involved in PE. Moreover, the absence of branching results in a more closely packed structure with a higher density and somewhat higher chemical resistance than LDPE, known as high-density polyethylene (HDPE). HDPE is more opaque than LDPE and it can withstand at higher processing temperatures. The molecular structure of PE classified by branching structure are illustrated schematically in Figure 1-8.

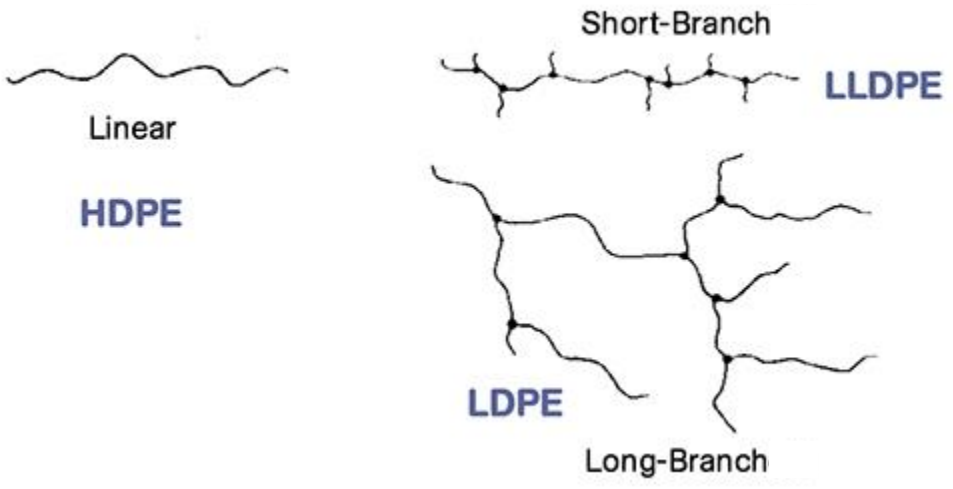

Figure 1-8 Molecular structure of polyethylene.[72]

1.4.2 Polypropylene

Polypropylene (PP) is classified as one type of polyolefins. Commercial production of PP began in 1957 and its usage has displayed strong growth from this date. In general, the Ziegler-Natta catalyst primarily consists of two components: a derivative of a transition metal such as titanium trichloride $TiCl_3$, and an organoaluminum compound such as triethylaluminum $Al(C_2H_5)_3$. In addition, the support and modifiers are usually incorporated. Ziegler-Natta catalyzed propylene comprises the majority of commodity grades resins with a comparatively broad molecular weight distribution (MWD) approximately 3.5. Continued research led to the discovery of metallocene catalyst, which consists of a bis(cyclopentadienyl) complex of a

transition metal and a methylaluminoxane.[74] As the catalysts contain only one type of active site, the comonomers react in an identical fashion. As a result, the catalysts provide LLDPE with narrower MWD approximately 2.0. Both Ziegler-Natta and metallocene catalysts are used commercially, the choice between the two depends largely on desired molecular weight distribution. These days, more researches tend to focus on the modification techniques, processing and applications rather than catalyst development.

The versatility of the polymer has sustained growth rates enabling PP to challenge the market share because of its ability for applying in various fields of applications. PP possesses high tensile and compressive strength as well as high heat distortion temperature. Moreover, it is highly resistant to most alkalis and acid, organic solvents, degreasing agents and electrolytic attack. On the contrary, it is less resistance to aromatic, aliphatic and chlorinated solvents and UV. However, its cost performance is relatively good. Therefore, it is one of the most used resins in the world.

Most PP used is highly crystalline and geometrically regular, *i.e.*, isotactic. It is said that PP has an intermediate level of crystallinity between LDPE and HDPE; On the other hand, PP has higher service temperatures and tensile strength than PE. However, its properties are related to the crystallinity of the polymer, which depends on its tacticity. PP has three possible stereochemical configurations: isotactic (with all methyls on the same side of the chain), syndiotactic (with methyls on alternating sides of the chain), and atactic (without any regular order). Schematic illustration of tacticity for PP is shown in Figure 1-9. In this thesis, PP represents the isotactic one.

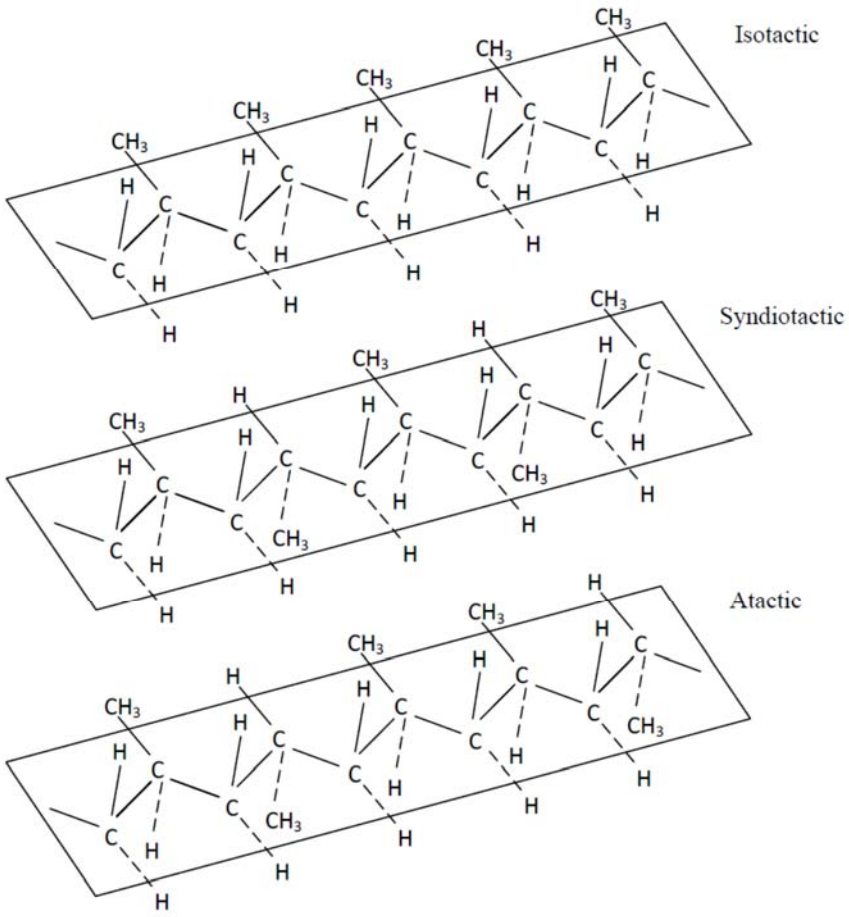

Figure 1-9 Tacticity of polypropylene.

1.5 Melt elasticity of polyolefins

Melt elasticity plays an important role in some processing operations such as fiber spinning, foaming and blow-molding.[44] It is well known that elastic properties in the molten

state are enhanced by broadening the molecular weight distribution and incorporation of long-chain branches. Apart from these methods, many approaches to enhance melt elasticity such as shear modification, blending of polyethylene and flexible nanofiber method have been reported recently.

1.5.1 Shear modification of long-chain branched polymer

It is well known that long-chain branches enhance the elastic features greatly in the molten state. Therefore, LDPE having long-chain branches shows higher melt elasticity than LLDPE. However, the elastic property of LDPE in the molten state is found to be depressed by applied processing history, which is known as "shear modification".[55] The mechanism of the shear modification was explained by Münstedt based on the tube model.[75] At equilibrium state, a branch polymer shows a prolonged characteristic time of the longest relaxation mechanism, because a simple reptation is not allowed by the branch parts. Further, the chain contraction between branch points is prohibited. After processing history, long-chain branches tend to align to the main chain by applied hydrodynamic force. Consequently, a branch part is dragged into a tube of a main chain, leading to decrease in "active" long-chain branches. Because the alignment of LCB to the main chain, a simple reptation is allowed. As a result, chain stretching occurs without the hindrance of branch parts as similar to a linear polymer. Moreover, the longest relaxation time, *i.e.*, reptation time, is also reduced.[76]

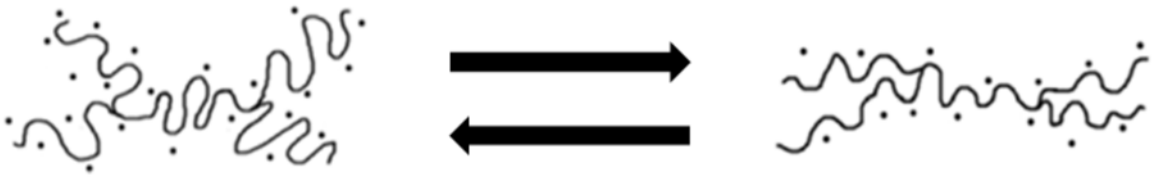

Figure 1-10 Schematics illustration of molecular conformation (left) before and (right) after the shear modification.

However, the branch points are in a low entropy state. Therefore, the conformation will recover to the initial one by entropic force after the cessation of flow. Yamaguchi and Gogos evaluated the rheological properties at recovery process from shear modification and found that the rheological properties after applied shear history are determined by the applied shear stress and the duration time of shearing.[77] This is reasonable because the degree of molecular orientation is proportional to the stress in a molten state.

1.5.2 Polyethylene blend

Although it is well known that LDPE shows marked melt elasticity as compared with LLDPE, the addition of LLDPE can enhance the melt elasticity of LDPE. This synergistic phenomenon was firstly reported by Utracki and Schlund.[78] Strain-hardening behavior is clearly detected for the blend with LLDPE having high viscosity. The drawdown force was also found

to be enhanced. This is attributed to the two following factors: enhancement of zero-shear viscosity and the marked strain-hardening behavior in elongational viscosity. It is believed that the addition of long linear chains makes the characteristic time of a tube for a branched polymer longer. Since the relaxation time of "surrounding linear chains" around a branched polymer is prolonged, tube dilation and constraint release are reduced.

1.5.3 Flexible nanofiber method

It has been found that the addition of flexible nanofibers can enhance the melt elasticity with slight increase in shear stress.[32] The high level of flexibility leads to the interdigitated state of the fibers. Then, the fibers cannot align to the flow direction independently, which is significantly different from rigid fibers such as glass fibers. Instead of the parallel orientation of the fiber, as observed in a system with rigid fibers, the network structure is deformed to the flow direction, retaining the topological interaction between fibers. Consequently, some parts of fibers near the coupling points have to bend to a great extent, providing large bending force. Moreover, friction force between the fibers would be enhanced by the deformation of network. The excess force will be responsible for the marked normal stress difference as energetic elasticity.

1.6 Objectives of this research

Since the drawdown force measured by a conventional capillary rheometer provides information on the elongational viscosity, which has a close relation with processability, it is employed in industry as one factor to investigate elastic behaviors of a molten polymer. Even though the drawdown force is often evaluated, the effect of extrusion condition such as die geometry, extrusion temperature, draw ratio, however, have not been clarified yet. The objective of this research is to investigate the effect of extrusion condition as well as mixing condition on the extrusion properties of polyolefins. In particular, the effect of die geometry and mixing condition on the stretchability and flow instabilities is intensively discussed as well as the mechanism is proposed. Furthermore, the effect of crystallization, which depends on short-chain branches in PE, on the drawdown force is evaluated. In addition, a new method to enhance the drawdown force at capillary extrusion for PP is studied.

References

(1) Macosko, C. W. *Rheology: Principles, Measurements, and Applications*; John Wiley & Sons: New York, **1994**.

(2) Vlachopoulos, J.; Strutt, D. *The Role of Rheology in Polymer Extrusion*; McMaster University Hamilton: Ontario **2003**.

(3) Benbow, J. J.; Howells, E. R. *Polymer* **1961**, *2*, 429.

(4) Bartenev, G. M.; Zelenev, Y. V. *Mater. Sci. Eng.* **1967**, *2*, 136.

(5) Joseph, S.; Oommen, Z.; Thomas, S. *Mater. Lett.* **2002**, *53*, 268.

(6) Yamaguchi, M.; Wagner, M. H. *Polymer* **2006**, *47*, 3629.

(7) Yamaguchi, M. *Polym. Eng. Sci.* **2006**, *46*, 1284.

(8) Dangtungee, R.; Supaphol, P. *Polym. Test.* **2008**, *27*, 951.

(9) Ono, K.; Yamaguchi, M. *J. Appl. Polym. Sci.* **2009**, *113*, 1462.

(10) Al-Muslimawi, A.; Tamaddon-Jahromi, H. R.; Webster, M. F. *J. Non-Newtonian Fluid Mech.* **2013**, *191*, 45.

(11) Malik, M. Y.; Zehra, I.; Nadeem, S. *Alexandria Eng. J.* **2014**, *53*, 427.

(12) Sarkar, D.; Gupta, M. *CAE and Related Innovations for Polymer Processing* **2000**, *90*, 309.

(13) Wagner, M. H. *Rheol. Acta* **1979**, *18*, 681.

(14) Axtell, F. H.; Haworth, B. *Polym. Test.* **1990**, *9*, 53.

(15) Walczak, K.; Gupta, M.; Koppi, K. A.; Dooley, J.; Spalding, M. A. *Polym. Eng. Sci.* **2008**, *48*, 223.

(16) Liang, J.-Z.; Zhong, L. *Polym. Test.* **2010**, *29*, 972.

(17) Wagner, M. H.; Rolón-Garrido, V. H. *Ibreo-American J. Rheology* **2013**, *1*, 19.

(18) Thévenon, A.; Fulchiron, R. *Polym. Test.* **2013**, *32*, 691.

(19) Münstedt, H. *J. Rheol.* **1979**, *23*, 421.

(20) Ishizuka, O.; Koyama, K. *Polymer* **1980**, *21*, 164.

(21) Muller, R.; Froelich, D. *Polymer* **1985**, *26*, 1477.

(22) Meissner, J.; Hostettler, J. *Rheol. Acta* **1994**, *33*, 1.

(23) Bernnat, A., Institut für Kunststofftechnologie Universität Stuttgart, **2001**.

(24) Muke, S.; Ivanov, I.; Kao, N.; Bhattacharya, S. N. *J. Non-Newtonian Fluid Mech.* **2001**, *101*, 77.

(25) Schulze, J. S.; Lodge, T. P.; Macosko, C. W.; Hepperle, J.; Münstedt, H.; Bastian, H.; Ferri, D.; Groves, D. J.; Kim, Y. H.; Lyon, M.; Schweizer, T.; Virkler, T.; Wassner, E.; Zoetelief, W. *Rheol. Acta* **2001**, *40*, 457.

(26) Wagner, M. H.; Bastian, H.; Bernnat, A.; Kurzbeck, S.; Chai, C. *Rheol. Acta* **2002**, *41*, 316.

(27) Sentmanat, M. *Rheol. Acta* **2004**, *43*, 657.

(28) Gupta, M. *Adv. Polym. Tech.* **2002**, *21*, 98.

(29) Nitta, K.-H. *Structure and Properties of Polyolefin Materials*; Transworld Reserach Network: India, **2012**.

(30) Laun, H. M.; Münstedt, H. *Rheol. Acta* **1976**, *15*, 517.

(31) Münstedt, H.; Laun, H. M. *Rheol. Acta* **1981**, *20*, 211.

(32) Md Ali, M. A. B.; Okamoto, K.; Yamaguchi, M.; Kasai, T.; Koshirai, A. *J. Polym. Sci. Polym. Phys.* **2009**, *47*, 2008.

(33) Mieda, N.; Yamaguchi, M. *J. Non-Newtonian Fluid Mech.* **2011**, *166*, 231.

(34) Hingmann, R.; Marczinke, B. *J. Rheol.* **1994**, *38*, 573.

(35) Kim, J. M.; Keffer, D. J.; Kröger, M.; Edwards, B. J. *J. Non-Newtonian Fluid Mech.* **2008**, *152*, 168.

(36) Malkin, A. Y. *J. Non-Newtonian Fluid Mech.* **2013**, *192*, 48.

(37) Cox, W. P.; Merz, E. H. *J. Polym. Sci.* **1958**, *28*, 619.

(38) Morrison, F. A.; Oxford University Press: New York, **2001**.

(39) Trouton, F. T. *Proceedings of the Royal Society of London* **1906**, *A77*, 426.

(40) Mackley, M. R.; Hassell, D. G. *J. Non-Newtonian Fluid Mech.* **2011**, *166*, 421.

(41) Meissner, J. *Rheol. Acta* **1971**, *10*, 230.

(42) Cogswell, F. N. *Polym. Eng. Sci.* **1972**, *12*, 64.

(43) Binding, D. M. *J. Non-Newtonian Fluid Mech.* **1988**, *27*, 173.

(44) Yamaguchi, M. *Melt Elasticity of Polyolefins, Impact of Elastic Properties on Foam Processing in Polymeric Foam*; CRC Press: New York, **2004**.

(45) Ansari, M.; Zisis, T.; Hatzikiriakos, S. G.; Mitsoulis, E. *Polym. Eng. Sci.* **2012**, *52*, 649.

(46) Bagley, E. B. *J. Appl. Phys.* **1957**, *28*, 624.

(47) Mitsoulis, E.; Hatzikiriakos, S. *Rheol. Acta* **2003**, *42*, 309.

(48) Liang, J.-Z. *Polym. Test.* **2000**, *20*, 29.

(49) Liang, J.-Z.; Li, R. K. Y.; Tang, C. Y.; Cheung, S. W. *J. Appl. Polym. Sci.* **2000**, *76*, 419.

(50) Liang, J.-Z.; Yang, J.; Tang, C.-Y. *Polym. Test.* **2010**, *29*, 624.

(51) Piau, J.-M.; El Kissi, N.; Toussaint, F.; Mezghani, A. *Rheol. Acta* **1995**, *34*, 40.

(52) Yamaguchi, M. *J. Appl. Polym. Sci.* **2001**, *82*, 1277.

(53) Robert, L.; Vergnes, B.; Demay, Y. *J. Non-Newtonian Fluid Mech.* **2003**, *112*, 27.

(54) Miller, E.; Rothstein, J. *Rheol. Acta* **2004**, *44*, 160.

(55) Siriprumpoonthum, M.; Mieda, N.; Anh Doan, V.; Nobukawa, S.; Yamaguchi, M. *J. Appl. Polym. Sci.* **2012**, *124*, 429.

(56) Koopmans, R.; Doelder, J. D.; Molenaar, J. In *Polymer Melt Fracture*; CRC Press: New York, **2010**.

(57) Malkin, A. Y.; Arinstein, A.; Kulichikhin, V. G. *Prog. Polym. Sci.* **2014**, *39*, 959.

(58) Kalman, B. M.; Savvas, G. H. In *Polymer Processing Instabilities*; CRC Press: New York, **2004**.

(59) Denn, M. M. *Annu. Rev. Fluid Mech.* **2001**, *33*, 265.

(60) Lee, H.-y.; Kim, D. H.; Son, Y. *Polymer* **2006**, *47*, 3929.

(61) Fernández, M.; Francisco Vega, J.; Santamaría, A.; Muñoz-Escalona, A.; Lafuente, P. *Macromol. Rapid Commun.* **2000**, *21*, 973.

(62) Yamaguchi, M.; Miyata, H.; Tan, V.; Gogos, C. G. *Polymer* **2002**, *43*, 5249.

(63) Allal, A.; Vergnes, B. *J. Non-Newtonian Fluid Mech.* **2007**, *146*, 45.

(64) Pol, H. V.; Joshi, Y. M.; Tapadia, P. S.; Lele, A. K.; Mashelkar, R. A. *Ind. Eng. Chem. Res.* **2007**, *46*, 3048.

(65) Cogswell, F. N. *J. Non-Newtonian Fluid Mech.* **1977**, *2*, 37.

(66) Kharchenko, S. B.; McGuiggan, P. M.; Migler, K. B. *J. Rheol.* **2003**, *47*, 1523.

(67) Bigio, D.; Meillon, M. G.; Kharchenko, S. B.; Morgan, D.; Zhou, H.; Oriani, S. R.; Macosko, C. W.; Migler, K. B. *J. Non-Newtonian Fluid Mech.* **2005**, *131*, 22.

(68) Dubrocq-Baritaud, C.; Darque-Ceretti, E.; Vergnes, B. *J. Non-Newtonian Fluid Mech.* **2011**, *166*, 847.

(69) Kazatchkov, I. B.; Yip, F.; Hatzikiriakos, S. G. *Rheol. Acta* **2000**, *39*, 583.

(70) Hong, Y.; Coombs, S. J.; Cooper-White, J. J.; Mackay, M. E.; Hawker, C. J.; Malmström, E.; Rehnberg, N. *Polymer* **2000**, *41*, 7705.

(71) Kotera, S.; Yamaguchi, M. *J. Fluorine Chem.* **2015**, *176*, 20.

(72) Michael, S. In *Plastics Technology* **2012**, 17.

(73) Andrew J. Peacock *Handbook of Polyethylene*; Marcel Dekker: New York, **2000**.

(74) Kaminsky, W. *J. Polym. Sci. Polym. Chem.* **2004**, *42*, 3911.

(75) Münstedt, H. *Soft Matter* **2011**, *7*, 2273.

(76) Doi, M., Edwards, S.F. *The Theory of Polymer Dynamics*; Oxford University Press: New York, **2007**.

(77) Yamaguchi, M.; Gogos, C. G. *Adv. Polym. Technol.* **2001**, *20*, 261.

(78) Utracki, L. A.; Schlund, B. *Polym. Eng. Sci.* **1987**, *27*, 1512.

Chapter 2

Effect of Die Geometry on Drawdown Force for Polyolefins

2.1 Introduction

Rheological responses of a molten polymer under elongational flow have received much attention in both academic and industrial fields, because they are important for polymer characterization and the quality of a product obtained by various processing operations in which a polymer melt with free surface is deformed, such as blow-molding, thermoforming, extrusion coating, foaming and spinning.[1-3] Therefore, numerous researchers have evaluated the elongational viscosity to predict the processability.[4-12]

Cogswell and Binding proposed the method to measure the uniaxial elongational viscosity by a pressure-driven capillary rheometer,[13,14] in which the elongational strain rate is calculated considering the convergence flow at the die entry.[15] However, it is not so easy to remove the stress contribution from shear flow by this method. Moreover, the growth curve of the elongational viscosity cannot be detected directly, although it has been recognized to be important for processability. Up to now, several elongational rheometers have been available in order to investigate the transient curves of elongational viscosity. One of the most well-

known rheometers was developed by Meissner, which consists of rotary clamps, so called "Meissner-type" rheometer.[16-23] Later, Sentmanat fabricated a dual wind-up extensional rheometer, composed of two counter-rotating drums, in which the ends of a sample are allowed to be stretched. This is called Sentmanat Extensional Rheometer (SER) and was originally used for an elastomer.[24,25] However, these rheometers are not available for low viscous melts. Therefore, the drawdown force, defined as the force needed to stretch a polymer melt uniaxially, is often evaluated to predict elongational viscosity, because the measurement is not difficult with minimal experimental error.[26-28] Furthermore, measurements can be performed even for a low viscous melt. Although the strain-hardening behavior, *i.e.*, upturn departure of the elongational viscosity from the linear region, is not evaluated directly by the drawdown force measurement, it is valuable to obtain the information on the rheological response under elongational flow. At present, therefore, it is widely used especially in industry. However, the effect of the measurement conditions such as draw ratio, temperature and die geometry has not been clarified yet. In this study, the effect of extrusion conditions on the drawdown force using a conventional capillary rheometer is clarified using polyolefins. In particular, the effect of die geometry is investigated in detail for polypropylene (PP). In addition, this effect is also studied using polyethylene (PE) to reveal the relationship of molecular structure and the sensitivity to die geometry, because various types of PE with different molecular structure are commercially available. It is well known that the crystallization behavior is strongly affected by the short-chain branches. For example, the solidification rate depends on the branch content and its distribution.[29] The difference in the crystallization rate must play an important role in the

drawdown force measurements. Furthermore, long-chain branches are known to be responsible for the strain-hardening behavior in the transient elongational viscosity owing to the chain stretching. Although the effect of short- and long-chain branches in PE on the elongational viscosity at a constant temperature has been widely reported,[9,28,30-33] such effect on the drawdown force has not been discussed yet. This topic is intensively studied in this research. The results will provide fundamental information on the extrusion processing and so on.

2.2 Experimental

2.2.1 Materials and Sample Preparation

Polyolefins employed in this study were PP and PE. In the case of PP, three samples with different molecular weights, denoted as PP-H, PP-M and PP-L in this study. All of them are commercially available homopolymers. The characteristics of the samples are shown in Table 2-1. PE used in this work were commercially available high-density polyethylene (HDPE) and linear low-density polyethylene (LLDPE) having different molecular weights. Characteristics for all types of PE are also summarized in Table 2-1, in which the numeral in the sample code denotes the value of the melt flow rate (MFR) at 190 ^{o}C. For example, HDPE-5 is the high-density polyethylene whose MFR is 5 g/10 min. HDPE-1, HDPE-5 and LLDPE-2 were produced by Ziegler-Natta catalyst, whereas LLDPE-1 was prepared by a metallocene catalyst. The number of short-chain branches per 1000 backbone carbon atoms were

characterized by the carbon nuclear magnetic resonance spectroscopy (^{13}C-NMR). LLDPE-1 is a copolymer of ethylene and 1-hexene, while LLDPE-2 is that of ethylene and 1-butene.

The crystallization temperature *Tc*, shown in Table 2-1, was evaluated by a differential scanning calorimeter (DSC 820, Mettler-Toledo, USA). The samples were heated to 190 °C at a heating rate of 30 °C/min to erase the thermal history, followed by cooling down to 25 °C at a cooling rate of 10 °C/min to evaluate the crystallization temperature.

Table 2-1 Characteristics of materials

Type	Sample	Mn	Mw	Number of SCB[1]	MFR (g/10 min)[2]	Density (kg/m^3)	Tc (°C)[3]	Grade (Maker)
PP	PP-H	4.5x10^4	2.6x10^5	-	5	N/A	114.0	FY4 (Japan Polypropylene)
	PP-M	4.3x10^4	2.1x10^5	-	10	N/A	115.0	K1008 (Chisso)
	PP-L	4.0x10^4	2.0x10^5	-	20	N/A	118.0	K1800 (Chisso)
PE	HDPE-1	1.7x10^4	1.0x10^5		0.95	961	116.4	#5110 (Tosoh)
	HDPE-5	1.2x10^4	7.5x10^4	-	5.0	965	115.7	#4000 (Tosoh)
	LLDPE-1	3.8x10^4	1.0x10^5	18.4 (Butyl)	1.0	915	100.1	SP1510 (Prime Polymer)
	LLDPE-2	2.6x10^4	1.1x10^5	18.0 (Ethyl)	2.0	-	104.6	FS144 (Tosoh)

[1] Number of short-chain branches per 1000 backbone carbons

[2] Melt flow rate at 2.16 kgf and 230 °C and for PP and 190 °C for PE

[3] Measured by DSC at -10 °C/min

2.2.1.1 Polypropylene

Thermal stabilizers such as tris(2,4-di-tert-butylphenyl)phosphate (Irgafos168, Ciba, Switzerland) and pentaerythritol tetrakis(3-(3,5-di-tert-butyl-4-hydroxyphenyl)propionate) (Irganox1010, Ciba, Switzerland) were added into the sample using an internal batch mixer (Labo-Plastmill, Toyoseiki, Japan) with a blade rotational speed of 30 rpm at 200 °C for 3 min. The amount of each thermal stabilizer was 5000 ppm. Moreover, 1,3:2,4-bis-O-(4-methylbenzylidene)-D-sorbitol (GelAll MD, New Japan Chemical, Japan) was used as a nucleating agent. The amount of the nucleating agent was 1 wt%. The sample was prepared by melt-mixing at 240 °C, which is higher than the dissolution temperature of the nucleating agent.[34] Then, the sample was compressed into a flat sheet using a compression-molding machine (IMC-180C, Imoto, Japan) at 230 °C for 3 min and cut into small pieces after quenching.

2.2.1.2 Polyethylene

Pure PE samples were used as a pellet form for the measurements. Besides the pure samples, two blends were prepared by the addition of 1 wt% of HDPE-5 into either LLDPE-1 or LLDPE-2 using an internal batch mixer (Labo-Plastmill, Toyoseiki, Japan). A blade rotation speed, temperature and mixing time were 30 rpm, 160 °C and 3 min, respectively. During melt mixing, 5000 ppm of a thermal stabilizer, 6-[3-(3-*t*-butyl-4-hydroxy-5-methylphenyl)propoxy]-2,4,8,10-tetra-*t*-butyldibenzo [d,f] [1,3,2] dioxaphosphepin (Sumilizer® GP, Sumitomo

Chemical, Japan), and 1000 ppm of calcium stearate were added. The samples obtained were compressed into a flat sheet at 200 °C for 3 min prior to the measurements.

2.2.2 Measurements

The frequency dependence of oscillatory shear moduli such as storage modulus *G'* and loss modulus *G"* was measured using a cone-and-plate rheometer (AR2000, TA instruments, USA) with a cone angle of 4° at various temperatures such as 190, 210, 230 and 250 °C.

Drawdown force was evaluated using a capillary rheometer (140 SAS-2002, Yasuda Seiki Seisakusyo, Japan) equipped with a tension detector (DT-413G-04-3, Nidec-Shimpo, Japan) and a set of rotating rolls as shown in Figure 2-1. Circular dies with an entrance angle of 180° and the length-to-diameter ratio *L*/*D* of 10/1, 20/1, 40/1, 20/2 and 40/2 (mm/mm) were used. The shear rates at the die wall were 124, 21.4 and 15.5 s^{-1}. The experiments were performed at 190, 210 and 230 °C with various draw ratios such as 2, 4.6, 5, 6, 9, 13 and 20. The draw ratio can be calculated from equation 2-1.

$$\text{Draw ratio} = \frac{\text{stretch rate } (= 2\pi RN)}{\text{extrusion rate } (= \frac{Q}{A})} \tag{2-1}$$

where *R* is the radius of rotating wheels, *N* is the number of rotation per second, *Q* is the volume flow rate and *A* is the cross-section area of die exit.

The flow curve was evaluated by the capillary rheometer equipped with various circular dies having a constant diameter of 1 mm at 190, 210 and 230 °C. The shear stress and shear rate were calculated by the Hagen-Poiseuille law with Bagley and Weissenberg-Rabinowitch corrections. During the extrusion, swell ratio of the extrudate was measured online by a laser beam.

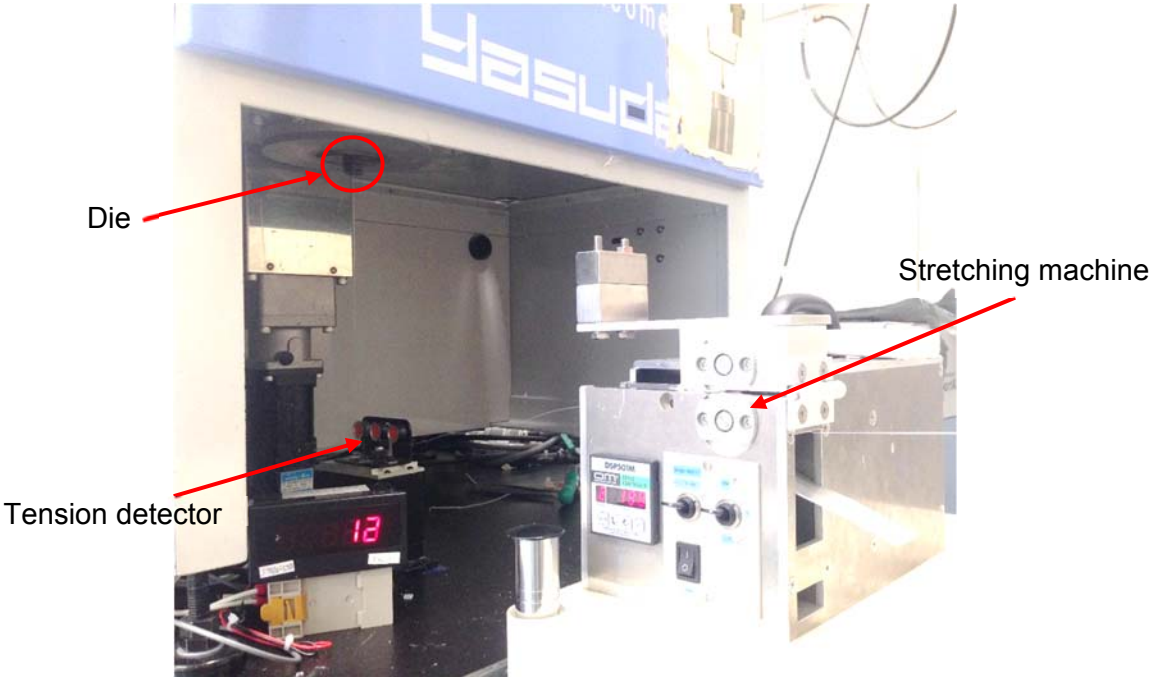

Figure 2-1 Experimental setup for drawdown force measurement using a capillary rheometer.

Wide-angle X-ray diffraction patterns (WAXD) were provided by an XRD diffractometer (R-AXIS IIc, Rigaku, Japan). The strands, extruded at 190 °C and stretched at a

draw ratio of 9, were employed as the samples. The measurements were performed using a graphite monochromatized CuKα radiation beam focused via a 0.3 mm pinhole collimator with a flat 20 × 20 cm^2 imaging plate (IP) detector of 1900 × 1900 pixels. The sample was exposed to the X-ray beam perpendicular to the strand axis for 7 min.

2.3 Results and discussion

2.3.1 Effect of extrusion condition on the drawdown force

Figure 2-2 shows the master curves of frequency dependence of oscillatory shear moduli such as storage modulus *G'* and loss modulus *G"* for PP-H, PP-M and PP-L at the reference temperature of 190 °C. Because the samples are homopolymers without long-chain branches, the time-temperature superposition principle is applicable. The flow activation energy is about 45 kJ/mol for all samples, which is almost identical to the values reported previously.[9,35,36]

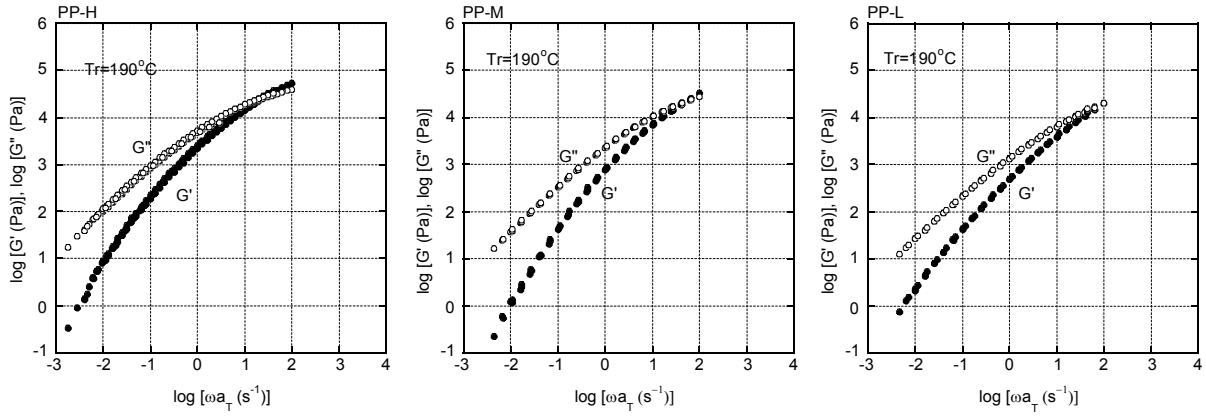

Figure 2-2 Master curves of frequency dependence of oscillatory shear moduli such as storage modulus *G'* (closed symbols) and loss modulus *G"* (open symbols) for PP-H, PP-M and PP-L at the reference temperature of 190 °C.

Furthermore, *G'* and *G"* are proportional to ω^2 and ω, respectively in the low frequency region, demonstrating that the rheological terminal zone is observed. Therefore, the weight-average relaxation time τ_w is estimated by the product of zero-shear viscosity η_0 and steady-state shear compliance J_e^0 as follows;

$$\eta_0 = \lim_{\omega \to 0} \frac{G''}{\omega} \tag{2-2}$$

$$J_e^0 = \lim_{\omega \to 0} \frac{G'}{G''^2} \tag{2-3}$$

$$\tau_w = \eta_0 J_e^0 \tag{2-4}$$

As summarized in Table 2-2, both η_0 and J_e^0 roughly correspond with the GPC data.

Table 2-2 Rheological parameters in the terminal zone at 190 °C

Samples	η_0 **(Pa s)**	J_e^0 **(Pa^{-1})**	τ_w **(s)**
PP-H	9.85×10^{3}	1.08×10^{-3}	10.6
PP-M	3.80×10^{3}	8.38×10^{-4}	3.2
PP-L	2.75×10^{3}	4.26×10^{-4}	1.2

Figure 2-3 shows the master curve of shear viscosity as a function of shear rate at the reference temperature of 190 °C for PP. As seen in the figure, all samples show non-Newtonian behavior in the experimental range. The shift factors at 210 and 230 °C are almost identical to those obtained at the oscillatory measurements. In the experimental range, flow instabilities like melt fracture are not detected for all samples.

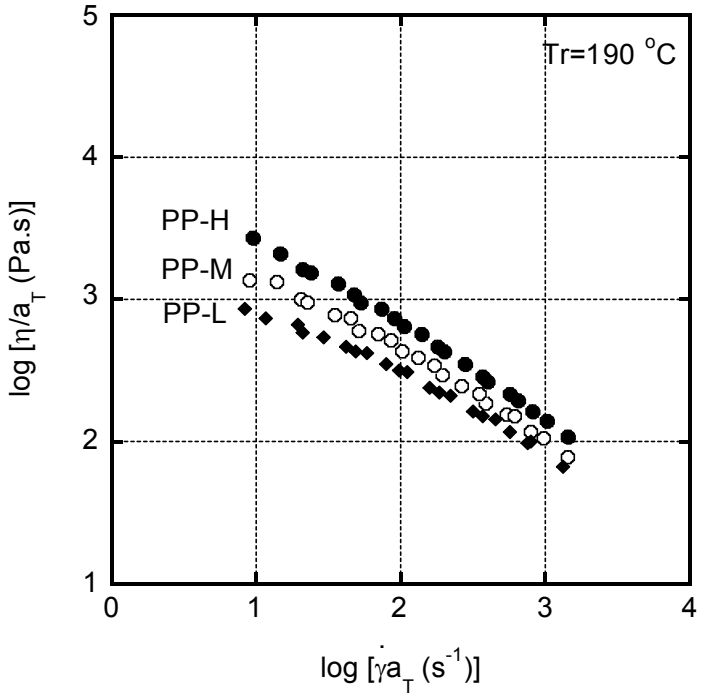

Figure 2-3 Master curves of shear viscosity as a function of shear rate at the reference temperature of 190 °C for PP-H (closed circles), PP-M (open circles) and PP-L (closed diamonds).

The drawdown force is investigated using various dies at 190, 210 and 230 °C. The results obtained at a draw ratio of 20 for PP-H are shown in Figure 2-4. The applied shear rate at the die wall is 15.5 s^{-1}.

It should be noted that the drawdown force increases with increasing the die length. For example, the values at the long die (L/D=40/1) are almost twice as large as those at the short

die (L/D=10/1). Such strong impact of the die length on the drawdown force has not been reported to the best of my knowledge. A similar trend is confirmed when the dies with 2 mm diameter are employed.

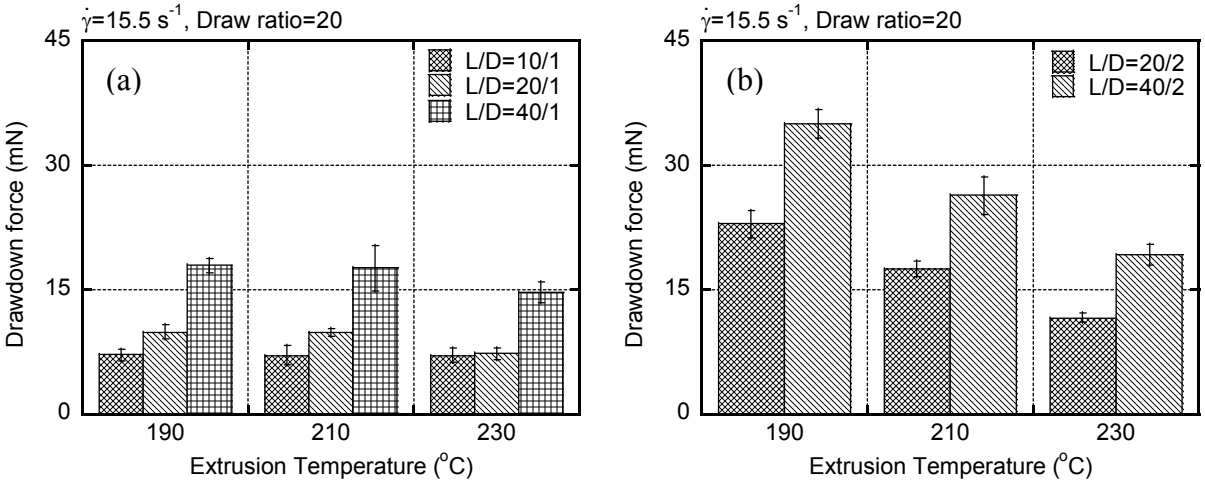

Figure 2-4 Drawdown force of PP-H extruded from dies having various lengths and diameters at a draw ratio of 20. The extrusion temperature at the die and reservoir was controlled at 190, 210 and 230 °C. The diameters of the dies were (a) 1 mm and (b) 2 mm.

Figure 2-5 shows the drawdown force at various draw ratios. As increasing the draw ratio, the drawdown force decreases rapidly and then keeps almost a constant value (constant force, not constant stress). The magnitude of the drawdown force seems to be independent of the shear rate at the die exit. This is a typical phenomenon as reported by Bernnat[23] and Lau et

al.[37] Moreover, the enhancement of the drawdown force for the long die is clearly detected in the wide range of the draw ratio and shear rate.

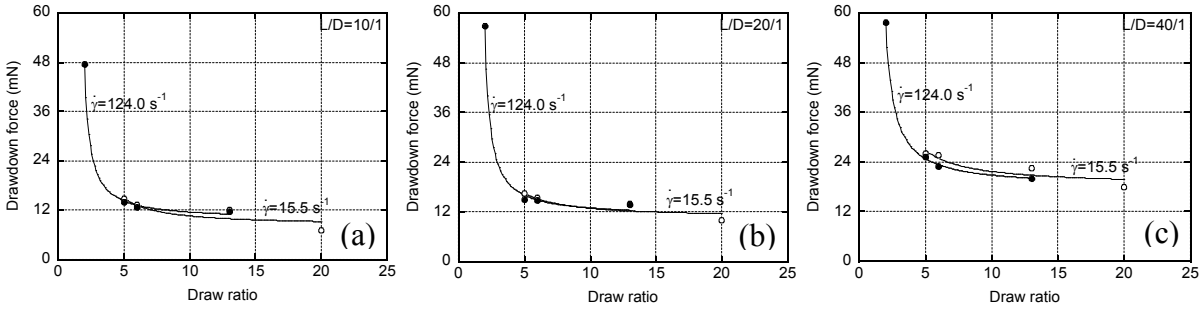

Figure 2-5 Drawdown force of PP-H extruded at various shear rates, 15.5 s^{-1} (open symbols) and 124 s^{-1} (closed symbols), and various draw ratios using dies with *L*/*D* of (a) 10/1, (b) 20/1 and (c) 40/1 at 190 °C.

It is well known that a large value of the drawdown force is detected for a polymer melt with high molecular weight, *i.e.*, long relaxation time, as shown in Figure 2-6. This is reasonable because not only shear viscosity but also elongational viscosity increases with increasing the relaxation time.

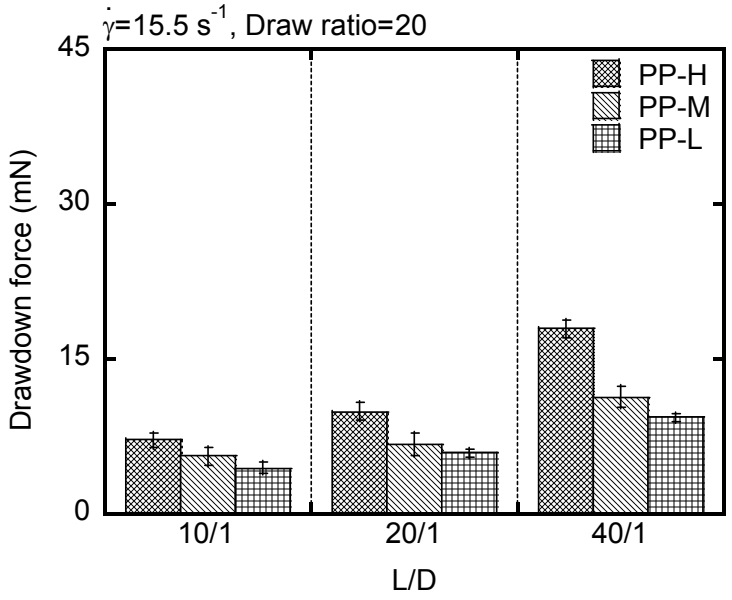

Figure 2-6 Drawdown force of PP-H, PP-M and PP-L extruded from dies having various lengths at a draw ratio of 20. The diameter of the dies was 1 mm, and the extrusion temperature at the die was controlled at 190 °C.

Since the relaxation time is affected also by the experimental temperature, the drawdown force is plotted against the relaxation time for all samples at various temperatures. As seen in Figure 2-7, the data of drawdown force obtained by the same die are on a single curve, irrespective of the experimental temperature and the molecular weight of the samples. Furthermore, it should be noted that the effect of the die length on the drawdown force is pronounced for a melt having a long relaxation time, which will be explained later.

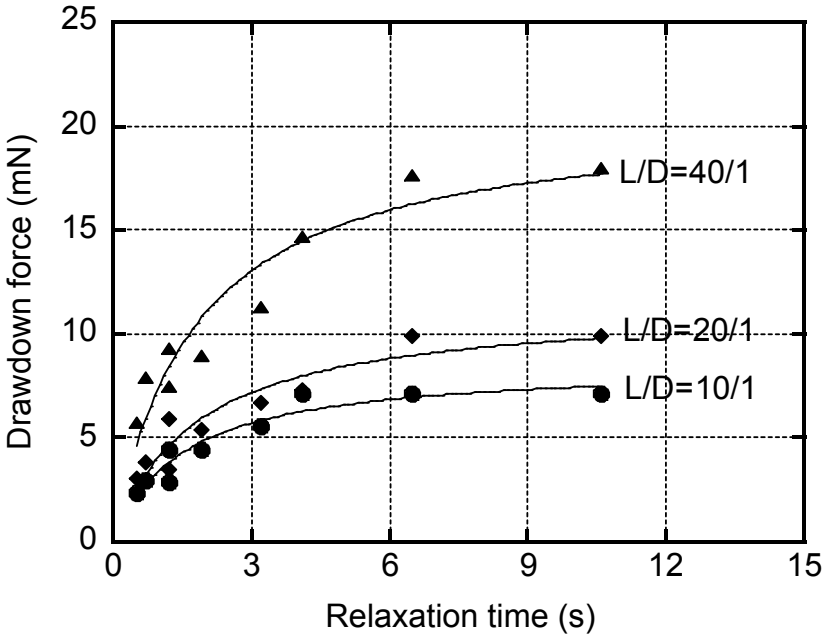

Figure 2-7 Drawdown force as a function of relaxation time for PP-H, PP-M and PP-L extruded from various dies; *L*/*D* = 10/1 (circles), 20/1 (diamonds) and 40/1 (triangles). The extrusion temperature at the die was controlled at 190, 210 and 230 °C. The drawdown force was measured at 15.5 s^{-1} and at a draw ratio of 20.

It has been known that the entanglement density at the die exit affects the Barus effect. For the better understanding of the drawdown force enhancement, therefore, the swell ratio is evaluated using various dies without stretching an extruded strand for PP-H (Figure 2-8).

As reported previously,[38-42] the swell ratio decreases with increasing the die length. In general, the swell ratio is mainly determined by the following two origins, *i.e.*, the primary normal stress difference and memory effect. The latter one becomes important when a short die

is used, because the density of entanglement couplings at the die exit is still higher than that in the steady-state under shear flow. In the case of a very long die, the swell ratio is determined by the normal stress difference as discussed by Tanner.[43,44] Therefore, Figure 2-8 demonstrates that the entanglement density is not in the steady-state at least for the short dies. The same phenomenon is observed for PP-M and PP-L as shown in Figure 2-9.

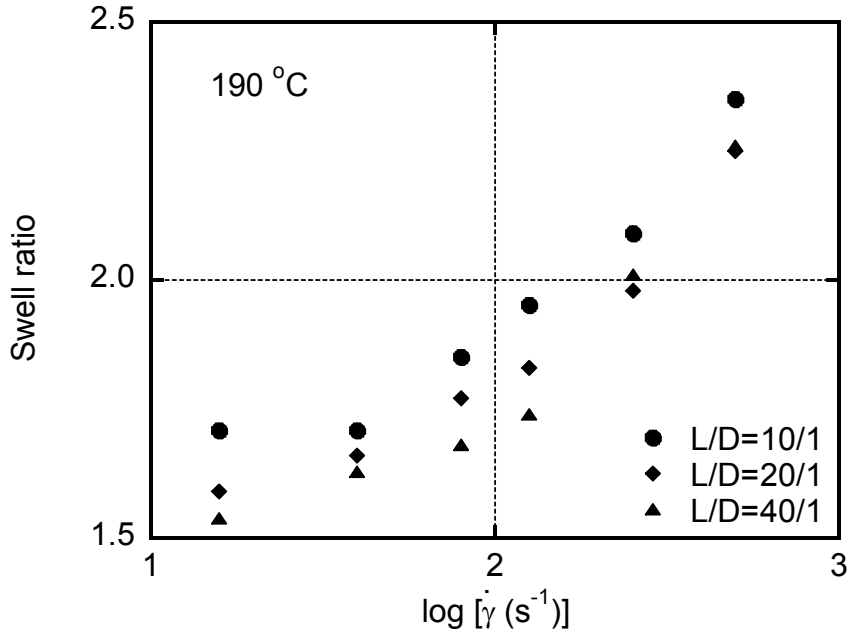

Figure 2-8 Shear rate dependence of swell ratio of PP-H using dies with *L*/*D*=10/1 (circles), 20/1 (diamonds) and 40/1 (triangles) at 190 °C.

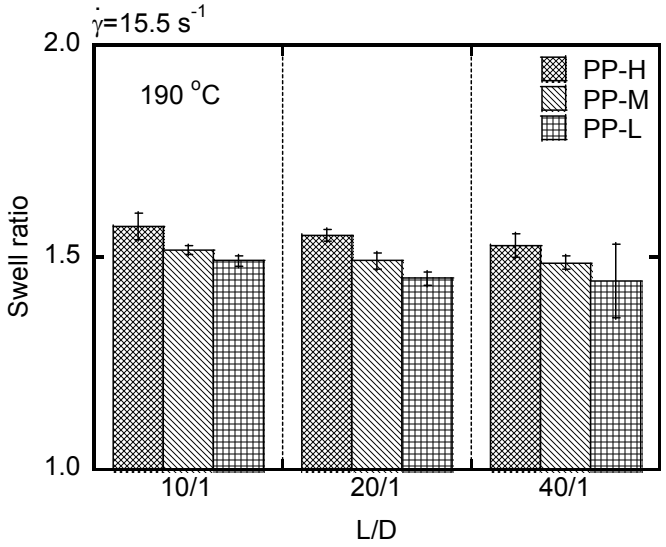

Figure 2-9 Swell ratio of PP-H, PP-M and PP-L extruded from various dies at 190 °C. The shear rate at the die wall was 15.5 s^{-1}.

The rheological response in the transient shear flow has been studied by both experimental and theoretical approaches.[45,46] According to them, shear stress shows a maximum, called overshooting, around at an applied strain of 2 for a simple polymer melt.[46] After passing the overshooting, the shear stress decreases and reaches to a plateau value, at which the entanglement density is in the steady-state. The overshooting of the shear stress is marked at a high Weissenberg number (the product of relaxation time and shear rate) condition. Moreover, a large shear strain, *i.e.*, a long residence time in the capillary die, is required to be a plateau value of the shear stress at a high Weissenberg number condition.

Figure 2-10 illustrates the distribution of the applied shear strain, calculated by the product of the shear rate and the residence time in the capillary dies, as a function of the distance from the center of a die with 1 mm diameter; *i.e.*, $r = 0$ at the center and $r = 0.5$ at the die wall. Both Bagley and Weissenberg-Rabinowitch corrections are performed.

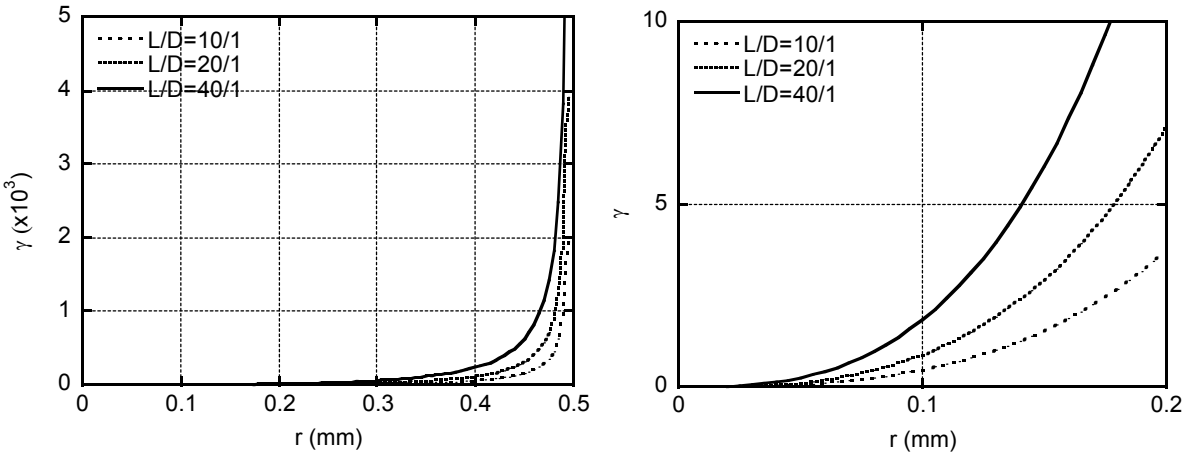

Figure 2-10 Distribution of applied shear strain at the die exit. The results were calculated considering both Bagley and Weissenberg-Rabinowitch corrections. The right figure shows applied shear strain near the center of the die.

It is clearly seen in the figure that the entanglement density at the die exit (at least $r < 0.1$ mm) is not in the steady-state even for the long die. This should be prominent for a melt with long relaxation time because of the high Weissenberg number. The difference in the entanglement density presumably affects the crystallization rate. In fact, the pronounced

crystallization rate due to few entanglement couplings was observed at fiber spinning for nascent powders of PE, poly(tetrafluoroethylene) and poly(acrylonitrile).[47-50] Rapid crystallization from an ordered melt having few entanglement couplings was also detected for PP, recently.[51] As similar to these phenomena, the drawdown force enhancement for a long die is attributed to the rapid crystallization due to few entanglement couplings. Because of the prompt solidification of an extruded strand, the deformation, *i.e.*, stretching, occurs in a restricted area near the die exit. This situation leads to the enhanced strain rate in the molten region of a strand, and results in the high elongational viscosity/stress. In contrast, the extrusion temperature affects the drawdown force slightly as shown in Figure 2-6. The result indicates that the relaxation time has stronger impact on the drawdown force. The insensitivity to the extrusion temperature would be attributed to the rapid cooling process of a thin strand in this study. In the case of a die with a large diameter, on the contrary, extrusion temperature should have a strong impact on the drawdown force. Since the cooling rate, and thus the crystallization rate, decreases for a thick strand owing to the low thermal conductivity of a polymer, the temperature at the die exit becomes important to decide the solidification time.

The prompt solidification will provide the high level of molecular orientation of the extruded strands, because the rapid crystallization prohibits the orientation relaxation. Based on this concept, the molecular orientation of the stretched strand is examined by wide-angle XRD measurements. Figure 2-11(a) exemplifies the 2D-diffraction pattern for the stretched strand of PP-H, which was extruded from the die with L/D=40/1 at 190 °C. Similar profiles are obtained for all samples. The diffraction patterns are ascribed to monoclinic α-form crystals.

Furthermore, as indicated by the strong peaks in the equator for (110), (040) and (130) planes, the chain axis orients to the flow direction. The degree of orientation is quantitatively compared by the azimuthal intensity distribution of (040) plane (Figure 2-11(b)). Moreover, Hermans' orientation function *f*, defined by equation (2-5), is calculated using the Wilchinsky's method (equation (2-6)).[52,53] Besides, the degree of crystallinity X_c is also calculated from equation (2-7).

$$f = \frac{3\left\langle \cos^2 \phi \right\rangle - 1}{2} \tag{2-5}$$

$$\left\langle \cos^2 \phi \right\rangle = 1 - 1.090\left\langle \cos^2 \phi_{110} \right\rangle - 0.901\left\langle \cos^2 \phi_{040} \right\rangle \tag{2-6}$$

$$X_c = \frac{\sum A_{cryst}}{\sum A_{cryst} + \sum A_{amorp}} \tag{2-7}$$

where ϕ is the angle that a segment makes with the stretching direction, and A_{cryst} and A_{amorp} are the peak areas of crystalline and amorphous parts, respectively.

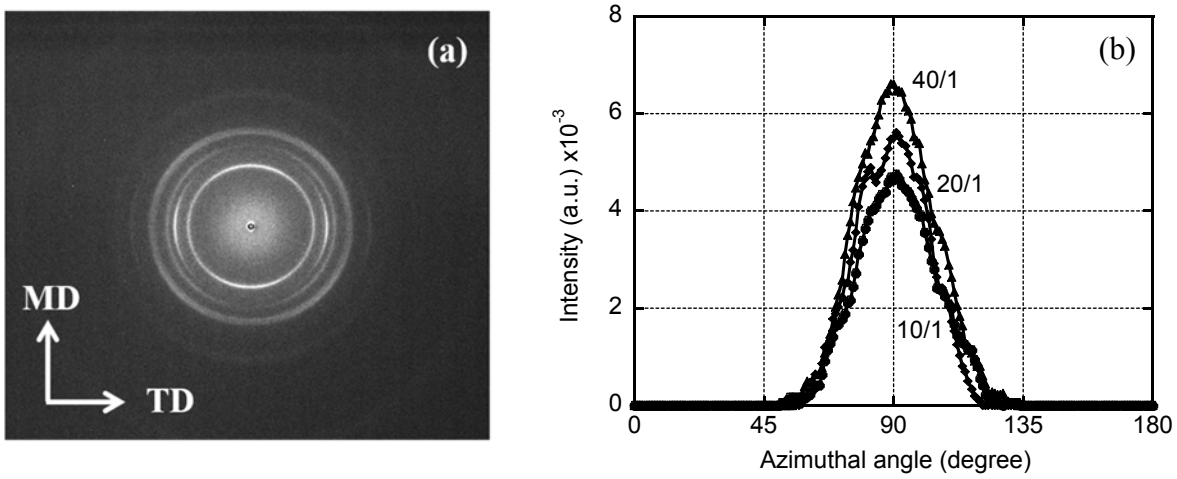

Figure 2-11 (a) 2D-WAXD pattern for the strand of PP-H extruded from the die (*L*/*D*=40/1), and (b) azimuthal intensity distribution of (040) plane for the strands of PP-H extruded from various dies; *L*/*D* = 10/1 (circles), 20/1 (diamonds) and 40/1 (triangles). The draw ratio was 9, and the die was controlled at 190 °C.

As shown in Table 2-3, both orientation function and the degree of crystallinity increase with increasing the die length, indicating that crystallization occurs rapidly and hence prohibits the orientation relaxation in a strand extruded from a long die. The results support the mechanism of the drawdown force enhancement for a long die.

Table 2-3 Hermans' orientation function and degree of crystallinity of PP-H extruded from various dies at 190 °C

L/D	Hermans' orientation function (*f*)	Crystallinity (%)
10/1	0.01	45
20/1	0.04	47
40/1	0.05	52

2.3.2 Effect of nucleating agent on the drawdown force

In order to confirm the effect of crystallization rate on the drawdown force, a sample containing the nucleating agent, 1,3:2,4-bis-O-(4-methylbenzylidene)-D-sorbitol, is prepared using PP-H. The details of the nucleating agent[34] and its effect on the rheological properties[54,55] were explained elsewhere. Due to a large number of crystalline nuclei, it can shorten the induction time at the crystallization process. As seen in Figure 2-12, the drawdown force increases greatly by the addition of the nucleating agent. The result also supports the mechanism of the drawdown force enhancement for a long die.

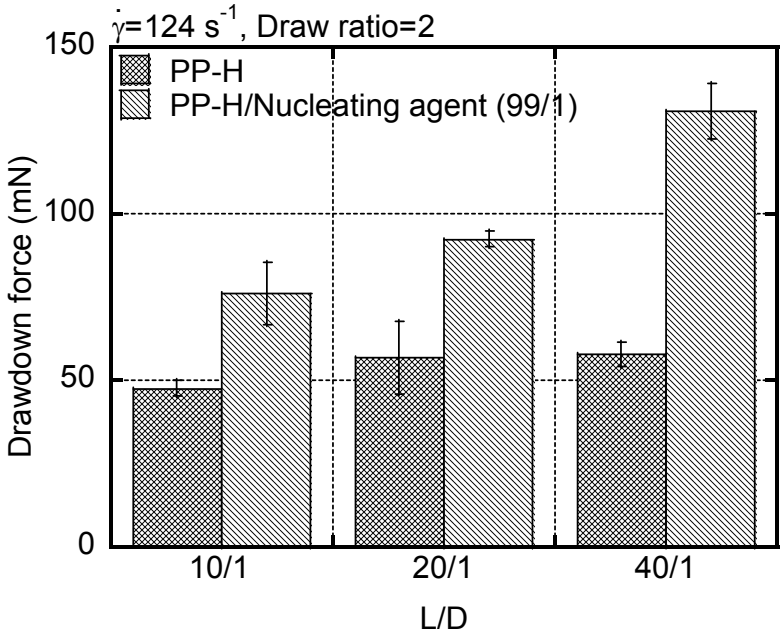

Figure 2-12 Drawdown force evaluated by various dies with different lengths for PP-H and its blend with 1% of the nucleating agent. The shear rate was 124 s^{-1} and the draw ratio was 2.

2.3.3 Effect of short-chain branches in polyethylene on crystallization

It was found from the experimental results using PP that the drawdown force increases with the length of a die, which is pronounced for a melt with long relaxation time. Therefore, the drawdown force is sensitive to the die length at low temperature for a high molecular weight material. Furthermore, a stretched strand with a large drawdown force is found to have high level of molecular orientation. These results suggest that the melt passing through a long die has low density of entanglement couplings and thus shows rapid crystallization. As mentioned,

crystallization process for PE is strongly affected by the short-chain branches. Consequently, the crystallization behavior should also affect the drawdown force of PE.

Figure 2-13 shows the oscillatory shear moduli for the materials used in this study. As seen in the figure, the order in loss modulus corresponds with MFR. In the case of HDPE-1, the storage moduli in the low frequency region are relatively high, suggesting that it has broad molecular weight distribution. Furthermore, the storage moduli in the low frequency region for LLDPE-2 is slightly higher than those for LLDPE-1. This is also attributed to the difference in the molecular weight distribution. Since LLDPE-1 is produced by a metallocene catalyst, it has narrow molecular weight distribution.

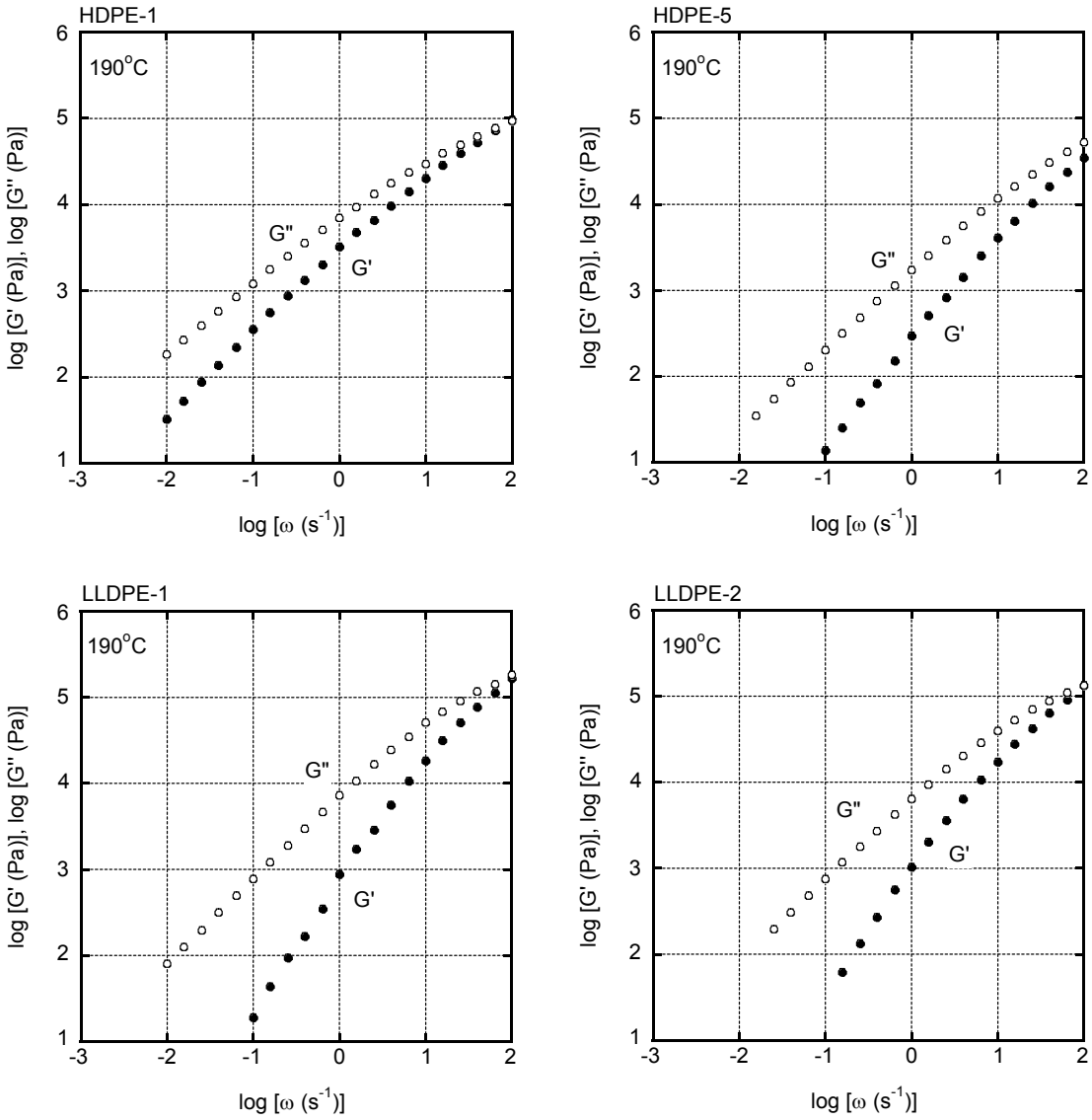

Figure 2-13 Angular frequency dependence of oscillatory shear moduli such as storage modulus *G'* and loss modulus *G"* for HDPE-1, HDPE-5, LLDPE-1 and LLDPE-2 at 190 °C.

The drawdown forces evaluated using various dies with different length are shown in Figure 2-14. As seen in the values of LLDPE samples, the molecular weight distribution does not affect the drawdown force significantly. Furthermore, it should be noted that the drawdown force increases with increasing the die length for HDPE, which is a similar phenomenon of PP. The applied flow history in a long die reduces the density of entanglement couplings due to chain orientation and then leads to rapid crystallization. In the case of LLDPE, in contrast, the drawdown force values are not sensitive to the die length. This is attributed to the low T_c of LLDPE as summarized in Table 2-1. In other words, the temperature difference between circumstance and the sample is pronounced for LLDPE. This is the same situation of the high extrusion temperature, at which the drawdown force is less sensitive to the die length as demonstrated using PP. Consequently, the drawdown force of HDPE-5 is almost the same as those of LLDPE samples when using the long die. Moreover, the results demonstrate that a great attention have to be paid to compare the drawdown force of PE samples having different crystallization temperatures.

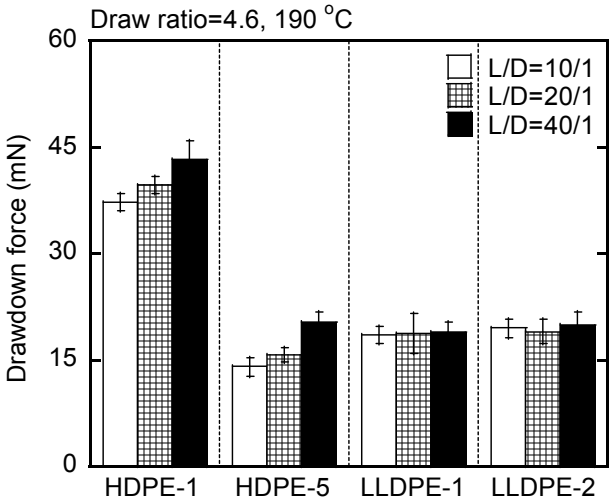

Figure 2-14 Drawdown force evaluated using various dies at 21.4 s^{-1} and at a draw ratio of 4.6 for HDPE-1, HDPE-5, LLDPE-1 and LLDPE-2. The extrusion was carried out at 190 °C.

The reduction of entanglement couplings in a long die also affects the extrudate swell as mentioned. As shown in Figure 2-15, the swell ratio decreases with increasing the die length for HDPE-1 and LLDPE-1 with an intense fashion of HDPE-1. The result demonstrates that the swell ratio of a melt with long relaxation time is sensitive to the die length. Furthermore, it is barely affected by the crystallization temperature of the sample. This is reasonable because the enlargement of strand diameter, *i.e.*, extrudate swell, occurs immediately after the die exit, *i.e.*, prior to the crystallization.

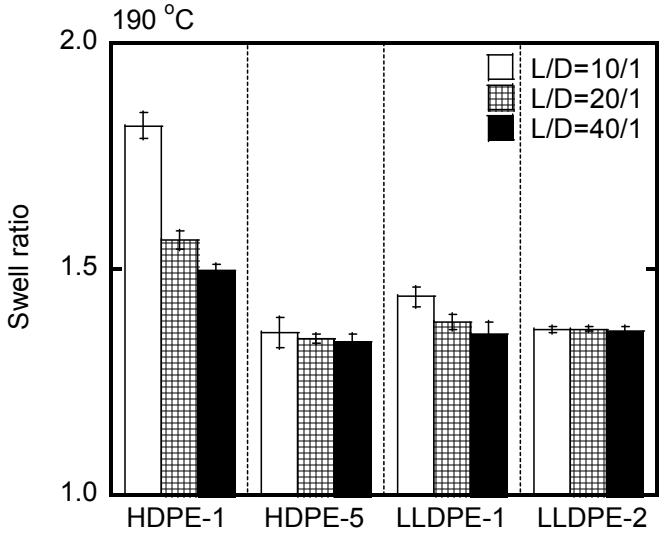

Figure 2-15 Swell ratio of HDPE-1, HDPE-5, LLDPE-1 and LLDPE-2 evaluated using various dies at 190 °C. The apparent shear rate at die wall is 21.4 s^{-1}.

As mentioned, the drawdown force is often measured to predict the elongational viscosity. Besides, the current study reveals that the drawdown force contains the information on crystallization process, which is affected by the flow history in a die for a polymer with high crystallization temperature. The latter information is, of course, also important to predict the processability at various processing operations, such as stability of a tubular-blown film, neck-in at T-die extrusion, and expansion ratio at foaming. Considering the role of crystallization on the drawdown force, we performed further experiments on the drawdown force measurements using LLDPE blends containing 1 wt% of HDPE-5. As shown in Figure 2-16, the drawdown force values of both LLDPE samples become sensitive to the die length by the HDPE addition, *i.e.*, increase with increasing the die length, which is significantly different from the trend of

the neat LLDPE. This behavior is attributed to the nucleating effect of HDPE for LLDPE. As a result, the reduction of entanglement couplings applied in a long die, *i.e.*, chain orientation, cannot be relaxed before crystallization.

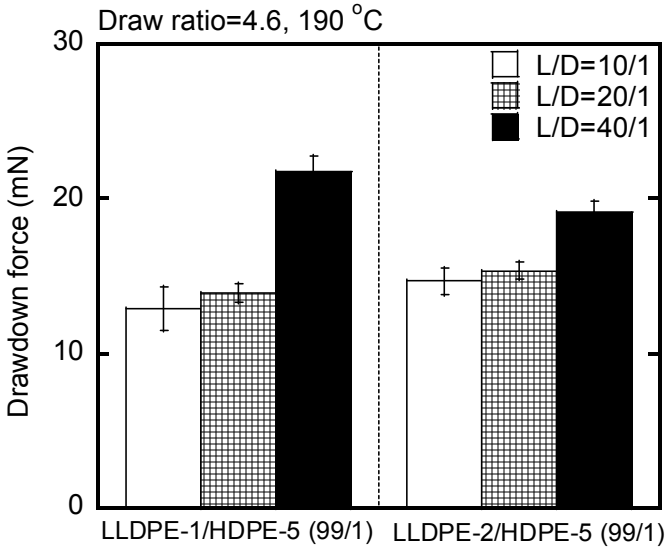

Figure 2-16 Drawdown force of the blends evaluated using various dies at a draw ratio of 4.6; (left) LLDPE-1/HDPE-5 (99/1) and (right) LLDPE-2/HDPE-5 (99/1). The extrusion was carried out at 190 °C. The data should be compared with those in Figure 2-14.

2.4 Conclusion

The effect of the measurement conditions on the drawdown force is studied using various dies with different lengths and diameters. Three types of PP (PP) having different molecular weights and four types of PE (PE) having different short-chain branches are

employed to investigate the effect of die geometry on the drawdown force. It is found that the drawdown force measured by a long die is greatly larger than that by a short die in a wide range of the draw ratio and shear rate at the die exit. The effect of the die length is pronounced for a melt with long relaxation time and for a die with small diameter. The drawdown force enhancement is attributed to the prompt solidification. The decrease in the entanglement couplings after passing through a long die is responsible for the rapid crystallization. This is confirmed by the marked molecular orientation of the stretched strand extruded from a long die. Since the melt with a high Weissenberg number shows marked overshooting of shear stress at the start-up flow, it takes a long time to be in the steady-state from the viewpoints of the entanglement density. Consequently, the effect of the die length is pronounced for a melt with long relaxation time. This phenomenon is also detected for HDPE. Furthermore, the addition of a nucleating agent also enhances the drawdown force of PP owing to the rapid crystallization. In the case of LLDPE, however, the die length barely affects the drawdown force, because the orientation applied in a long die will be relaxed prior to the crystallization. After blending with a small amount of HDPE, the drawdown force of LLDPE increases with increasing the die length. This is attributed to the nucleating effect of HDPE.

The experimental results obtained in this study demonstrate that the drawdown force includes the information on not only elongational viscosity but also crystallization behavior. In addition, the die length affects the extrudate swell especially for a polymer with long relaxation time regardless of the crystallization temperature. These results will provide the information on the die design to enhance the processability.

References

(1) Meissner, J.; Raible, T.; Stephenson, S. E. *J. Rheol.* **1981**, *25*, 1.

(2) Yamaguchi, M.; Takahashi, M. *Polymer* **2001**, *42*, 8663.

(3) Koyama, K. *Nihon Reoroji Gakkaishi* **2006**, *34*, 267.

(4) Axtell, F. H.; Haworth, B. *Polym. Test.* **1990**, *9*, 53.

(5) Takahashi, T.; Takagi, Y.; Minagawa, K.; Iwakura, K.; Koyama, K. *Polymer* **1994**, *35*, 4472.

(6) Okamoto, M.; Kojima, A.; Kotaka, T. *Polymer* **1998**, *39*, 2149.

(7) Zatloukal, M. *J. Non-Newtonian Fluid Mech.* **2003**, *113*, 209.

(8) Wagner, M.; Kheirandish, S.; Yamaguchi, M. *Rheol. Acta* **2004**, *44*, 198.

(9) Yamaguchi, M.; Wagner, M. H. *Polymer* **2006**, *47*, 3629.

(10) Yokohara, T.; Nobukawa, S.; Yamaguchi, M. *J. Rheol.* **2011**, *55*, 1205.

(11) Sitticharoen, W.; Harnnarongchai, W.; Intawong, N.; Sombatsompop, N. *J. Appl. Polym. Sci.* **2012**, *124*, 3751.

(12) Thévenon, A.; Fulchiron, R. *Polym. Test.* **2013**, *32*, 691.

(13) Cogswell, F. N. *Polym. Eng. Sci.* **1972**, *12*, 64.

(14) Binding, D. M. *J. Non-Newtonian Fluid Mech.* **1988**, *27*, 173.

(15) Feigl, K.; Tanner, F. X.; Edwards, B. J.; Collier, J. R. *J. Non-Newtonian Fluid Mech.* **2003**, *115*, 191.

(16) Meissner, J. *Rheol. Acta* **1971**, *10*, 230.

(17) Ishizuka, O.; Koyama, K. *Polymer* **1980**, *21*, 164.

(18) Münstedt, H.; Laun, H. M. *Rheol. Acta* **1981**, *20*, 211.

(19) Muller, R.; Froelich, D. *Polymer* **1985**, *26*, 1477.

(20) Meissner, J.; Hostettler, J. *Rheol. Acta* **1994**, *33*, 1.

(21) Muke, S.; Ivanov, I.; Kao, N.; Bhattacharya, S. N. *J. Non-Newtonian Fluid Mech.* **2001**, *101*, 77.

(22) Schulze, J. S.; Lodge, T. P.; Macosko, C. W.; Hepperle, J.; Münstedt, H.; Bastian, H.; Ferri, D.; Groves, D. J.; Kim, Y. H.; Lyon, M.; Schweizer, T.; Virkler, T.; Wassner, E.; Zoetelief, W. *Rheol. Acta* **2001**, *40*, 457.

(23) Wagner, M. H.; Bastian, H.; Bernnat, A.; Kurzbeck, S.; Chai, C. *Rheol. Acta* **2002**, *41*, 316.

(24) Sentmanat, M. *Rheol. Acta* **2004**, *43*, 657.

(25) Wagner, M. H.; Rolón-Garrido, V. H. *Ibreo-American J. Rheology* **2013**, *1*, 19.

(26) Bernnat, A., Institut für Kunststofftechnologie Universität Stuttgart, **2001**.

(27) Yamaguchi, M.; Suzuki, K.-I. *J. Appl. Polym. Sci.* **2002**, *86*, 79.

(28) Mieda, N.; Yamaguchi, M. *J. Non-Newtonian Fluid Mech.* **2011**, *166*, 231.

(29) Gelfer, Y.; Winter, H. H. *Macromolecules* **1999**, *32*, 8974.

(30) Münstedt, H.; Kurzbeck, S.; Egersdörfer, L. *Rheol. Acta* **1998**, *37*, 21.

(31) Sugimoto, M.; Masubuchi, Y.; Takimoto, J.; Koyama, K. *Macromolecules* **2001**, *34*, 6056.

(32) Ajji, A.; Sammut, P.; Huneault, M. A. *J. Appl. Polym. Sci.* **2003**, *88*, 3070.

(33) Kim, J.; Kim, D. H.; Son, Y. *Polymer* **2009**, *50*, 4998.

(34) Tenma, M.; Yamaguchi, M. *Polym. Eng. Sci.* **2007**, *47*, 1441.

(35) Yamaguchi, M.; Miyata, H. *Macromolecules* **1999**, *32*, 5911.

(36) Md Ali, M. A. B.; Okamoto, K.; Yamaguchi, M.; Kasai, T.; Koshirai, A. *J. Polym. Sci. Polym. Phys.* **2009**, *47*, 2008.

(37) Lau, H. C.; Bhattacharya, S. N.; Field, G. J. *Polym. Eng. Sci.* **1998**, *38*, 1915.

(38) Vlachopoulos, J. *Rheol. Acta* **1974**, *13*, 223.

(39) Liang, J. -Z. *Polym. Test.* **2000**, *20*, 29.

(40) Liang, J. -Z. *Polym. Test.* **2002**, *21*, 927.

(41) Liang, J. -Z. *Polym. Test.* **2008**, *27*, 936.

(42) Liang, J. -Z.; Yang, J.; Tang, C. -Y. *Polym. Test.* **2010**, *29*, 624.

(43) Tanner, R. I. *J. Polym. Sci. Polym. Phys.* **1970**, *8*, 2067.

(44) Sun, J.; Phan-Thien, N.; Tanner, R. *Rheol. Acta* **1996**, *35*, 1.

(45) Yamaguchi, M. In *Polymeric Foams*; CRC Press: New York, **2004**.

(46) Doi, M., Edwards, S .F. *The Theory of Polymer Dynamics*; Oxford University Press: New York, **2007**.

(47) Kanamoto, T.; Ohama, T.; Tanaka, K.; Takeda, M.; Porter, R. S. *Polymer* **1987**, *28*, 1517.

(48) Sano, A.; Iwanami, Y.; Matsuura, K.; Yokoyama, S.; Kanamoto, T. *Polymer* **2001**, *42*, 5859.

(49) Sawai, D.; Miyamoto, M.; Kanamoto, T.; Ito, M. *J. Polym. Sci. Polym. Phys.* **2000**, *38*, 2571.

(50) Sawai, D.; Watanabe, D.; Morooka, N.; Kuroki, H.; Kanamoto, T. *J. Polym. Sci. Polym. Phys.* **2006**, *44*, 3369.

(51) Phulkerd, P.; Arayachukeat, S.; Huang, T.; Inoue, T.; Nobukawa, S.; Yamaguchi, M. *J. Macromol. Sci. Part B Polym. Phys.* **2014**, *53*, 1222.

(52) Wilchinsky, Z. W. *J. Appl. Phys.* **1960**, *31*, 1969.

(53) Bao, R.; Ding, Z.; Zhong, G.; Yang, W.; Xie, B.; Yang, M. *Colloid Polym. Sci.* **2012**, *290*, 261.

(54) Tenma, M.; Mieda, N.; Takamatsu, S.; Yamaguchi, M. *J. Polym. Sci. Polym. Phys.* **2008**, *46*, 41.

(55) Uematsu, H.; Aoki, Y.; Sugimoto, M.; Taniguchi, T.; Koyama, K. *Rheol. Acta* **2008**, *47*, 237.

Chapter 3

Enhancement of Drawdown Force for Polypropylene by Blending Acrylate Polymers

3.1 Introduction

Polypropylene (PP), classified as one type of polyolefins, occupies the large demand for commodity plastics in the market due to its versatile properties such as good mechanical properties, high heat distortion temperature and good cost performance. However, processing methods are limited because of its low melt elasticity.[1-4] Recently, numerous studies have been carried out in order to improve the processability of PP at some processing operations such as T-die extrusion, blow-molding, foaming, spinning and thermoforming, at which high melt elasticity is required. Several approaches have been proposed to enhance melt elasticity of PP for improvement of its processability.[5-8] One of the methods to enhance melt elasticity is the incorporation of long-chain branches,[7,9,10] because it can provide strain-hardening behavior in elongational viscosity. Another well-known technique is to add high molecular weight fraction. However, it is not easy to enhance the elasticity efficiently, because a very high molecular

weight fraction has to be homogeneously mixed for this purpose. In 2000, Yamaguchi and Miyata reported that melt elasticity of PP is enhanced by blending a small amount of a weak gel, such as cross-linked ethylene-1-hexene-ethylidene norbornene terpolymer (gEHDM). The strain-hardening behavior in the elongational viscosity was clearly detected for this system.[11] Md Ali et al. reported the enhancement of elastic nature of a molten PP by blending fine fibers prepared from polytetrafluoroethylene (PTFE).[12] It was found that a binary blend of PP and PTFE shows marked strain-hardening behavior as well as Barus effect. Later, it was revealed that various flexible fibers have capacity to enhance the melt elasticity.[13-15] They found that blending a small amount of fibers with high aspect ratio greatly provides the strain-hardening behavior in elongational viscosity.

Since the drawdown force has a close relation with elongational viscosity, it is one approach to examine melt elasticity of a polymer. Moreover, it has a direct relation with processability because the measurement is performed with non-isothermal condition as similar to actual processing operations.

In this study, a new method to enhance the drawdown force of PP at capillary extrusion by blending acrylate polymers, *i.e.*, poly(isobutyl methacrylate) PIBM and poly(methyl methacrylate) PMMA having low molecular weight is proposed. This method will have strong impact on the industry because it has never been reported that an immiscible polymer with low viscosity enhances the melt elasticity of PP.

3.2 Experimental

3.2.1 Materials and sample preparation

Two types of commercially available propylene homopolymer (PP) having different melt flow rate (MFR), *i.e.*, 5 and 10 g/10 min denoted as PP-H and PP-M, respectively, were employed in this study. In addition, a random copolymer of propylene and 3 wt% of ethylene (Japan Polypropylene, Japan), denoted as PP-random in this thesis, was also used. Poly(isobuthyl methacrylate) PIBM and poly(methyl methcrylate) PMMA, provided by Mitsubishi Rayon, Japan, having low molecular weight were used as additives. Characteristics of the PP samples are summarized in Table 3-1.

Table 3-1 Characteristics of materials

Samples	**M_n**	**M_w**	**MFR (g/10 min)**	**T_c (°C) (-10 °C/min)**	**Grade (Maker)**
PP-H	$4.5x10^4$	$2.6x10^5$	5	114.0	FY4 (Japan Polypropylene)
PP-M	$4.3x10^4$	$2.1x10^5$	10	115.0	K1008 (Chisso)
PP-random	-	-	10	92.7	R-730 (Prime Polymer)

PP and 5 wt% of either PIBM or PMMA were mixed together with the presence of 5,000 ppm of thermal stabilizers, such as tris(2,4-di-tert-butylphenyl)phosphate (Irgafos168, Ciba, Switzerland) and pentaerythritol tetrakis(3-(3,5-di-tert-butyl-4-hydroxyphenyl)propionate) (Irganox1010, Ciba, Switzerland), using an internal mixer (Labo-Plastmill, Toyoseiki, Japan)

with a blade rotational speed of 30 rpm at 200 °C for 3 minutes. Then, the mixed sample was compressed into a flat sheet at 230 °C for 3 minutes.

3.2.2 Measurements

A rheometer (AR2000, TA instruments, USA) equipped with cone-and-plate and parallel plates was used to evaluate the frequency dependence of oscillatory shear moduli such as storage modulus *G'* and loss modulus *G"*. The experiment was carried out using frequency sweep mode with angular frequency range from 100-0.01 rad/s at various temperatures, *i.e.*, 110, 120, 130, 140, 150, 190, 210 and 230 °C.

Drawdown force and swell ratio were measured using a capillary rheometer (140 SAS-2002, Yasuda Seiki Seisakusyo, Japan) equipped with dies having various *L/D* ratios, *i.e.*, 10/1 and 40/1. A set of rotating wheels and a tension detector were attached to the capillary rheometer in order to evaluate the drawdown force at a draw ratio of 2.4, whereas the swell ratio was obtained by measuring the diameter of an extrudate using an on-line laser beam without stretching. The applied shear rate and temperature in the die and reservoir were controlled at 124 s^{-1} and 190 °C, respectively.

A differential scanning calorimeter (DSC 820, Mettler-Toledo, USA) was used to analyze thermal properties. The sample was heated from 25 to 190 °C with the heating rate of 30 °C/min. Then, it was cooled down to 25 °C with various cooling rates, *i.e.*, 1, 10, 30, 100 and 300 °C, prior to heating up to 190 °C.

An X-ray diffractometer (R-AXIS IIc, Rigaku, Japan) was employed to investigate the degree of orientation of the samples. The strands extruded from the dies with various lengths, *i.e.*, 10 and 40 mm, at a draw ratio of 4 were irradiated using a graphite monochromatized CuKα radiation beam focused via a 0.3 mm pinhole collimator with a flat 20 × 20 cm^2 imaging plate (IP) detector of 1900 × 1900 pixels. The sample was exposed to the X-ray beam perpendicular to the strand axis in the through view direction for 7 min.

Morphology of the dispersed acrylate polymers in PP matrix was observed using a scanning electron microscope (SEM) (S400, Hitachi, Japan). The strand extruded from the die with *L/D* = 40/1 without stretching was cut along the extrusion direction (side-section) using a razor blade. Then, the sample was soaked into acetone for overnight in order to dissolve the acrylate polymer. After that, it was dried up in ambient temperature and observed by SEM. Deformation of the dispersed phase was further confirmed by the measurement of lateral expansion of a strand after dipping into a silicone oil bath at 170 °C for 10 seconds.

3.3 Results and Discussion

3.3.1 Rheological properties

Figure 3-1 shows the master curves of frequency dependence of oscillatory shear moduli such as storage modulus *G'* and loss modulus *G"* for PP-H, PP-random, PIBM and PMMA at the reference temperature of 190 °C. Zero-shear viscosities obtained from the terminal zone of

the master curves shown in Table 1. It indicates that viscosities of both PIBM and PMMA are much lower than that of pure PP-H at extrusion temperatures. In addition, the shift factors obtained from the master curves at the reference temperature of 190 °C are plotted as a function of temperature as shown in Figure 3-2. The apparent activation energies, which are calculated using the shift factor in the temperature range from 190 to 230 °C, are 45, 119 and 143 kJ/mol for PP-H, PIBM and PMMA, respectively.

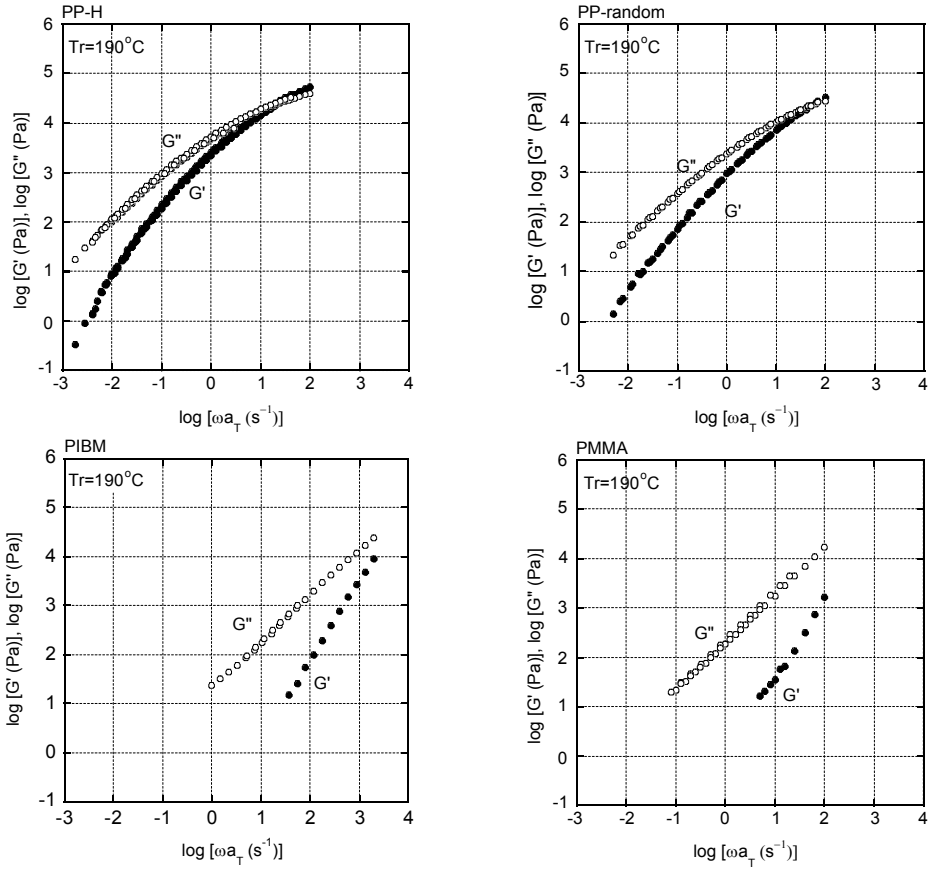

Figure 3-1 Master curves of frequency dependence of oscillatory shear moduli such as storage modulus *G'* (closed symbols) and loss modulus *G"* (open symbols) for PP-H, PP-random, PIBM and PMMA at the reference temperature of 190 °C.

Table 3-2 Zero-shear viscosity of materials

Samples	**η_0 (Pa s) at 190 °C**
PP-H	9,850
PIBM	43
PMMA	280

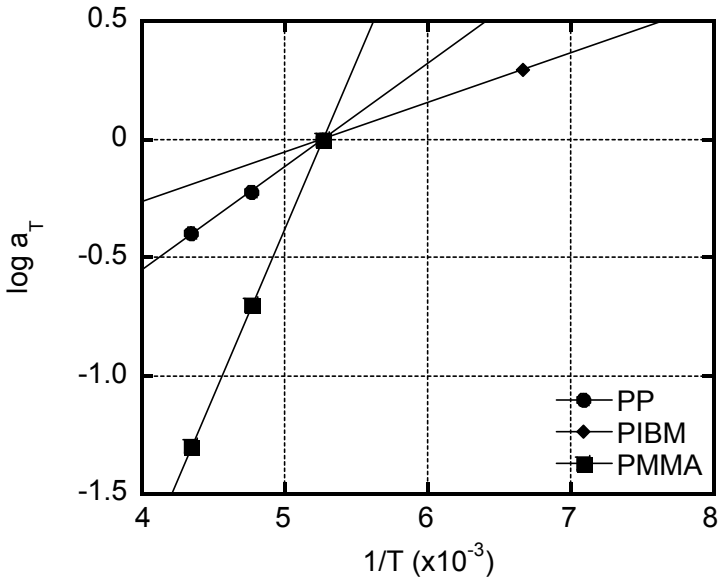

Figure 3-2 Shift factors as a function of temperature obtained from the master curves at the reference temperature of 190 °C for PP-H, PIBM and PMMA.

Master curves of frequency dependence of oscillatory shear moduli such as storage modulus *G'* and loss modulus *G"* for the blends of PP-H/PIBM (95/5) and PP-H/PMMA (95/5) are shown in Figure 3-3. As compared with the neat PP-H, viscoelastic properties of the blends are almost the same with those of the neat PP-H. In other words, blending with neither PIBM nor PMMA does affect the linear viscoelastic properties of PP-H.

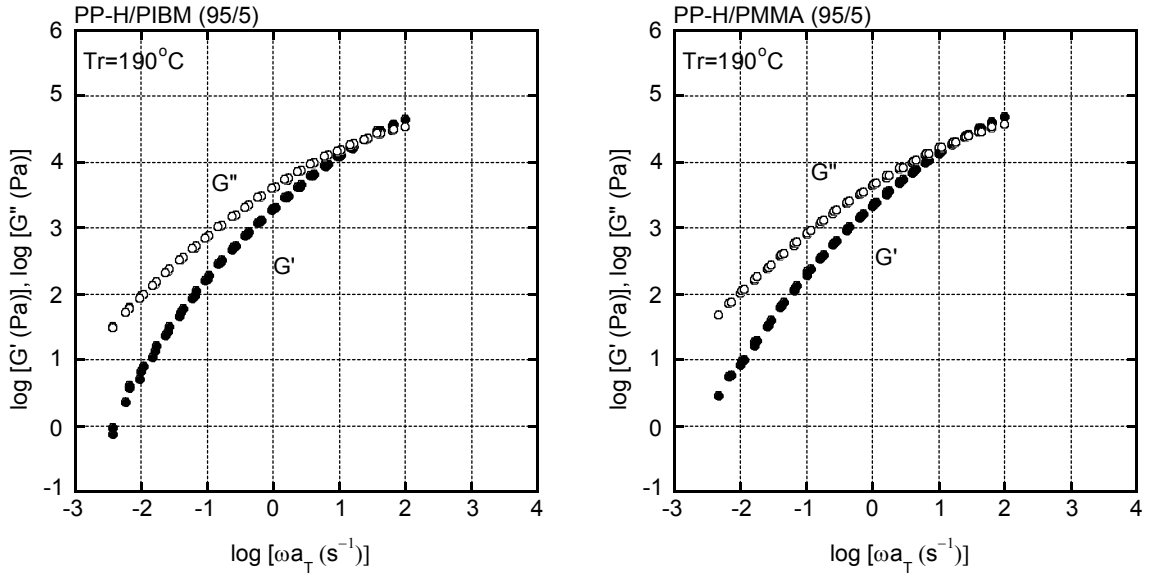

Figure 3-3 Master curves of frequency dependence of oscillatory shear moduli such as storage modulus *G'* (closed symbols) and loss modulus *G"* (open symbols) for PP-H/PIBM (95/5) and PP-H/PMMA (95/5) at the reference temperature of 190 °C.

3.3.2 Drawdown force

Drawdown force is plotted as a function of die length for PP-H, PP-H/PIBM (95/5) and PP-H/PMMA (95/5) as shown in Figure 3-4. It should be noted that the blend with an acrylate

polymer exhibits a high value of the drawdown force with an intense fashion of PIBM. This is a surprisingly result because the acrylate polymers show much lower viscosity than PP. To the best of my knowledge, ultra high molecular weight fraction is usually needed to enhance the drawdown force and this phenomenon is expected only in a miscible system.[6,9,10] In the case of an immiscible blend, the drawdown force enhancement has never been reported, especially by the addition of a low viscous polymer. Remarkably, in this study, PIBM and PMMA are found to be able to enhance the drawdown force of PP-H, even though both of them possess significantly low viscosity compared with the neat PP-H.

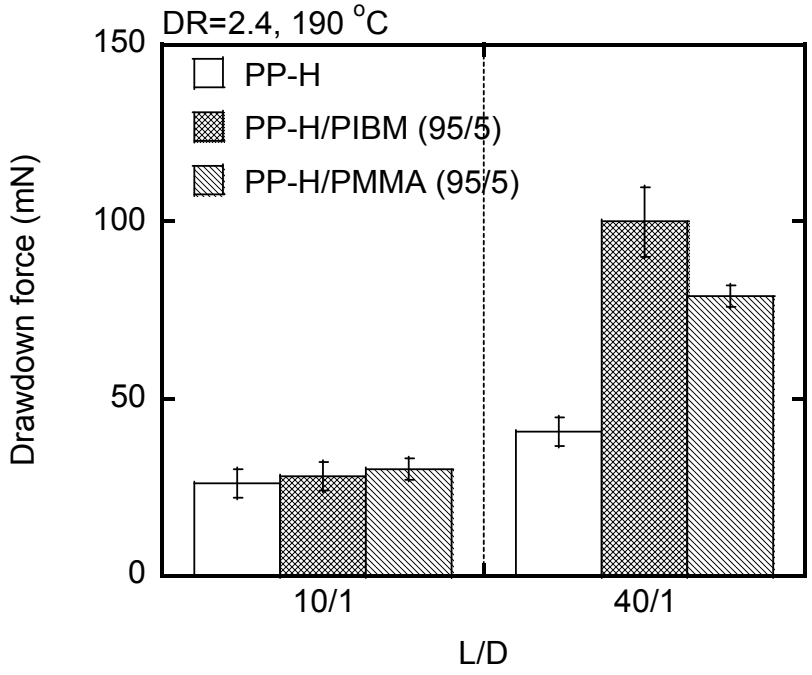

Figure 3-4 Drawdown force of PP-H, PP-H/PIBM (95/5) and PP-H/PMMA (95/5) extruded at 124 s^{-1} and stretched at a draw ratio of 2.4. The temperature was controlled at 190 °C.

The swell ratio, known as Barus effect, is shown in Figure 3-5 as a function of die length. It is well known that the swell ratio decreases with die length, because it is affected by the entanglement couplings.[16] Generally, the swell ratio for viscoelastic fluids is mainly determined by the primary normal stress difference and memory effect.[6] The elastic recovery from the deformation is responsible for high level of the swell ratio. As seen in the figure, the swell ratio of PP-H, PP-H/PIBM (95/5) and PP-H/PMMA (95/5) decreases with an increase of the die length. However, the swell ratios of the blends are almost similar to the neat PP-H.

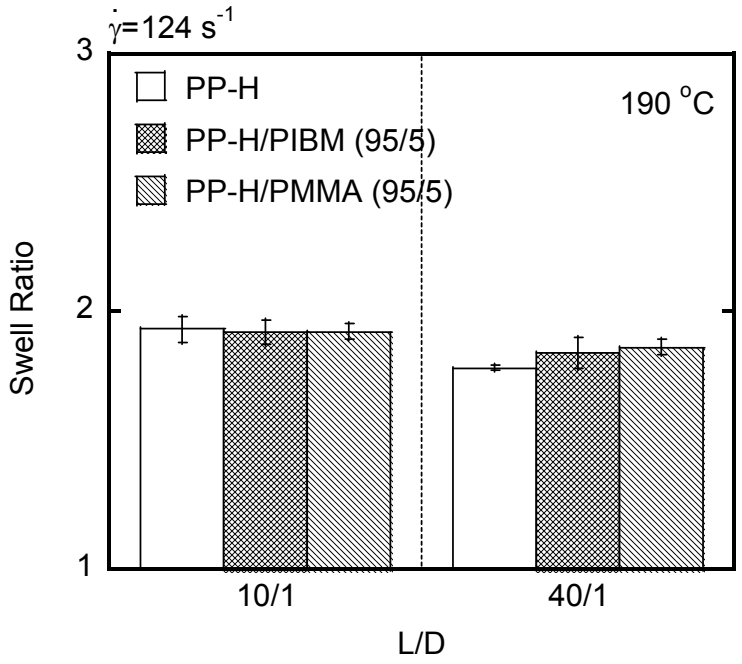

Figure 3-5 Swell ratio of PP-H, PP-H/PIBM (95/5) and PP-H/PMMA (95/5) extruded at 124 s^{-1}. The temperature was controlled at 190 °C.

Further, stretchability of PP-H and the blends with PIBM and PMMA is examined by changing the draw ratio. A maximum draw ratio at which the strand can be stretched without any rupture is defined as the maximum draw ratio. As shown in Figure 3-6, the maximum draw ratio of the blends is obviously lower than that of neat PP-H when they are extruded using a die with L/D = 40/1. In particular, PP-H/PIBM (95/5) shows significantly poor stretchability. This result indicates that the addition of PIBM reduces the stretchability due to the high level of an elongational stress. In the case of PP-H/PMMA (95/5), the stretchability is higher than that of the blend with PIBM but lower than that of the neat PP-H. This result is found to correspond with the drawdown force. Furthermore, the enhancement of the drawdown force is pronounced for a long die as discussed in the previous chapter. Because a long die provides low level of entanglement couplings, crystallization of the PP chains takes place rapidly as the melt leaves the die, resulting in high level of the drawdown force. This behavior is confirmed by 2D X-ray diffraction (2D-XRD) patterns. Since the rapid crystallization prohibits orientation relaxation, the strand extruded from a long die exhibits high degree of orientation. This phenomenon is also observed in the case of the blends.

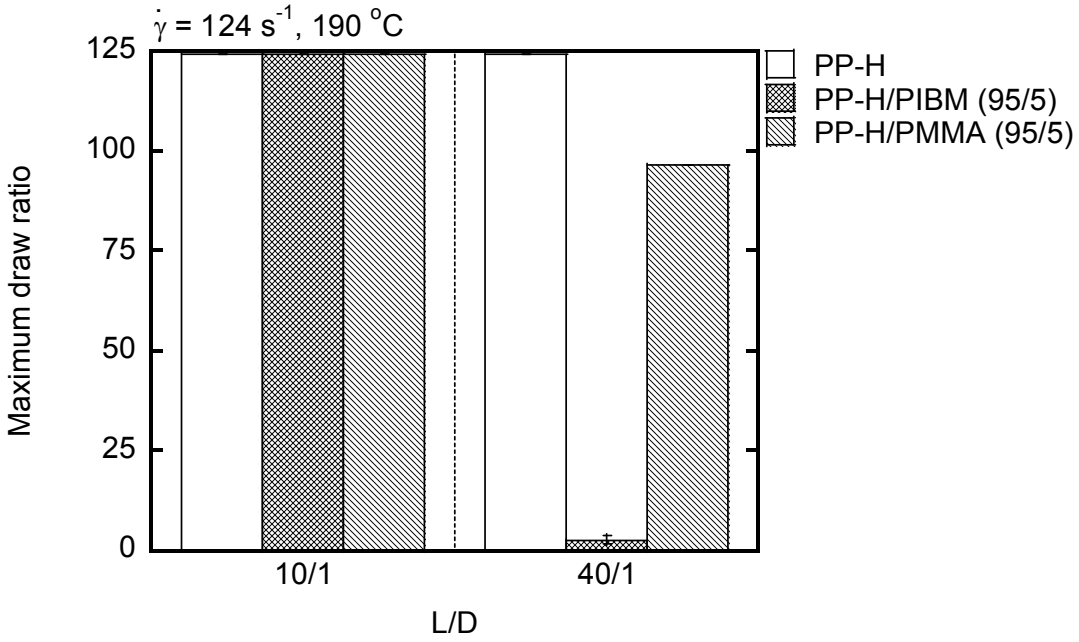

Figure 3-6 Maximum draw ratio of PP-H, PP-H/PIBM (95/5) and PP-H/PMMA (95/5) extruded at 124 s^{-1} and 190 °C. The experiment was carried out 3 times as represented with error bar.

3.3.3 Crystallization and orientation

As the enhancement of the drawdown force is observed for PP-H by blending acrylate polymers with low viscosity, further experiments are performed in order to clarify the mechanism. In the previous chapter, I mentioned that the crystallization process has a strong impact on the drawdown force at capillary extrusion. Therefore, the effect of the addition of an acrylate polymer on the PP crystallization has to be clarified to consider the mechanism.

It has been previously reported that the cooling rate has strong influence on the crystallization temperature T_c and glass transition temperatures T_g of a polymer.[17-19] Normally, both T_c and T_g decrease with the cooling rate. Figure 3-7 shows the effect of cooling rate on T_c of PP-H and T_g's of PIBM and PMMA. As seen in the figure, T_c of PP-H seems to be sensitive to the cooling rate, because it drastically decreases with the cooling rate. On the contrary, T_g's for both PIBM and PMMA are less sensitive to the cooling rate. Further, T_g of PMMA is located at a higher temperature than T_c of PP-H at a high cooling rate, *e.g.*, 300 °C/min, indicating that solidification of PMMA takes place earlier than the crystallization of PP-H. Since the actual cooling rate near the die exit at capillary extrusion is quite high, *e.g.*, > 6000 °C/min, and it has been reported that T_c of isotactic PP is around 60 °C in this range of the cooling rate,[19-21] it is, therefore, possible to consider that the solidification of the acrylate polymers occurs faster than the crystallization of PP-H at the drawdown force measurement.

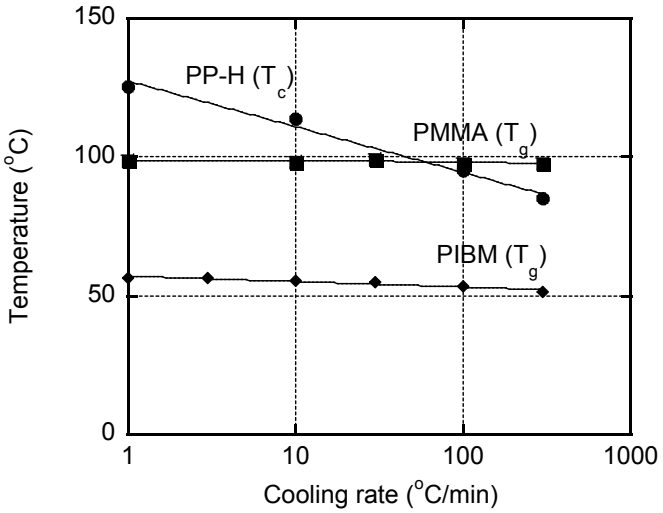

Figure 3-7 Crystallization temperature T_c for neat PP-H and glass transition temperature T_g's for PIBM and PMMA as a function of cooling rate.

Moreover, the crystallization behavior of PP-H and the blends is investigated as shown in Figure 3-8. As seen in the figure, T_c*'s* of the blends are almost the same as the neat PP at a cooling rate of 10 °C/min. This result indicates that acrylate polymers has no nucleation effect on the crystallization of PP-H under the quiescent condition, at least at this condition. However, in the case of a high cooling rate, *i.e.*, 100 °C, T_c of the blend with PMMA slightly shift to a higher temperature while this behavior cannot be detected for the blend with PIBM, indicating that PMMA shows nucleating ability slightly. This result is reasonable because T_g of PMMA is higher than that of PIBM (Figure 3-7). Considering the cooling rate, T_g*'s* of both PIBM and PMMA are located at lower temperatures than that of PP-H at a cooling rate of 10 °C/min, suggesting that the acrylate polymers are in a liquid state at this condition. Hence, they cannot exhibit the nucleation effect on the crystallization of PP-H. On the contrary, PMMA solidifies before the crystallization of PP-H at a cooling rate of 100 °C/min. As it is well known that the presence of a solid surface in contact with a polymer melt usually results in heterogeneous nucleation,[22] the rigid PMMA, solidified at the high cooling rate, can act as a nucleating agent, which shortens the induction time in the crystallization process. Therefore, a slight shift of T_c for the blend with PMMA is observed at a high cooling rate.

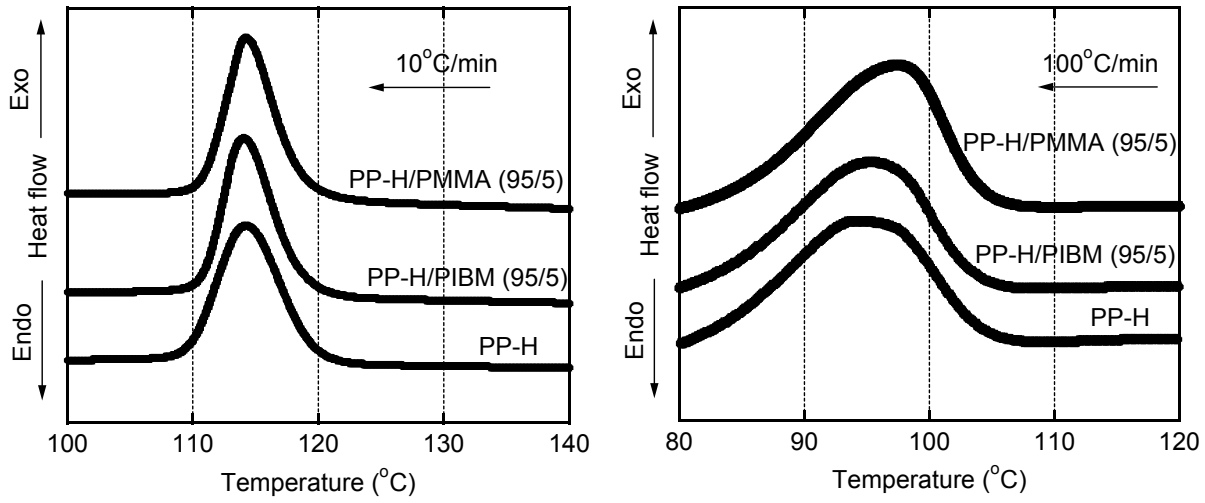

Figure 3-8 Crystallization peaks for strands of PP-H, PP-H/PIBM (95/5) and PP-H/PMMA (95/5) cooling from 190 to 25 °C with a cooling rate of 10 (left) and 100 (right) °C/min.

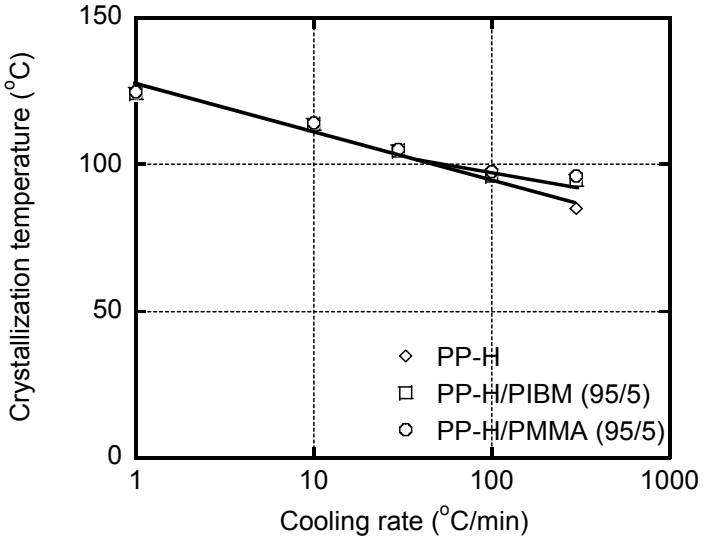

Figure 3-9 Crystallization temperature T_c for neat PP-H, PP-H/PIBM (95/5) and PP-H/PMMA (95/5) as a function of cooling rate.

Figure 3-9 shows the effect of cooling rate on T_c*'s* of the blends. As seen in the figure, T_c*'s* of both PP-H/PIBM (95/5) and PP-H/PMMA (95/5) slightly deviate from the T_c of neat PP-H at high cooling rates, ***e.g.***, ≥ 100 °C/min. Moreover, the T_c*'s* of the blends become less sensitive to the cooling rate than that of the neat PP-H. This result confirms that acrylate polymers slightly show nucleation effect on crystallization process of PP-H under quiescent condition at a high cooling rate.

Although acrylate polymers do not/little show the nucleation effect on the crystallization of PP-H at the quiescent condition, ***i.e.*** without flow field, they strongly affect the crystallization process of PP-H in the flow condition, ***i.e.***, at capillary extrusion. Since it has been known that the rapid crystallization prohibits orientation relaxation, 2D-XRD was used to determine the degree of molecular orientation for PP and the blends in order to confirm the effect of acrylate polymers. Figures 3-10 and 3-11 show 2D-diffraction patterns for the strand of PP-H and the blend with PIBM extruded from dies with various lengths and stretched at a draw ratio of 4. As seen in the result, PP chains orient to the flow direction for both neat and the blend. Moreover, azimuthal intensity distribution becomes narrow for the strand extruded from a long die, indicating that the long die provides high level of molecular orientation. Furthermore, the blend with PIBM shows the obviously high level of molecular orientation as confirmed by the narrow distribution of azimuthal intensity. This result strongly supports that the enhancement of the drawdown force for the blend is ascribed to the rapid crystallization.

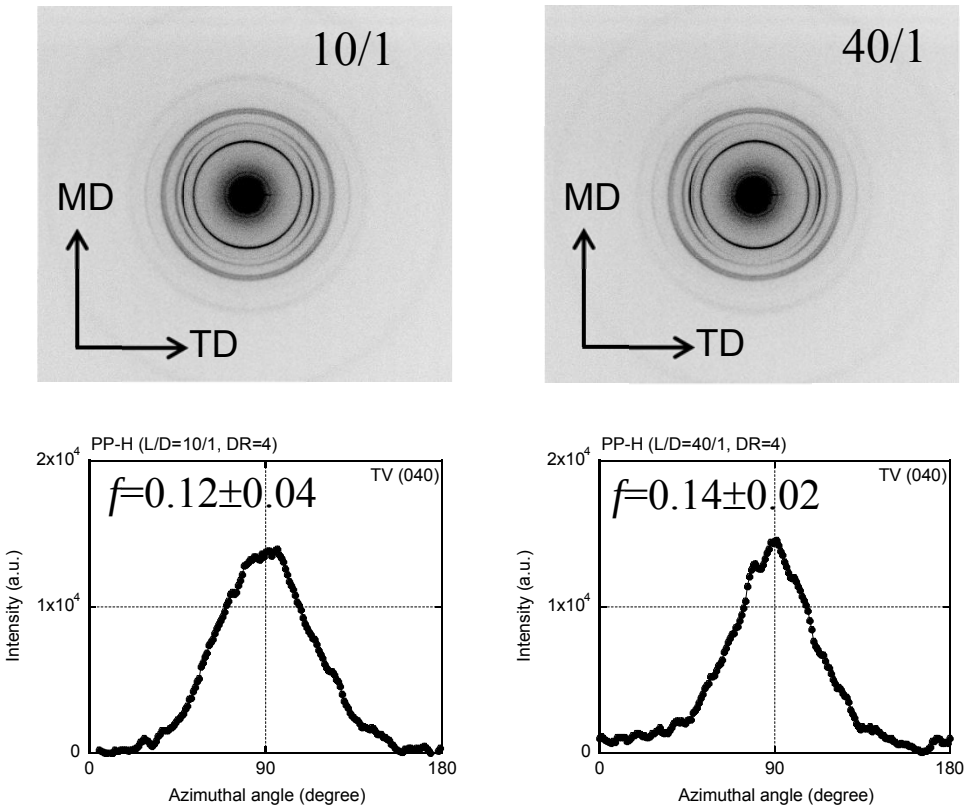

Figure 3-10 2D-diffraction patterns for the strand of PP-H extruded from the dies with 1 mm having various lengths, *i.e.*, 10 and 40 mm, at 190 °C and stretched at a draw ratio of 4. The plots below the figures represent the azimuthal intensity distribution of (040) plane obtained from each figure. In the figure, Hermans' orientation function *f* is noted with experimental error.

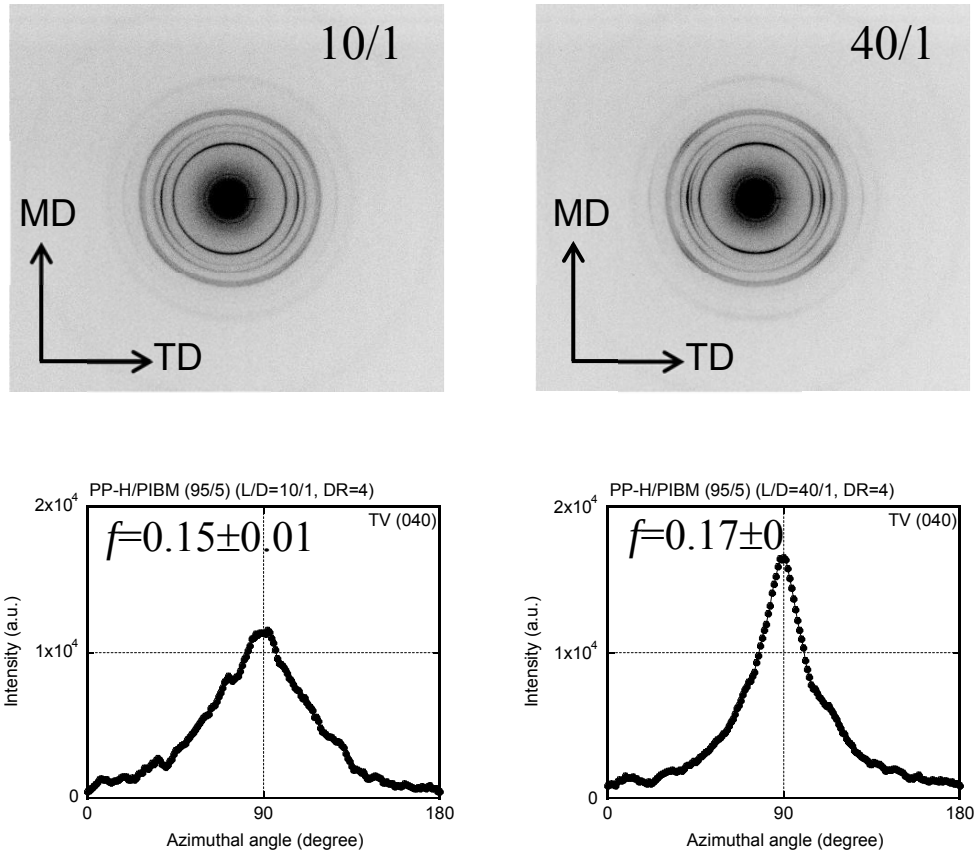

Figure 3-11 2D-diffraction patterns for the strand of PP-H extruded from the dies with 1 mm having various lengths, *i.e.*, 10 and 40 mm, at 190 °C and stretched at a draw ratio of 4. The plots below the figures represent the azimuthal intensity distribution of (040) plane obtained from each figure. In the figure, Hermans' orientation function *f* is noted with experimental error.

3.3.4 Morphology of dispersed phase

Since PIBM and PMMA possess low viscosity at the extrusion condition, they exist in the PP matrix as dispersed liquid droplets during the flow. Therefore, the deformation of droplets in a matrix has to be considered to understand the unique rheological behavior. In general, the size of droplets is determined by the interfacial tension as well as the mixing performance including the stress, type of flow, and the distributive performance. When the viscosity of droplets is much lower than that of the matrix, droplets deform into fibrous shape by the hydrodynamic force.[23,24] Therefore, droplets of the acrylate polymers presumably deform during the flow in the flow direction. The deformation must give rod-like or ellipsoidal shape of the dispersion in the PP matrix. To confirm it, the deformation of the dispersed phase is observed by SEM.

As shown in Figure 3-12, both PIBM and PMMA deform in the flow direction. Furthermore, the droplet size of PIBM seems to be smaller than that of PMMA. This is presumably attributed to the lower interfacial tension with PP for PIBM. Therefore, the deformed PIBM has higher aspect ratio, whereas PMMA droplets deform into ellipsoidal shape. This morphology must be determined in a die or immediately after passing through a die. Then, the deformed droplets will behave like rigid fibers because of the glassification as discussed previously.

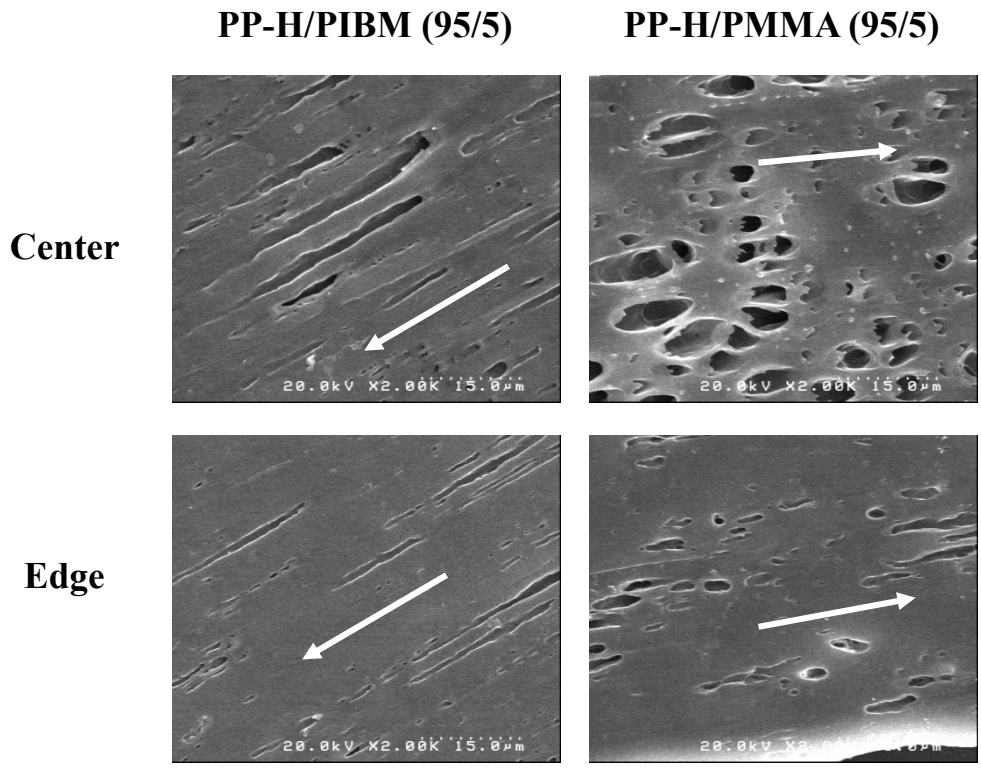

Figure 3-12 Morphology of the dispersed phase for the strand of PP-H/PIBM-L (95/5) and PP-H/PMMA-L (95/5) extruded from a die with L/D = 40/1 without stretching. The arrows in the images represent the flow direction.

Although PMMA possesses higher T_g than PIBM, the drawdown force enhancement for PMMA is low as compared with PIBM. This would be attributed to the size of droplets. The elongational stress in a suspension with rigid fibers was discussed by the theoretical and experimental approaches. Among them, the slender-body theory was successfully developed to predict the elongational stress considering the excess deformation of a matrix between

fibers,[25,26] which was well summarized by Laun[27] as shown in Figure 3-13. According to the slender-body theory, the elongational viscosity η_E of a continuous phase with long slender particles depends on aspect ratio as well as volume fraction of the particles as the following equation,

$$\eta_E = 3\eta_c + \frac{4}{3}\eta_c \frac{\phi_d \left(\frac{l}{d}\right)^2}{ln\left(\frac{\pi}{\phi_d}\right)} \tag{3-1}$$

where η_E is the elongational viscosity of a suspension, η_c is the shear viscosity of a continuous phase, ϕ_d is the volume fraction of dispersion and l/d is the length-to-diameter ratio of fibers.

Following this theory, the excess stress generated by large shear deformation between the neighboring fibers is responsible for the enhancement of the elongational viscosity of a suspension. Since the distance between the fibers is determined by the number of fibers, the fine dispersion provides high elongational viscosity on average.

Therefore, the blend with PIBM, which has small and thin fibers with high aspect ratio, should possess high elongational viscosity as compared with the blend with PMMA, because PMMA dispersion has lower aspect ratio. As well known that the drawdown force has a close relation with elongational viscosity at elongation flow, this explanation, therefore, has an agreement with the drawdown force result, in which PIBM exhibits a great ability for the drawdown force enhancement compared with PMMA.

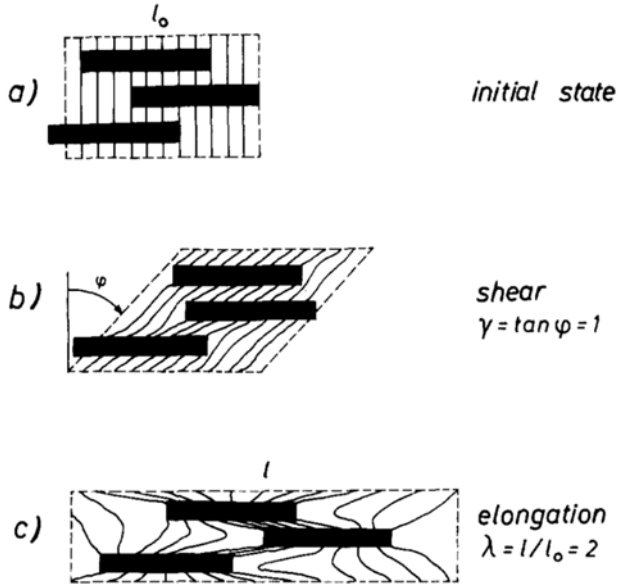

Figure 3-13 Schematic illustration of deformation of polymer matrix caused by rigid fibers in simple shear and uniaxial elongational flow.[27]

3.3.5 Effect of molecular structure of polypropylene

The proposed mechanism is further confirmed using PP-random, which has a lower crystallization temperature than PP homopolymer having the same MFR. As seen in Figure 3-14, the enhancement of the drawdown force by blending both PIBM and PMMA is not so obvious when using PP-M. On the contrary, this phenomenon is obviously detected when using PP-random having the same MFR. This is because PP-M has higher T_c than PP-random. Therefore, the crystallization of PP-M after the die exit must take place faster than that of PP-random. As a result, the PP-M matrix cannot deform greatly with the rigid fibers/particles as compared with that of PP-random, resulting in low enhancement of the drawdown force. This

result strongly confirms that the mechanism of the drawdown force enhancement is due to the prompt solidification of the acrylate polymer, which occurs prior to the crystallization of PP. Therefore, it can act as rigid fibers/particles, resulting in an increase of the elongational stress generated by large shear deformation for the PP matrix and thus, enhancement of the drawdown force.

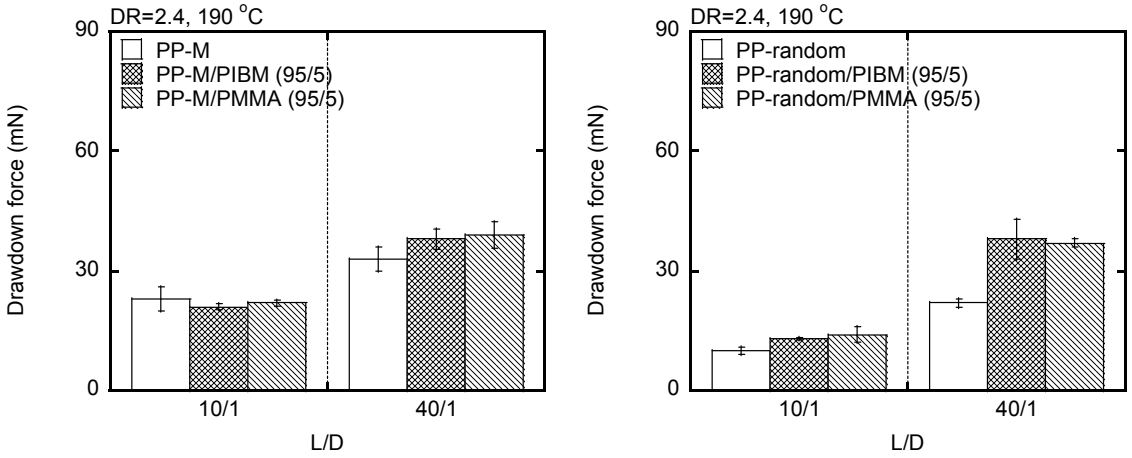

Figure 3-14 Drawdown force of PP-M (homopolymer) and PP-random and their blends with 5 %wt of PIBM and PMMA stretched at a draw ratio of 2.4. The temperature was controlled at 190 °C.

Further, the deformation of the dispersed phase is confirmed by measuring the lateral expansion of the strand after dipping into silicone oil bath at 170 °C as shown in Figure 3-15. After dipping, PP matrix as well as the dispersed phase is melted immediately. Then, the

interfacial tension tends to pull the droplets back to spherical shape. Therefore, the deformed dispersed-phase returns to the original shape, *i.e.*, spherical droplet. High level of the deformation will provide high level of the lateral expansion as well as vertical shrinkage. Based on this technique, the level of deformation can be determined from the level of the lateral expansion of the strand. Since there is no dispersed phase in the pure PP system, the level of strand expansion for the pure system depends on the degree of orientation. As discussed previously, the enhancement of the drawdown force for a long die is due to the reduction of entanglement coupling density, *i.e.*, chain orientations. In the case of pure PP, PP-H shows the high value of the drawdown force compared with PP-M because it possesses long relaxation time and thus high degree of the orientation. In the case of the pure polymers having the same MFR, PP-M exhibits high degree of orientation than PP-random, leading to high level of the drawdown force. Therefore, the level of strand expansion for the pure polymers is considered based on the degree of orientation. For example, the expansion level for the strand of PP-H is lower than those of PP-M and PP-random because PP-H exhibits high degree of orientation, which prohibits the vertical shrinkage. In the case of the blends, the drawdown force enhancement by the additives is, in contrast, pronounced for the PP-random, especially when using a long die. The drawdown force values of the blends for PP-random and PP-M extruded from the die with L/D = 40/1 are almost the same. This behavior is discussed based on the level of strand expansion. PP-random exhibits a high level of strand expansion compared with that of PP-M. In particular, this behavior is obviously detected for the strand extruded from a long die, indicating that PIBM and PMMA deform greatly in the PP-random matrix. This result

suggests that the prompt solidification of PP-M reduces the deformation of the dispersion, leading to low level of the expansion as compared with PP-random having the same MFR. Furthermore, this phenomenon correlates with the drawdown force value.

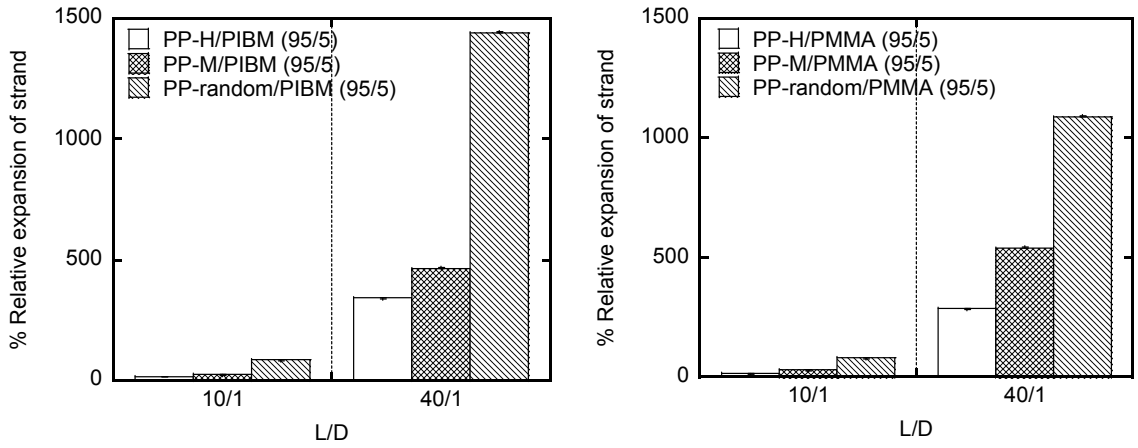

Figure 3-15 Percentage of relative expansion of strand after dipping into silicone oil bath at 170 °C as compared with the original strand.

3.4 Conclusion

Drawdown force enhancement of PP at capillary extrusion is studied by blending acrylate polymers, such as PIBM and PMMA, which have significantly low shear viscosity at the processing temperature of PP. Although it has been generally understood that the drawdown force is enhanced by blending high molecular weight materials, a new approach to enhance the drawdown force for PP using a low viscous material is proposed. The mechanism of this phenomenon is found to be attributed to prompt solidification of PIBM and PMMA at the rapid cooling condition like the drawdown force measurements. In the die, droplets of the acrylate polymers deform to the flow direction. Once their solidification takes place, they will act as rigid fibers/particles depending on the level of the deformation. This situation occurs by the difference in the cooling rate dependence of solidification temperatures, *i.e.*, crystallization temperature of PP is more sensitive to the cooling rate than the glass transition temperature of the acrylate polymers. Then, the drawdown force is enhanced by the excess stress generated by large shear deformation of a matrix between the fibers/particles. Therefore, the droplet size is an important factor to determine the level of drawdown force enhancement. Furthermore, the solidified deformed-droplets presumably exhibit nucleation effect, which can accelerate the crystallization process of PP, in the flow condition. This phenomenon is confirmed by DSC as well as the degree of orientation obtained from 2D-XRD.

References

(1) Ryu, S. H.; Gogos, C. G.; Xanthos, M. *Polymer* **1991**, *32*, 2449.

(2) Liang, J. -Z. *Polym. Test.* **2008**, *27*, 936.

(3) Tabatabaei, S. H.; Carreau, P. J.; Ajji, A. *Chem. Eng. Sci.* **2009**, *64*, 4719.

(4) Liang, J. Z.; Du, Q.; Wei, L. Y.; Tsui, C. P.; Tang, C. Y.; Law, W. C.; Zhang, S. D. *Polym. Test.* **2015**, *45*, 179.

(5) Lau, H. C.; Bhattacharya, S. N.; Field, G. J. *Polym. Eng. Sci.* **1998**, *38*, 1915.

(6) Yamaguchi, M. *Melt Elasticity of Polyolefins, Impact of Elastic Properties on Foam Processing in Polymeric Foam*; CRC Press: New York, **2004**.

(7) Yamaguchi, M.; Wagner, M. H. *Polymer* **2006**, *47*, 3629.

(8) Li, Y.; Yao, Z.; Chen, Z.-h.; Qiu, S.-l.; Zeng, C.; Cao, K. *Polymer* **2015**, *70*, 207.

(9) Azizi, H.; Ghasemi, I. *Polym. Test.* **2004**, *23*, 137.

(10) Lugão, A. B.; Artel, B. W. H.; Yoshiga, A.; Lima, L. F. C. P.; Parra, D. F.; Bueno, J. R.; Liberman, S.; Farrah, M.; Terçariol, W. R.; Otaguro, H. *Radiat. Phys. Chem.* **2007**, *76*, 1691.

(11) Yamaguchi, M.; Miyata, H. *Polym. J.* **2000**, *32*, 164.

(12) Md Ali, M. A. B.; Okamoto, K.; Yamaguchi, M.; Kasai, T.; Koshirai, A. *J. Polym. Sci. Polym. Phys.* **2009**, *47*, 2008.

(13) Yokohara, T.; Nobukawa, S.; Yamaguchi, M. *J. Rheol.* **2011**, *55*, 1205.

(14) Yamaguchi, M.; Fukuda, K.; Yokohara, T.; Ali, M. A. B. M.; Nobukawa, S. *Macromol. Mater. Eng.* **2012**, *297*, 654.

(15) Yamaguchi, M.; Yokohara, T.; Bin Md Ali, M. A. *Nihon Reoroji Gakkaishi* **2013**, *41*, 129.

(16) Liang, J.-Z.; Li, R. K. Y.; Tang, C. Y.; Cheung, S. W. *J. Appl. Polym. Sci.* **2000**, *76*, 419.

(17) Moynihan, C. T.; Easteal, A. J.; Wilder, J.; Tucker, J. *J. Phys. Chem.* **1974**, *78*, 2673.

(18) Buchholz, J.; Paul, W.; Varnik, F.; Binder, K. *J. Chem. Phys.* **2002**, *117*, 7364.

(19) Gradys, A.; Sajkiewicz, P.; Minakov, A. A.; Adamovsky, S.; Schick, C.; Hashimoto, T.; Saijo, K. *Mater. Sci. Eng.* **2005**, *413–414*, 442.

(20) Mollova, A.; Androsch, R.; Mileva, D.; Gahleitner, M.; Funari, S. S. *Eur. Polym. J.* **2013**, *49*, 1057.

(21) Schawe, J. E. K. *Thermochim. Acta* **2015**, *603*, 85.

(22) Bogoeva-Gaceva, G.; Grozdanov, A. *J. Serb. Chem. Soc.* **2006**, *71*, 483.

(23) Macosko, C. W. *Rheology: Principles, Measurements, and Applications*; John Wiley & Sons: New York, **1994**.

(24) Larson, R. G. *The Structure and Rheology of Complex Fluids*; Oxford University Press: New York, **1998**.

(25) Batchelor, G. K. *J. Fluid Mech.* **1971**, *46*, 813.

(26) Mewis, J.; Metzner, A. B. *J. Fluid Mech.* **1974**, *62*, 593.

(27) Laun, H. M. *Colloid Polym. Sci.* **1984**, *262*, 257.

Chapter 4

Rheological Properties of Mixing Condition on Flow Instability for Polyethylene Blends

4.1 Introduction

Flow instability of a molten polymer at extrusion is not only an interesting research topic in academia but also industrially relevant, since it limits product quality and production rate at processing operations.[1-4] Generally, flow instability at capillary extrusion is categorized into three types. The first type is surface melt fracture known as shark-skin failure, of which an extrudate begins losing glossy appearance from the presence of small amplitude with high frequency of distortions on the surface due to cohesive failure near die exit or unstable slippage at high shear stress. When apparent shear stress is beyond the critical value, macroscopic slippage between polymer and wall takes place, resulting in alternating of periodic rough and smooth regions on the surface of an extrudate. This phenomenon is called stick-slip instability or spurt flow.[5] The last type is gross melt fracture, which is caused by a swirling motion of a

melt due to the high elongational stress by converging flow at the die entrance, giving rise to volumetric distortion.[6] Over the past decades, numerous researchers have intensively studied the flow instability, involving the mechanism in both microscopic and macroscopic levels, in order to control and overcome this phenomenon.[7-14] It is generally understood that shark-skin failure occurs beyond the critical shear stress at die exit while gross melt fracture is detected beyond the critical elongational stress at die entry. Furthermore, various methods to eliminate flow instability have been proposed, such as use of additives, coating the die wall with a low surface energy material,[15] design of capillary dies,[16] control of processing temperature,[17] considering molecular structure of a polymer[18,19] and blending with a linear polymer.[20] The most common method is to use fluoropolymer-based polymer processing aids. Dubrocq-Baritaud et al. reported the use of copolymers of vinylidene fluoride and hexafluoropropylene for postponing the surface defects. They found that these additives possess the ability to reduce die pressure and delay the onset of shark-skin by creating the slippage at the die wall.[21] Kotera et al. studied flow instability of ethylene–tetrafluoroethylene copolymer (ETFE) at capillary extrusion. They reported that ETFE exhibits various types of flow instability. Interestingly, quasi-stable flow region, so-called super-extrusion, is detected in the wide range of shear rates between shark-skin and wavy melt fracture regions due to steady slippage, suggesting that ETFE can be processed at a high output rate condition.[22]

For polyethylene, the type of flow instability appeared at a low shear rate at capillary extrusion depends on the molecular structure.[23] Low-density polyethylene (LDPE) having long-chain branches exhibits gross melt fracture prior to shark-skin failure. This is attributed to

marked strain-hardening in elongational viscosity, leading to high elongational stress. On the contrary, shark-skin failure is detected before gross melt fracture for linear low-density polyethylene (LLDPE) and high-density polyethylene (HDPE) when the applied shear stress is above the critical value. Mieda et al. studied flow instability of binary blends composed of LLDPE and LDPE.[24] According to them, blends containing LLDPE with high shear viscosity show anomalous rheological response and exhibit shark-skin failure at low shear stress comparing with pure LLDPE. Siriprumpoonthum et al. investigated the effect of shear history on the flow instability of LDPE.[23] It has been reported that prolonged shear history with high shear stress provides the shark-skin failure of LDPE prior to gross melt fracture, suggesting that LDPE with intense shear history behaves like linear polyethylene in the molten state. However, the effect of molecular aggregation state decided by an applied mixing condition on the flow instability has not been reported yet to the best of my knowledge. In this research, the relation between mixing condition and flow instability at capillary extrusion is investigated using blends of two types of LLDPE having different molecular weights. The results obtained in this study provide the information on the importance of melt-mixing in an extruder because it greatly affects the onset of shark-skin failure.

4.2 Experimental

4.2.1 Materials

Materials used in this study were two types of ethylene-1-hexene copolymers as LLDPE. They have different molecular weights, denoted as L-PE and H-PE for low and high molecular weight LLDPE, respectively. The molecular weights were characterized by a gel permeation chromatography (GPC) (Alliance GPS 2000, Waters, USA) by comparing with a linear polyethylene standard as described in a previous work.[25] Other characteristics of the materials are shown in Table 4-1. The number of short-chain branches per 1000 backbone carbon atoms was determined by the carbon nuclear magnetic resonance spectroscopy (^{13}C-NMR).

Table 4-1 Characteristics of the materials

Sample	Mw	Mn	MFR (g/10min)[#]	Number of SCB[*]	Density (kg/m^3)
H-PE	1.55x10^5	6.25x10^4	0.2	19.8	908
L-PE	2.43x10^4	1.01x10^4	205	8.5	939

[#] Melt flow rate at 190 °C and 2.16 kgf

* Number of short-chain branches per 1000 backbone carbons

4.2.2 Sample preparation

As a thermal stabilizer, 6-[3-(3-t-butyl-4-hydroxy-5-methylphenyl)propoxy]-2,4,8,10-tetra-*t*-butyldibenzo[d,f][1,3,2]dioxaphosphepin (Sumilizer® GP, Sumitomo Chemical, Japan) was employed with calcium stearate to avoid thermal degradation during mixing process. The blend ratio of H-PE and L-PE was 60/40 wt%. The melt-blending was carried out by various methods as described below.

Three different types of extruders were used as mixing devices in this study. The first one was a single-screw extruder with full-flight screw (EXU-40, Placo, Japan), denoted as SSE in this thesis. The diameter of the screw D_s is 40 mm and L_s/D_s ratio, in which L_s is defined as the axial extruder length, is 28. The screw rotational speed and output rate were 80 rpm and 14 kg/h, respectively. Temperatures in the barrel were controlled as follows; C1/160, C2/170, C3/180, C4/200 and D/200 °C. The second device was a co-rotating twin-screw extruder (PCM46-35-2V, Ikegai, Japan), denoted as TSE-1. The screw diameter D_s is 46 mm with L_s/D_s ratio of 35. The screw rotational speed and output rate during the operation were controlled at 300 rpm and 44 kg/h, respectively. The temperature profile was as follows; C1/150 °C, C2/160 °C, C3/170 °C, C4/170 °C, C5/170 °C, C6/180 °C, C7/180 °C, C8/180 °C, C9/200 °C, AD/200 °C and D/200 °C. The third one was a co-rotating twin-screw mixer (ULT15TWnano-15MG-NH-HKU, Technovel, Japan) operated by a closed discharge condition for 5 min, denoted as TSE-2. The screw diameter D_s is 15 mm with L_s/D_s ratio of 15. The operation was performed

with a screw rotational speed of 40 rpm. Temperature profile in the barrel was as follows; C1/110 °C, C2/190 °C, H/190 °C and D/190 °C.

The mixing was performed using three different conditions, defined as condition #1, #2 and #3, which are summarized in Figure 4-1. For the condition #1, H-PE and L-PE were firstly mixed by dry blending, followed with melt-mixing using TSE-1. The condition #2 was almost similar to the condition #1, but after mixing by TSE-1, the sample was mixed again using SSE. In the case of the condition #3, H-PE and L-PE were mixed by dry blending prior to melt-mixing using TSE-2.

The samples mixed by each method were compressed into a flat sheet using a compression-molding machine (IMC-180C, Imoto, Japan) at 230 °C for 10 min and quenched at 25 °C prior to cutting into small pieces.

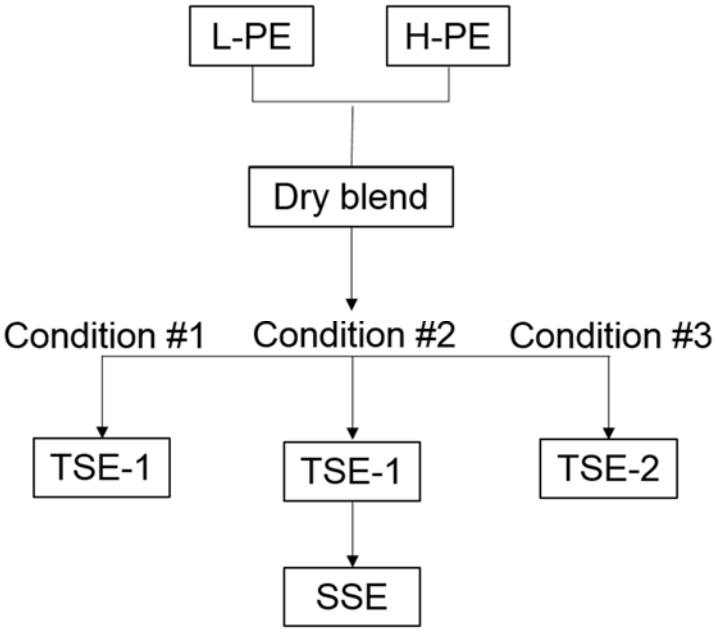

Figure 4-1 Schematic illustration of mixing methods.

4.2.3 Measurements

The frequency dependence of oscillatory shear moduli such as storage modulus *G'* and loss modulus *G"* was measured using a cone-and-plate rheometer (AR2000, TA instruments, USA) with a cone angle of 4° at various temperatures such as 130, 160 and 190 °C.

The flow curves and drawdown force were evaluated by a capillary rheometer (140 SAS-2002, Yasuda Seiki Seisakusyo, Japan) equipped with a circular die at 190 °C. The length and diameter of the die were 10 and 1 mm, respectively, and the entrance angle was 180°. In the case of drawdown force measurements, a tension detector was attached with a set of rotating wheels. In addition, the applied shear rate was controlled at 21.4 s^{-1} and the draw ratio was varied by adjusting a taking-up speed of the rotating wheels. The maximum value of the draw ratio at which a melt can be stretched without rupture at the applied shear rate of 14.6 s^{-1} was evaluated as a maximum draw ratio.

Appearance of the extrudates was observed by means of an optical microscope (S6E, Leica, Germany) and a scanning electron microscope (SEM) (S400, Hitachi, Japan). Prior to the SEM observation, the samples were coated by Pt-Pd and observed with the voltage of 20 kV.

4.3 Results and discussion

4.3.1 Rheological properties

Figure 4-2 shows the master curves of frequency dependence of oscillatory shear moduli such as storage modulus *G'* and loss modulus *G"* of the samples blended by various methods as described in the experimental section. As seen in the figure, *G'* and *G"* obtained from various temperatures can be superimposed onto each other for all samples, indicating that the time-temperature superposition principle is applicable. This is reasonable because the materials have linear structure with no long-chain branch. Moreover, both moduli for H-PE are much higher than those for L-PE. In case of H-PE/L-PE blends, both values are between those of H-PE and L-PE. Furthermore, the apparent activation energy E_a obtained from the master curve is 37.2, 39.6 and 38.3 kJ/mol for the blends of condition #1, #2 and #3, respectively. The flow activation energy is known to be determined by the number of short-chain branches for LLDPE as shown in the following equation.

$$E_a = 23.9 + 26.8\left[1 - exp\left(-\frac{n_{SCB}}{35.4}\right)\right] \quad (4\text{-}1)$$

where n_{SCB} is the number of short-chain branches per 1000 backbone carbon atoms.

Since the difference in the activation energy is within the experimental error, the number of short-chain branch does not change by the mixing method. In other words, it should be noted that the mixing method has no/little influence on the linear viscoelastic properties at least in this experimental range. It is also found that there is no long time relaxation mechanism associated with phase separation. The miscibility of this blend system is attributed to the small difference in the number of short-chain branches between H-PE and L-PE. It has been well known that the difference in short-chain branches must be larger than 40 per 1000 carbon atoms to show immiscibility in the molten state for LLDPE blends.[26-28]

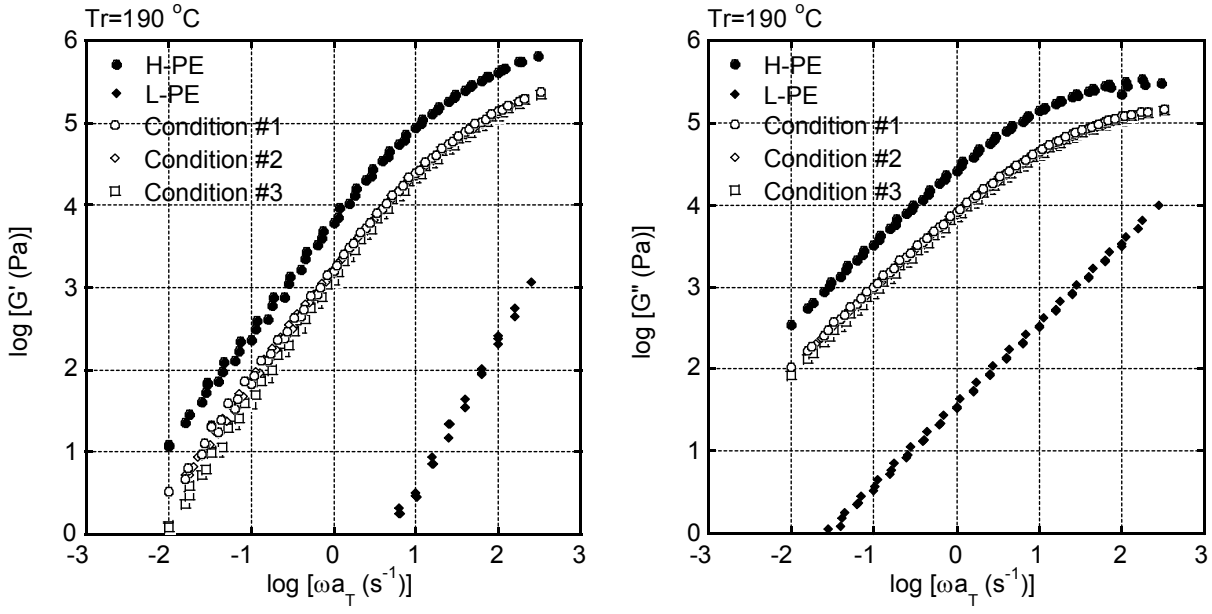

Figure 4-2 Master curves of frequency dependence of oscillatory shear moduli such as storage modulus *G'* (left) and loss modulus *G"* (right) at the reference temperature of 190 °C for H-PE, L-PE and the blends obtained by conditions #1, #2 and #3.

Figure 4-3 shows apparent shear stress as a function of apparent shear rate at wall at 190 °C. It indicates that H-PE and the blend samples exhibit non-Newtonian behavior in the high shear rate. Moreover, the blends possess the same shear viscosity during the flow condition. In the case of L-PE, however, only Newtonian behavior is detected in this range. This is reasonable because L-PE has very low molecular weight. Furthermore, this value is identical to the complex shear viscosity calculated by the oscillatory shear moduli.

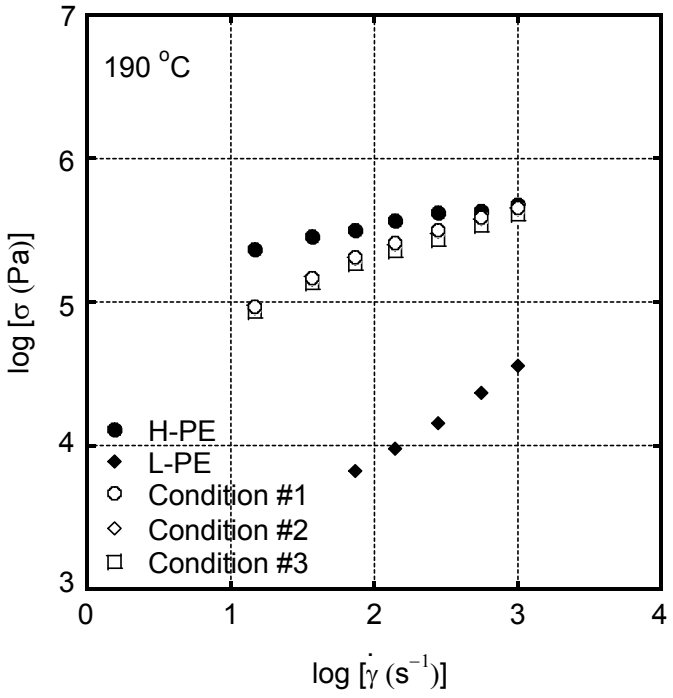

Figure 4-3 Apparent shear stress as a function of apparent shear rate at wall at 190 °C for H-PE, L-PE and the blends obtained by various mixing conditions.

4.3.2 Flow instability

Flow instability of the blends is investigated using a capillary rheometer at 190 °C. The shear rates were varied from 15 to 1000 s^{-1}. Appearance of the strands extruded from a capillary die was observed by the optical microscope. As seen in Figure 4-4, the strands of conditions #1 and #2 exhibit rough surface even at low apparent shear rates. The onset shear stress of shark-skin failure is 0.15 MPa (36 s^{-1}) at condition #1, whereas 0.20 MPa (73 s^{-1}) at the condition #2. In the case of the strand at the condition #3, however, the shark-skin is detected only at high shear stress, *i.e.*, 0.41 MPa. Consequently, the extrusion with smooth surface can be carried out at significantly high shear rate, *e.g.*, 1000 s^{-1}. It should be noted from the viewpoints of marked productivity. This result demonstrates that the H-PE/L-PE blend obtained by a good mixing condition hardly shows shark-skin failure. Regarding the mixing ability at the condition #3, TSE-2 provides intense mixing due to high level of elongational stress and relentless change of flow direction and thus, allows the materials to be mixed well.

Based on one of the possible mechanisms of shark-skin failure, which was proposed by Cogwell (1977), the surface fracture is caused by the crack, *i.e.*, cohesive failure due to high level of tensile stress at the die exit.[29] From the view point of entanglement couplings, homogeneous distribution of entanglement couplings is barely obtained by the poor mixing because of the low diffusivity of molecular chains, leading to mechanically weak points. Such weak points will be responsible for cohesive failure at tensile stretching at surface of a strand. Consequently, the sample with poor mixing exhibits the low onset shear stress for shark-skin

failure, even though the linear viscoelastic properties are almost identical to those of the sample with good mixing.

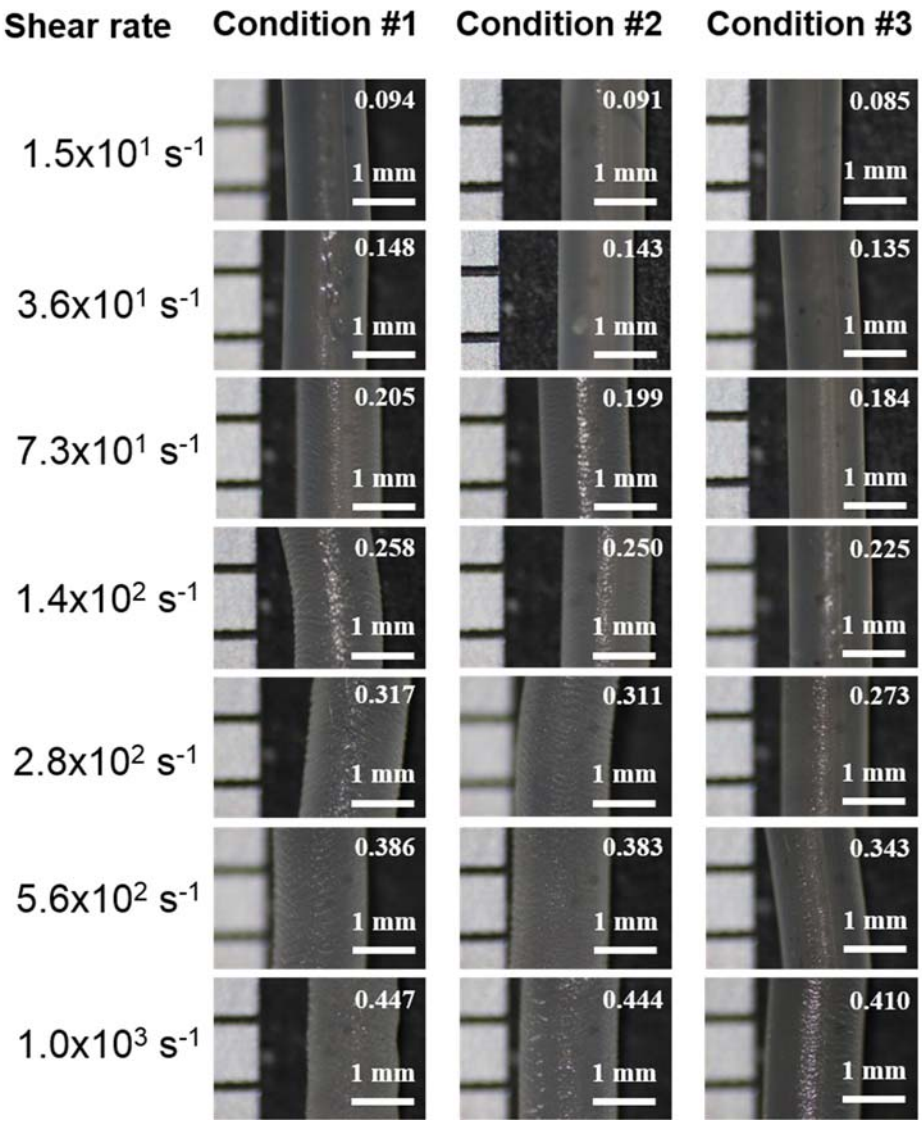

Figure 4-4 Appearance of the strands extruded from a capillary rheometer for the blends obtained by various mixing conditions. The numerals in the pictures represent the apparent shear stress at wall (Unit = MPa).

The surface roughness of the extrudates for the blends prepared by various methods is confirmed by SEM. Figure 4-5 illustrates surface morphology of the strands for the samples prepared by the conditions #1, #2 and #3 extruded from the capillary rheometer at apparent shear rates of 280 and 560 s^{-1}. It is clearly seen that the strand of the condition #1 shows the most severe surface failure at this shear stress. The shark-skin is also detected for the strand at condition #2. However, the amplitude of periodic distortion is smaller than that at condition #1 at the apparent shear rate of 280 s^{-1}. In the case of a strand at condition #3, it shows smooth surface without any defect even at a high apparent shear rate (560 s^{-1}). This result confirms that the surface roughness is mitigated and the onset of shark-skin failure is, moreover, postponed to a higher shear rate by good mixing.

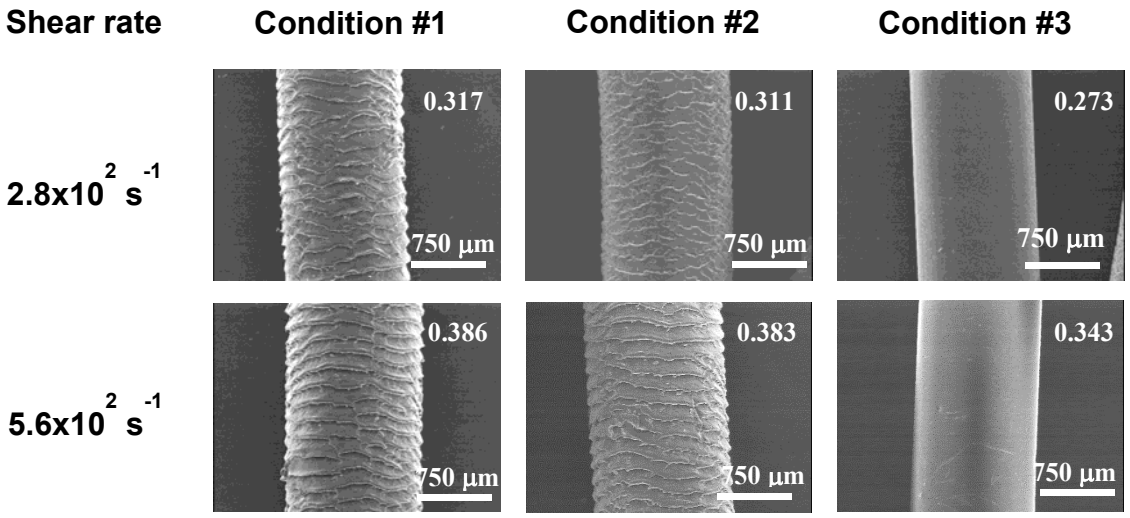

Figure 4-5 SEM photographs of the strands extruded from a capillary rheometer at the apparent shear rate of 280 and 560 s^{-1} for the blends obtained by various mixing conditions. The extrusion temperature were controlled at and 190°C. The numerals in the pictures represent the apparent shear stress at wall (Unit = MPa).

4.3.3 Drawability

Figure 4-6 shows the maximum draw ratio of the blends obtained by various mixing methods. The experiment was performed with an applied shear rate of 14.6 s^{-1} at 190 ^{o}C. As seen in the result, the blend prepared by the condition #3 shows the high value of the maximum draw ratio. Furthermore, the melt obtained by the condition #1 shows large derivation of the maximum draw ratio values as represented with the experimental error. This result correlates

with the low onset shear stress of shark-skin, indicating that the existence of mechanically-weak points associated with lacks of entanglement couplings due to poor mixing leads to the shark-skin failure. In other words, the melt prepared by the condition #1 is not in the equilibrium state from the viewpoints of entanglement couplings. In addition, sporadic lacks of entanglement couplings are responsible for the large derivation of the maximum draw ratio for the sample prepared by a poor mixing condition. This is reasonable because the mechanically-weak points will affect the elongation at break in the uniaxial stretching, although their contribution to the oscillatory moduli, *i.e.*, the rheological response under small strains, can be neglected.

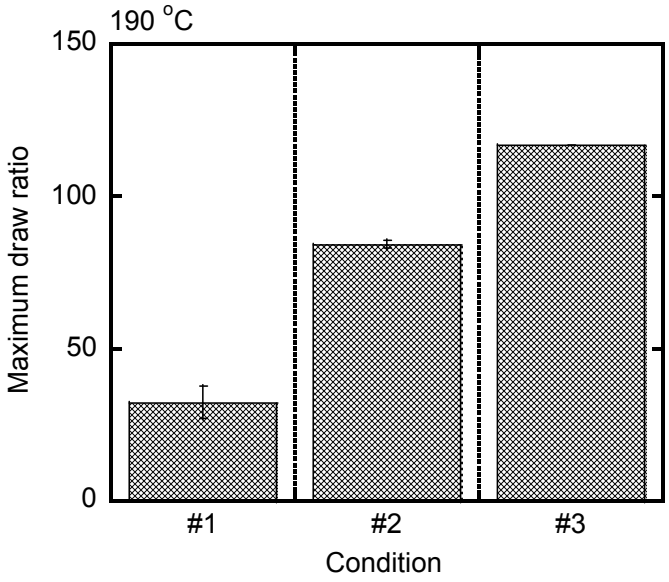

Figure 4-6 Maximum draw ratio at 190 °C for the blends obtained by various mixing conditions at 14.6 s^{-1}. The measurements were carried out at 3 times to evaluate the standard deviation which is shown by the error bar. The maximum draw ratio value for the blend obtained by condition #3 is the highest limitation of the machine.

Figure 4-7 shows the drawdown force of H-PE/L-PE blends obtained by various mixing conditions at 190 °C. As seen in the figure, the drawdown force values of the H-PE/L-PE blends are almost the same, although a large experimental error is detected for the extrudate of the blend obtained by the condition #1. The large experimental error for the melt with poor mixing suggests that the stretching cannot be performed well, corresponding to the existence of poor entanglement couplings. Moreover, the result strongly supports that the high level of maximum draw ratio, which is responsible for the mitigation of surface cracks, is not ascribed to the chain scission, leading to a low value of drawdown force.

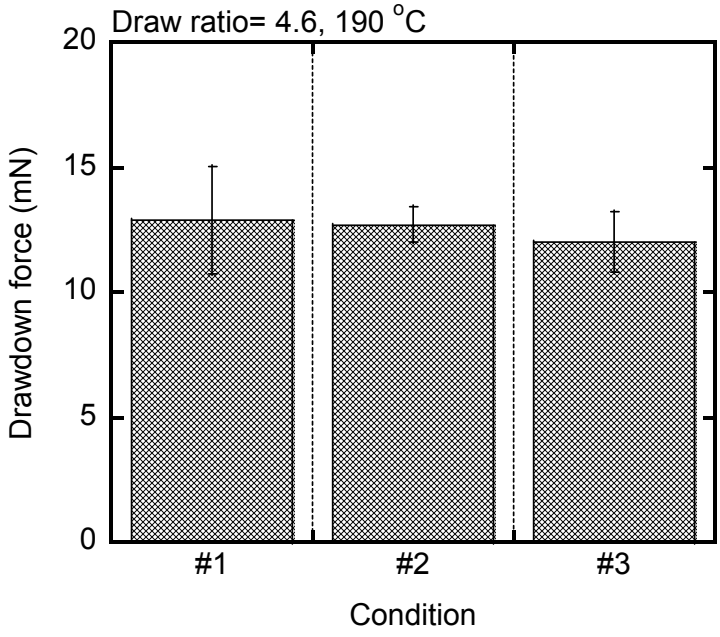

Figure 4-7 Drawdown force at various draw ratios of the blends obtained by various mixing conditions. The shear rate and the extrusion temperature were controlled at 21.4 s^{-1} and 190 °C, respectively.

4.4 Conclusion

Flow instability at capillary extrusion of LLDPE blends obtained by various mixing conditions is studied. In particular, the effect of mixing condition on the flow instability behavior, *i.e.*, the onset shear stress of the shark-skin failure, is investigated. To the best of my knowledge, the study on the shark-skin failure relating with the mixing ability in a mixer using bimodal mixture has not been carried out yet. It is found that the mixing condition strongly affects the onset stress even though all blends are composed of the same materials with almost the same linear viscoelastic properties. The LLDPE blend prepared by a good mixing condition, *e.g.*, a twin-screw mixer, shows the mitigation of shark-skin failure. Furthermore, the onset of shark-skin is found to be postponed to a higher shear rate comparing with the blends obtained by the poor mixing conditions. This phenomenon is attributed to the lack of mechanically weak points, *i.e.*, no defects of entanglement couplings, for a blend with good mixing. In contrast, the cohesive failure due to the abrupt stretching at the die exit occurs at weak points for the blends with poor mixing. Furthermore, the maximum draw ratio, stretchability of a polymer melt, is found to be sensitive to the homogeneity, *i.e.*, the degree of mixing.

References

(1) Migler, K. B.; Hatzikiriakos, S. G. In *Polymer Processing Instabilities*; CRC Press: New York, **2004**.

(2) Koopmans, R.; Doelder, J. d.; Molenaar, J. In *Polymer Melt Fracture*; CRC Press: New York, **2010**.

(3) Malkin, A. Y.; Arinstein, A.; Kulichikhin, V. G. *Prog. Polym. Sci.* **2014**, *39*, 959.

(4) Pérez-González, J.; Denn, M. M. *Ind. Eng. Chem. Res.* **2001**, *40*, 4309.

(5) Robert, L.; Vergnes, B.; Demay, Y. *J. Non-Newtonian Fluid Mech.* **2003**, *112*, 27.

(6) Yamaguchi, M. *J. Appl. Polym. Sci.* **2001**, *82*, 1277.

(7) Ramamurthy, A. V. *Adv. Polym. Technol.* **1986**, *6*, 489.

(8) Kim, Y. S.; Chung, C. I.; Lai, S. Y.; Hyun, K. S. *J. Appl. Polym. Sci.* **1996**, *59*, 125.

(9) Fernández, M.; Francisco Vega, J.; Santamaría, A.; Muñoz-Escalona, A.; Lafuente, P. *Macromol. Rapid Commun.* **2000**, *21*, 973.

(10) Hong, Y.; Coombs, S. J.; Cooper-White, J. J.; Mackay, M. E.; Hawker, C. J.; Malmström, E.; Rehnberg, N. *Polymer* **2000**, *41*, 7705.

(11) Piau, J. M.; Nigen, S.; El Kissi, N. *J. Non-Newtonian Fluid Mech.* **2000**, *91*, 37.

(12) Yamaguchi, M.; Miyata, H.; Tan, V.; Gogos, C. G. *Polymer* **2002**, *43*, 5249.

(13) Santamaría, A.; Fernández, M.; Sanz, E.; Lafuente, P.; Muñoz-Escalona, A. *Polymer* **2003**, *44*, 2473.

(14) Pol, H. V.; Joshi, Y. M.; Tapadia, P. S.; Lele, A. K.; Mashelkar, R. A. *Ind. Eng. Chem. Res.* **2007**, *46*, 3048.

(15) Piau, J.-M.; El Kissi, N.; Toussaint, F.; Mezghani, A. *Rheol. Acta* **1995**, *34*, 40.

(16) Arda, D. R.; Mackley, M. R. *J. Non-Newtonian Fluid Mech.* **2005**, *126*, 47.

(17) Miller, E.; Rothstein, J. *Rheol. Acta* **2004**, *44*, 160.

(18) Allal, A.; Vergnes, B. *J. Non-Newtonian Fluid Mech.* **2007**, *146*, 45.

(19) Ansari, M.; Inn, Y. W.; Sukhadia, A. M.; DesLauriers, P. J.; Hatzikiriakos, S. G. *Polymer* **2012**, *53*, 4195.

(20) Aguilar, M.; Expósito, M. T.; Vega, J. F.; Muñoz-Escalona, A.; Martínez-Salazar, J. *Macromolecules* **2004**, *37*, 681.

(21) Dubrocq-Baritaud, C.; Darque-Ceretti, E.; Vergnes, B. *J. Non-Newtonian Fluid Mech.* **2011**, *166*, 847.

(22) Kotera, S.; Yamaguchi, M. *J. Fluorine Chem.* **2015**, *176*, 20.

(23) Siriprumpoonthum, M.; Mieda, N.; Anh Doan, V.; Nobukawa, S.; Yamaguchi, M. *J. Appl. Polym. Sci.* **2012**, *124*, 429.

(24) Mieda, N.; Yamaguchi, M. *J. Non-Newtonian Fluid Mech.* **2011**, *166*, 231.

(25) Siriprumpoonthum, M.; Nobukawa, S.; Satoh, Y.; Sasaki, H.; Yamaguchi, M. *J. Rheol.* **2014**, *58*, 449.

(26) Alamo, R. G.; Graessley, W. W.; Krishnamoorti, R.; Lohse, D. J.; Londono, J. D.; Mandelkern, L.; Stehling, F. C.; Wignall, G. D. *Macromolecules* **1997**, *30*, 561.

(27) Schuman, T.; Stepanov, E. V.; Nazarenko, S.; Capaccio, G.; Hiltner, A.; Baer, E. *Macromolecules* **1998**, *31*, 4551.

(28) Agamalian, M.; Alamo, R. G.; Kim, M. H.; Londono, J. D.; Mandelkern, L.; Wignall, G. D. *Macromolecules* **1999**, *32*, 3093.

(29) Cogswell, F. N. *J. Non-Newtonian Fluid Mech.* **1977**, *2*, 37.

Chapter 5

General Conclusion

Rheological responses at capillary extrusion have been studied in this thesis. As well known, extrusion processing is one of the most important processing operations for polymers, especially polyolefins. Therefore, intensive study has been performed, in particular for the flow mechanism from a hopper, *i.e.*, the entrance of an extruder, to a die, *i.e.*, the exit of an extruder. After passing through the die, a polymer is exposed to open air and then the shape of products is determined. This shaping process is always focused in industry, because it directly decides the quality of a product. For example, surface roughness, which is called shark-skin failure, loses the gloss of a product. Moreover, the lack of drawability restricts applications, in which the rheological properties under elongational flow as well as the solidification process play an important role. In this thesis, therefore, the drawdown force, *i.e.*, the rheological response under uniaxial elongation at non-isothermal crystallization, is focused with surface roughness of an extrudate. They are the most important topics for the extrusion of polyolefins.

In this research, the origin of the drawdown force and its enhancement for polyolefins

are investigated at first. The extrusion conditions such as die geometry, ***i.e.***, die length and diameter, draw ratio and extrusion temperature is found to strongly affect the drawdown force. In particular, it was firstly revealed that the drawdown force is enhanced by a long capillary die for linear polyolefins, ***e.g.***, isotactic polypropylene (PP) and high-density polyethylene (HDPE). Furthermore, this phenomenon is pronounced for high molecular weight materials and at low extrusion temperature. The mechanism of the phenomenon is due to the decrease in the density of entanglement couplings in a long die, leading to prompt crystallization. The crystallization suppresses orientation relaxation, and thus results in high level of the drawdown force. On the contrary, polyolefin with low crystallization temperature, ***e.g.***, linear low-density polyethylene (LLDPE), hardly shows this phenomenon. In other words, slow crystallization relaxes the molecular orientation. Therefore, the drawdown force of LLDPE is less sensitive to the die length. Furthermore, the drawdown force enhancement by a long die for LLDPE is detected by the addition of a small amount of HDPE. This behavior is attributed to the nucleating effect of HDPE.

Moreover, the drawdown force is found to be enhanced by blending either poly(isobutyl methacrylate) PIBM or poly(methyl methacrylate) PMMA, even though these materials have low molecular weight. In particular, PIBM can greatly enhance the drawdown force by comparing PMMA. This is a new concept because it has been believed that only high molecular weight materials can enhance the drawdown force. In this work, it is, however, found that the low molecular weight materials also exhibit outstanding ability to enhance the drawdown force of PP. The mechanism of this behavior is attributed to the prompt solidification of PIBM and

PMMA at the processing condition. Considering the effect of the cooling rate, the crystallization temperature T_c of PP is sensitive to the cooling rate, *i.e.*, decrease with the cooing rate, whereas glass transition temperature T_g of PIBM and PMMA is less sensitive to the cooing rate. Since the actual cooling rate at capillary extrusion is quite high, *e.g.*, > 6000 °C/min, solidification of the low molecular weight materials presumably takes place earlier than the crystallization of PP. In addition, PIBM and PMMA are dispersed as liquid droplets in PP matrix. Therefore, they deform during the flow. The deformation gives rise to the change of the droplet shape. Since the interfacial tension of PMMA is higher than that of PIBM, the droplet size is larger than that of PIBM. When the solidification occurs, the deformed droplets will become rigid fiber-like/ ellipsoidal particles. Therefore, the rigid fibers/particles of PIBM have higher aspect ratio than those of PMMA. The existence of the rigid components provides the excess deformation of a matrix between fibers/particles, leading to high degree of molecular orientation and rapid crystallization.

The mechanism is, moreover, confirmed using PP having low T_c (PP-random) because it possesses the retardation of the crystallization compared with PP homopolymer having the same melt flow rate. Consequently, the effect of rigid particles on the drawdown force enhancement is pronounced for PP-random, suggesting that it has an agreement with the proposed mechanism.

As the rheological properties of a molten polymer after the die exit decide the processability at some processing operations, especially T-die extrusion, thermoforming and spinning, melt fracture including shark-skin failure is involved in one of the parameters to

predict processability. In this thesis, the effect of mixing condition on the flow instability and drawability of polyethylene blend is evaluated. It is found that the mixing method strongly affects the flow instability as well as drawability of the blends. On the other hand, it has no/little effect on linear viscoelastic properties of the blends. Good mixing condition is responsible for the decrease in the onset shear stress of shark-skin failure at capillary extrusion. The sporadic weak points of entanglement couplings will be the origin of the localized deformation under uniaxial elongation. In other words, mechanically-weak points provided due to the lack of mixing performance are exposed to the starting point of the deformation under non-linear elongational strain region. Because of the same origin, a blend prepared by poor mixing is lack of drawability at uniaxial stretching, which is also an origin of poor processability at various processing operations.

Finally, the techniques proposed in this thesis have to be considered not only for polyolefins but also for other polymers. The design of appropriate die geometry is probably a useful concept for improvement of processability at some processing operations in polymer processing industry. In addition, the approach to enhance melt elasticity by blending acrylate polymers may be able for further development in industrial scale.

Achievements

Publications

1. **Jiraporn Seemork**, Monchai Siriprumpoonthum, Youngjun Lee, Shogo Nobukawa, Masayuki Yamaguchi.
   Effect of Die Geometry on Drawdown Force of Polypropylene at Capillary Extrusion. *Advances in Polymer Technology* **2015**, 34, 21477 (1-7).

2. **Jiraporn Seemork**, Tomoki Itoh, Shogo Nobukawa, Masayuki Yamaguchi.
   Effect of Crystallization on Drawdown Force at Capillary Extrusion for Polyethylene. *Journal of the Society of Rheology, Japan* **2016**, 44, 23-27.

3. **Jiraporn Seemork**, Tomoki Itoh, Shogo Nobukawa, Hiroko Sasaki, Yasuo Satoh, Masayuki Yamaguchi.
   Impact of Mixing Condition on Flow Instability of Linear Low-Density Polyethylene Blends. *Submitted*

4. **Jiraporn Seemork**, Mohd Amran Bin Md Ali, Masayuki Yamaguchi.
   Enhancement of Drawdown Force for Polypropylene by Blending Acrylate Polymers. *Submitted*

Other Publications

1. Chavakorn Samthong, **Jiraporn Seemork**, Shogo Nobukawa, Masayuki Yamaguchi, Piyasan Praserthdam, Anongnat Somwangthanaroj.

Morphology, Structure, and Properties of Poly(lactic acid) Microporous Films Containing Poly(butylene terephthalate) Fine Fibers Fabricated by Biaxial Stretching. *Journal of Applied Polymer Science* **2015**, 132, 41415 (1-8).

2. Sunatda Arayachukiat, **Jiraporn Seemork**, Porntip Pan-In, Kittima Amornwachirabodee, Naunpun Sangphech, Titiporn Sansureerungsikul, Kamonluck Sathornsantikun, Chotima Vilaivan, Kazuki Shigyou, Prompong Pienpinijtham, Tirayut Vilaivan, Tanapat Palaga, Wijit Banlunara, Tsutomu Hamada, Supason Wanichwecharungruang.
   Bringing Macromolecules into Cells and Evading Endosomes by Oxidized Carbon Nanoparticles. *Nano Letters* **2015**, 15, 3370–3376.

3. Thapakorn Tree-Udom, **Jiraporn Seemork**, Kazuki Shigyou, Tsutomu Hamada, Naunpun Sangphech, Tanapat Palaga, Numpon Insin, Porntip Pan-In, Supason Wanichwecharungruang.
   Shape Effect on Particle-Lipid Bilayer Membrane Association, Cellular Uptake, and Cytotoxicity. *ACS Applied Materials & Interfaces* **2015**, 7, 23993−24000.

4. Ryuya Osato, Takumi Sako, **Jiraporn Seemork**, Sunatda Arayachukiat, Shogo Nobukawa, Masayuki Yamaguchi.
   Self-healing Properties of Poly(ethylene-co-vinyl acetate). *Colloid and Polymer Science* **2015**, *in press*, DOI: 10.1007/s00396-015-3817-z

5. Masayuki Yamaguchi, Chiyo Kanoh, **Jiraporn Seemork**, Shogo Nobukawa, Kaori Yanase.
   Effect of Foaming Method on Mechanical Properties of Aqueous Foams Prepared from Surfactant Solution. *Industrial & Engineering Chemistry Research* **2012,** 51, 14408−14413.

Presentations

International Conferences

Reviewed

1. **Jiraporn Seemork**, Monchai Siriprumpoonthum, Shogo Nobukawa, Masayuki Yamaguchi
   Drawdown Force Enhancement of Polypropylene Blends
   Eurofillers Polymer Blends 2015, Apr. 26-30, 2015, Montpellier, France

2. **Jiraporn Seemork**, Monchai Siriprumpoonthum, Shogo Nobukawa, Masayuki Yamaguchi
   Effect of Die Geometry on Uniaxial Elongational Response of Polypropylene
   31st International Conference of the Polymer Processing Society (PPS 31), Jun. 7-11, 2015, Jeju Island, Korea

3. **Jiraporn Seemork**, Shogo Nobukawa, Masayuki Yamaguchi
   Enhancement of Melt Tension for Polypropylene by Blending Poly(isobutyl methacrylate)
   13th International Conference on Advances in Foam Materials & Technology (FOAMS® 2015), Sep. 10-11, 2015, Kyoto, Japan

4. **Jiraporn Seemork**, Shogo Nobukawa, Masayuki Yamaguchi
   Effect of Die Geometry on Capillary Extrusion Properties for Polypropylene
   Polymer Processing Society Conference (PPS 2015), Sep. 21-25, 2015, Graz, Austria

5. **Jiraporn Seemork**, Shogo Nobukawa, Masayuki Yamaguchi
   Effect of Extrusion Condition on Elongational Properties of Polypropylene
   The 2nd International Conference on Polymer Materials Science (PMS 2016), Jan. 14-16, 2016, Bangkok, Thailand

Non-reviewed

1. **Jiraporn Seemork**, Monchai Siriprumpoonthum, Shogo Nobukawa, Masayuki Yamaguchi
   Effect of Die Length on the Extrusion Properties of Polypropylene
   International Symposium on Advanced Materials 2013, Oct.17-18, 2013, Japan Advanced Institute of Science and Technology, Ishikawa, Japan

2. **Jiraporn Seemork**, Shogo Nobukawa, Masayuki Yamaguchi
   Extensional Properties of Polypropylene at Capillary Extrusion with Various Die Geometries
   World Polyolefin Congress 2015 (WPOC2015), Nov. 23-27, 2015, Tokyo, Japan

Domestic Conferences

Non-reviewed

1. **Jiraporn Seemork**, Monchai Siriprumpoonthum, Shogo Nobukawa, Masayuki Yamaguchi
   Effect of Die Length on the Elongational Stress at Capillary Extrusion
   62nd Annual Meeting of Society of Polymer Science Japan, Sep. 11-13, 2013, Kanazawa, Japan

2. **Jiraporn Seemork**, Monchai Siriprumpoonthum, Shogo Nobukawa, Masayuki Yamaguchi
   Elongational Behavior of Polypropylene at Capillary Extrusion with Various Dies
   61st Rheology symposium, Sep. 25-27, 2013, Yamagata, Japan

Awards

1. JASSO Scholarship for Doctoral Students, April 2013 – March 2014.

2. Grant for Student Attending International Conferences, JAIST Research Grant to present at PPS 2015, Graz, Austria, September 2015.

3. Grant for PhD student, Chulalongkorn University Dutsadiphiphat Scholarship, June 2012-May 2016.

Thermoresponsive copolymers for controlled release of fragrances

1. Introduction

Fragrances are used in daily life products such as cosmetics and toiletries. However, volatility and reactive functionality of fragrance molecules have caused problems on short-life and instability of the fragrances. Many researches have been conducted in order to increase fragrance stability, which is responsible for prolonging the fragrance life-time. There are two categories of well-known fragrance prolongation technology. The first one is chemical derivation such as acetal, α-acyloxy ketones, β-mercapto ketones and Schiff base. The other technology is encapsulation or trapping of fragrance molecules in certain vehicles.

A thermoresponsive polymer is the polymer which undergoes a physical change when external thermal stimuli are presented. Thermoresponsive polymers have attracted much research interest because of their potential applications. The biocompatible thermoresponsive copolymers are being developed for various applications including drug delivery and gene delivery. Poly(ethylene glycol) is the most available thermoresponsive polymer for biological applications because of its hydrophilicity, non-toxicity, high flexibility and biocompatibility.

In this research, I demonstrate fragrance delivery system using thermoresponsive chitosan derivative in which the switching temperature can control the release of perfumery

aldehydes. The amphiphilic thermoresponsive chitosan derivative is synthesized for using as a fragrance controlled release system. The obtained polymer can self-assemble in aqueous media to form polymeric particles with spherical shape. Poly(ethylene glycol), a hydrophilic polymer, is grafted onto chitosan backbone in order to act as thermoresponsive residue in which upon self-assembling became particles' coronas, whereas perfumery aldehydes is grafted onto the chitosan to inherit hydrophobicity on which self-assembling became particles' core. The synthesized thermoresponsive polymer shows aggregation-dissociation behavior, corresponding with temperature trigger, leading to temperature dependence of the fragrance controlled release; significantly release of aldehyde from the particles is observed when the temperature is lower than lower critical solution temperature (LCST) whereas slower release is obvious at the temperature beyond the LCST. The LCST of system can be tuned by adjusting through salt concentration. This delivery system is completely biocompatible, therefore, it can be used in various applications.

2. Experimental

2.1 Materials and Chemicals

Chitosan (MW 30,000 Da, 85 % deacetylated) was purchased from Seafresh Chitosan Lab Co., Ltd (Thailand). Succinic anhydride, citral, vanillin, and 1-ethyl-3-(3-dimethyllaminopropyl) carbodiimide hydrochloride (EDCI.HCL) were obtained from Acros

organics (Geel Belgium). Pyridine and $ZnSO_4.7H_2O$ were purchased from CARLO ERBA (Val de Reuil, France). Polyethyleneglycol methyl ether (mPEG, Mw 5000) was purchased from Fluka (Missouri, USA). 1-Hydroxybenzotriazole (HOBt) was recrystallized in MeOH and other chemicals were analytical grade.

2.2 Methods

2.2.1 Synthesis of methoxy-terminated poly(ethylene oxide) carboxylic acid

Polyethyleneglycol methyl ether (mPEG 5000, 10.00 g) was reacted with succinic anhydride (4.00 g, 20 mole equivalent to mPEG) in DMF (20 mL) with a catalytic amount (2 drops) of pyridine at 60 °C overnight to achieve methoxy-terminated poly(ethylene oxide) carboxylic acid (mPEO-COOH). The obtained product was purified by dialysis against water using benzoylate dialysis tubing (MWCO 2000, Sigma-Aldrich, Missouri, USA) before drying by freeze dry method. Structural characterization of the product was achieved on a 400 MHz Varian mercury nuclear (^1H) magnetic resonance spectrometer (Varian Inc., Palo Alto, USA).

2.2.2 Synthesis of poly(ethylene oxide) grafted-chitosan (mPEO-CS)

Poly(ethylene oxide) grafted-chitosan (mPEO-CS) was synthesized by homogeneous coupling reaction in aqueous solution. Chitosan MW 3,000 (0.25 g, 1.53 mmole) was blended with HOBt (0.206 g, 1.53 mmole) followed with addition

of deionized water (20 mL) and stirred until a clear solution was obtained. Next, aqueous solution of mPEO-COOH (0.765 g, 0.153 mmole, 10 mL) was added drop-wise, following with the addition of aqueous EDCI.HCl (0.293 g EDCI, 1.53 mmole and 10 ml water) solution. The mixture was stirred at room temperature for 24 h. The obtained solution was precipitated in excess acetone and yellow crude gel was achieved. The crude gel was filtered and washed by acetone followed with ethanol for several times and then dried under vacuum at ambient temperature. The product was characterized using ^{1}H NMR. Attenuated total reflectance fourier transform infrared (ATR-FTIR) spectra were recorded with Nicolet 6700 FT-IR spectrometer (Thermo Electron Corporation, Madison, WI, USA) connected to a Continuμm™ infrared microscope equipped with a mercury-cadmium-telluride (MCT) detector.

2.2.3 Preparation of imine-mPEO-CS

mPEO-CS (90 mg) was dispersed in 30 mL of deionized water before addition (drop-wise) of each perfumery aldehyde (vanillin and citral), which was dissolved in ethanol (3 mL), under high-intensity ultrasound (40 kHz) at room temperature for 4 h. Hydrodynamic diameter of samples were acquired on a Zetasizer nanoseries instrument (Malvern Instrument, Worcestershire, UK) while morphological and aggregation-dissociation behavior images were achieved from JEM-2100 transmission electron microscope (JEOL, Tokyo, Japan) and confocal microscopes, Nikon Ti-E Inverted Microscope Confocal Nikon C1si-system (Nikon Corpopation, Tokyo, Japan) with differential interference contrast (DIC) mode, respectively.

2.2.4 Determination of critical micelle concentration

The 1000 μM of aliquot (10 mL) of pyrene solution was added into each clean test tube and dried under nitrogen, then 10 ml of citralidene-mPEO-CS in water (at various concentrations of 0.01, 0.1, 0.25, 0.35, 0.5, 0.6 g/L) were added. The samples were kept at room temperature overnight for equilibration. Then the samples were subjected to fluorescence spectroscopic analysis on PerkinElmer LS 55 Luminescence Spectrometer (PerkinElmer, Massachusetts, USA). Plot between ratio of fluorescent intensity at 372 to 382 nm and concentration of citralidene-mPEO-CS (g/L) was then constructed and critical micelle concentration (CMC) was estimated from the interception of curve fitting between two slopes.

2.2.5 Investigation of phase transition profile

Transmittance of the suspension of imine-mPEO-CS with polymer concentration of 3.0 g/L in a presence of various concentrations of $ZnSO_4.7H_2O$ (0, 0.8, 0.9, and 1 M for vanillidene-mPEO-CS and 0, 1, 1.3, and 1.5 M for citralidene-mPEO-CS) were measured using UV-visible spectrophotometer, CARY 100 Bio UV-Vis spectrophotometer (Varian Inc., Palo Alto, USA), equipped with temperature controller. Samples were heated up from 25 to 80 °C followed with cooled down from 80 to 25 °C with a rate 1 °C/min.

2.2.6 Hydrolysis of imine bond with temperature control

To investigate thermally controlled release profiles, suspension of vanillidene-mPEO-CS (30 mL) with polymer concentration 6.0 g/L was prepared, then phosphate buffer pH 1 (30 mL) and addition of $ZnSO_4.7H_2O$ (15.5 g) were added. Final concentrations of polymer and $ZnSO_4.7H_2O$ in the mixture were 3.0 g/L and 0.9 M, respectively. Whereas, citralidene-mPEO-CS was prepared with polymer concentration 3.0 g/L in deionized water (60 mL) and $ZnSO_4.7H_2O$ (25.9 g, 1.5 M) was added to it. Each uncovered vial containing 5 mL of the mixture was subjecting to the determination of vanillin or citral release with switching temperature every 2 days between 35 and 55 °C for vanillin and every 1 day between 30 and 40 °C for citral. The sample of vanillidene-mPEO-CS was collected on day 0, 2, 4, 6, 8, 10 whereas citralidene-mPEO-CS was collected on day 0, 1, 2, 3, 4, 5 by addition of 1.0 M HCl (1.0 mL) followed with addition of ethanol : H_2O (1 : 1) 15.0 mL for vanillin and hexane (15.0 mL) for citral. The collected vials were then capped with headspace aluminum crimp caps with PTFE/silicone septa. The mixtures in the vials were then subjected to UV-vis spectrophotometric analysis (Shimadzu Corporation, Kyoto, Japan) in order to quantitate aldehyde released.

2.2.7 Hydrolysis of imine bond with salt control

To demonstrate release profiles of both imine-mPEO-CS, at various salt concentration under constant temperature, the suspension of each imine-mPEO-CS in deionized water (200 mL) was prepared and divided into two parts, 100 mL each. The first part was added with $ZnSO_4.7H_2O$ (28.8 g, 1 M for vanillidene-mPEO-CS and 43.1 g, 1.5 M for citralidene-mPEO-

CS) while no salt was added to the other part. Then the samples were transferred into vials (5.0 mL for each vial). Each vial containing 5.0 mL of sample was kept uncovered at 40 °C. Collection of the samples was proceeded on day 0, 1, 2, 5, 8, 12, 15, 20, 26 for vanillidene-mPEO-CS while on day 0, 1, 2, 5, 7, 10, 15, 20 for citralidene-mPEO-CS with following method, 1 M HCl (1 mL) was added followed with addition of ethanol : H_2O (1 : 1) 15 mL for vanillin. Whereas, followed with addition of hexane (15 mL) for citral. Next, the vial was capped with headspace aluminum crimp caps, inserting with PTFE/silicone septa. Finally, each treated sample was subjected to UV-vis spectroscopic analysis for aldehyde quantification.

3. Results and Discussion

3.1 Synthesis and characterization

Methoxy-terminated poly(ethylene oxide) carboxylic acid (mPEO-COOH) was synthesized from reaction between polyethyleneglycol methyl ether and succinic anhydride at 60 ^oC, pyridine was used as catalyst. The product is white powder and well-dissolved in aqueous media. ^1H NMR spectrum showed methylene protons of succinyl group at chemical shift of 2.51 ppm. This could imply that the succinyl group was successfully grafted on the polyethyleneglycol chain. Next, mPEO-COOH was grafted on the chitosan backbone by homogeneous coupling reaction in aqueous media. Appearance of product is light yellow solid.

The product was characterized by mean of ^{1}H NMR. methylene protons peak of mPEG moiety at 3.56-3.72 ppm. ATR-FTIR spectrum of mPEO-CS showed new absorption peak at 1731 cm^{-1} corresponding to C=O stretching of an ester bond and an increase of absorption peak at 2877 cm^{-1} corresponding to C-H stretching (Figure 2). These indicated that mPEO-COOH was grafted on amino group of chitosan. A mPEO-COOH substitution degree, which was evaluated from NMR spectroscopic method, was 0.168. Two aldehydes, vanillin and citral, were used in the preparation of imine-mPEO-CS. ATR-FTIR spectrum of vanillidene-mPEO-CS showed new absorption peak at 1635 and 1509 cm^{-1} corresponding to C=N stretching vibration of the imine bond and C=C stretching vibration of aromatic, respectively. By subjecting the obtained vanilidene-mPEO-chitosan to acid hydrolysis followed with hexane extraction and quantifying the released vanillin by UV-vis absorption spectroscopy, the substitution degree of vanillin of 0.15 could be obtained. On the other hand, ATR-FTIR spectrum of citralidene-mPEO-CS showed the absorption peak at 1638 and 1615 cm^{-1} which represented C=N stretching vibration of imine bond and C=C stretching vibration of aliphatic, respectively. Using similar hydrolysis/extraction and UV-vis absorption analysis as stated for the vanilidene-mPEO-chitosan, the degree of citral substitution of 0.12 could be obtained.

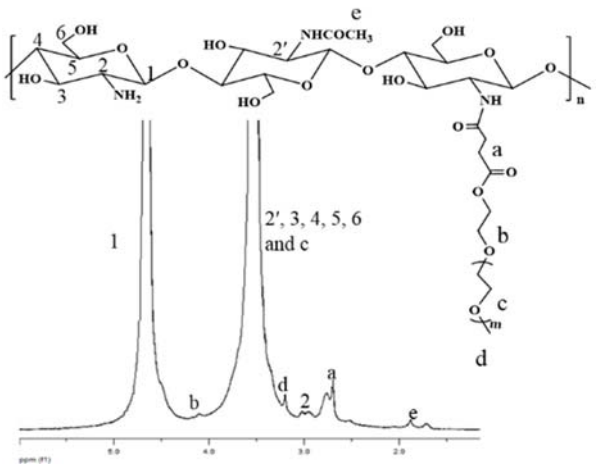

Figure 1 ^{1}H NMR spectrum of mPEO-CS.

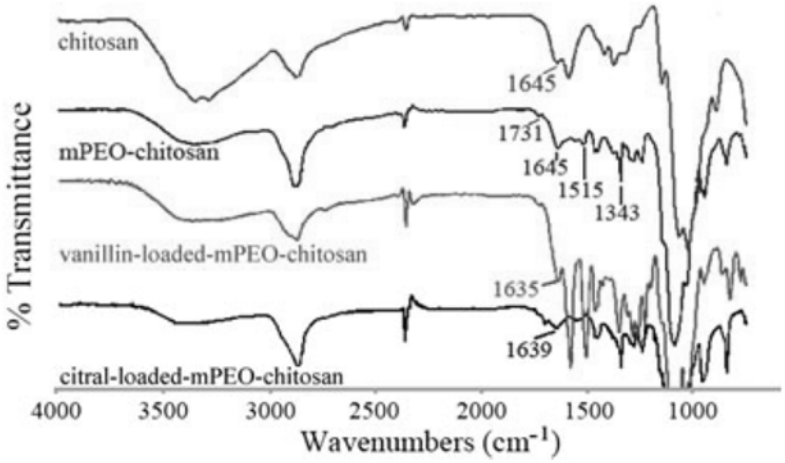

Figure 2 ATR-FTIR spectra of chitosan, mPEO-CS, vanillidene-mPEO-CS and citralidene-mPEO-CS.

3.2 Size and morphological characterization

The suspension of vanillidene-mPEO-CS and citralidene-mPEO-CS was prepared in aqueous media and morphology was observed using TEM. Spherical shape could be clearly observed in TEM photographs. Dynamic light scattering technique was used to determine hydrodynamic diameter (mean value ± S.D.) of the products which were ~ 452.03 ± 46.4 (PDI of 0.345 ± 0.07) and 306.67 ± 51.4 (PDI of 0.427 ± 0.03) nm for vanillidene-mPEO-CS and citralidene-mPEO-CS, respectively. The spherical sizes of non-hydrated vanillidene- and citralidene-mPEO-CS observed by TEM were less than the hydrated one, indicating swelling of the particles in water. Critical aggregation concentration of citralidene-mPEO-CS was determined using fluorescence spectroscopy by measuring pyrene probe. When the polymer concentration was low, no aggregates of polymer could be formed thus environment of pyrene would be hydrophilic (no hydrophobic interior of any self-assembled architecture to associate with). In contrast, when the polymer concentration was increased over 0.35 g/L, polymer could form into polymeric aggregates, so pyrene molecules could move into the hydrophobic core of the micellar aggregates. Therefore, pyrene's environment would change to the hydrophobic one. The critical micelle concentration of citralidene-mPEO-CS was 0.47 g/L as determined from the sudden change in I_{372}/I_{382} ratio of pyrene fluorescence signal, which resulted from the change in the pyrene environment as described.

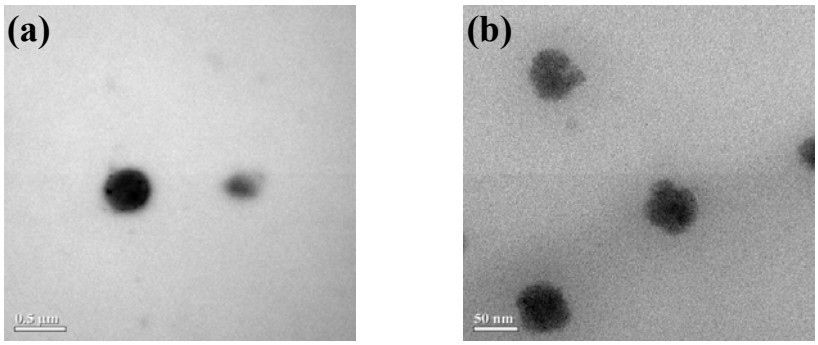

Figure 3 TEM photographs of (a) vanillidene-mPEO-CS and (b) citralidene-mPEO-CS.

Table 1 Hydrodynamic diameter of mPEO-CS and both imine-mPEO-CSs

Samples	**Hydrodynamic diameter**		**Zeta potential**
	(nm)	**PDI**	**(mV)**
mPEO-CS	577.67±15.04	0.492±0.07	+28.3±0.35
Vanillidene-mPEO-CS	452.03±46.4	0.345±0.07	+24.9±0.21
Citralidene-mPEO-CS	306.67±51.4	0.427±0.03	+24.3±0.32

3.3 Phase transition behavior of imine-mPEO-CS

Vanillidene-mPEO-CS suspension (3 g/L) with $ZnSO_4.7H_2O$ (0, 0.8, 0.9 and 1 M) and citralidene-mPEO-CS suspension (3 g/L) with $ZnSO_4.7H_2O$ (0, 1, 1.3 and 1.5 M) were measured to investigate temperature dependence of aggregation-dissociation. A transparent suspension of sample was heated from 25 ^oC to 80 ^oC before cooled down to 25 ^oC. Then,

percent of transmittance was plotted against temperature. For vanillidene-mPEO-CS with 0 M of $ZnSO_4.7H_2O$ the percent of transmittance did not change in this temperature range. However, the transmittances suddenly decreased at 55, 45, and 35 ^oC by the addition of 0.8, 0.9 and 1 M $ZnSO_4.7H_2O$, respectively. In a similar fashion, the citralidene-mPEO-CS suspension with 0 M of $ZnSO_4.7H_2O$ showed no change in the percent transmittance in the tested temperature range. However, in the presence of 1, 1.3, and 1.5 M $ZnSO_4.7H_2O$, the transmittances suddenly decreased at 65, 43 and 35 ^oC, respectively. The temperature values which showed the sudden change were the Lower Critical Solution Temperature (LCST) of the system. The sudden change indicated the switch from associated particles at the temperatures below LCST to dissociated particles at the temperatures above the LCST. The change thus corresponded to the switch from big particles (association of many nanoparticles) which could reflect light effectively to the small dissociated particles that could reflect light less effectively.

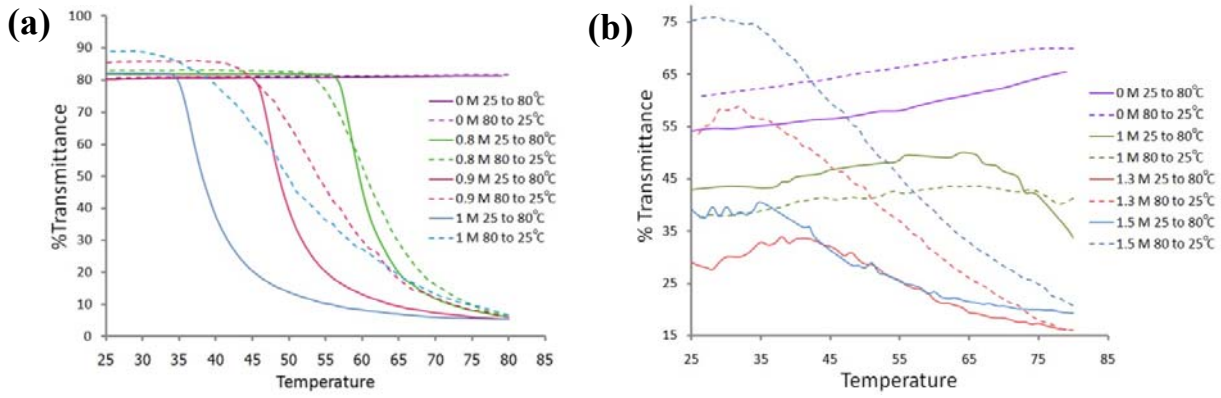

Figure 4 Phase transition profiles of (a) vanillidene-mPEO-CS and (b) citralidene-mPEO-CS at various $ZnSO_4$ concentrations.

Confocal laser fluorescent microscope with differential interference contrast mode was used to demonstrate phase transition behavior of the self-assembled polymeric micelles of vanillidene-mPEO-CS and citralidene-mPEO-CS at the polymer concentration of 3 g/L in the presence of 0.9 and 1.5 M of $ZnSO_4.7H_2O$, respectively. When temperature was below LCST, vaillidene-mPEO-CS particles (Figure 5a) and citralidene-mPEO-CS particles (Figure 5c), dissociated as water molecules could well-hydrate the hydrophilic chains of the mPEO corona. In contrast, when the temperature reached the LCST, aggregation of particles could be observed (Figure 5b, 5d). The aggregation was caused by the de-hydration of water molecules along the mPEO corona of the particles, leading to increased interaction among mPEO chains from the same and different particles.

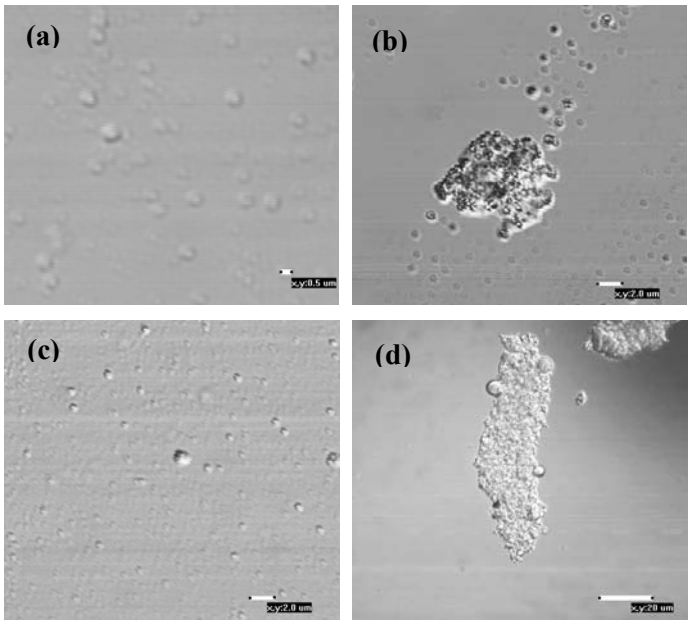

Figure 5 Morphology of vanillidene-mPEO-CS with 0.9 M $ZnSO_4$ at temperature (a) below LCST and (b) above LCST, and citralidene-mPEO-CS with 1.5 M $ZnSO_4$ at temperature (c) below LCST and (d) above LCST.

3.4 Thermally controlled release of imine-mPEO-CS

As described in the previous section, the self-assembled polymeric nanoparticles could be in the aggregated or dissociated states depending on the temperature. Here, we reported investigation of thermally controlled release profiles of vanillidene-mPEO-CS and citralidene-mPEO-CS in the presence of $ZnSO_4.7H_2O$ (0.9 M for vanillidene-mPEO-CS and 1.5 M for citralidene-mPEO-CS). Our idea was that hydrolysis of imine bond to release out the fragrant aldehydes should be fast when the particles were dissociated as the water molecules could more easily diffuse into the particles' core where the imine bonds situated. In contrast, when the particle associated, the imine hydrolysis should be halt as no water could get into the imine sites. As seen in figure 3.16 and 3.17, rate of release of both vanillin and citral from mPEO-CS nanoparticles at temperature above LCST (55 and 40 ^oC for vanillin and citral, respectively) were more slowly than those at the temperature below LCST. Furthermore, the release of vanillin from vanillidene-mPEO-CS particle while it was on dissociated state was obviously slower as compared with citral. This may be the effect of molecular structure, vanillin of which molecule possesses aromatic ring that can allow the delocalization of electron leading to stronger imine bond. Therefore, the hydrolysis of vanillin' imine bond should be more difficult than that in case of citral.

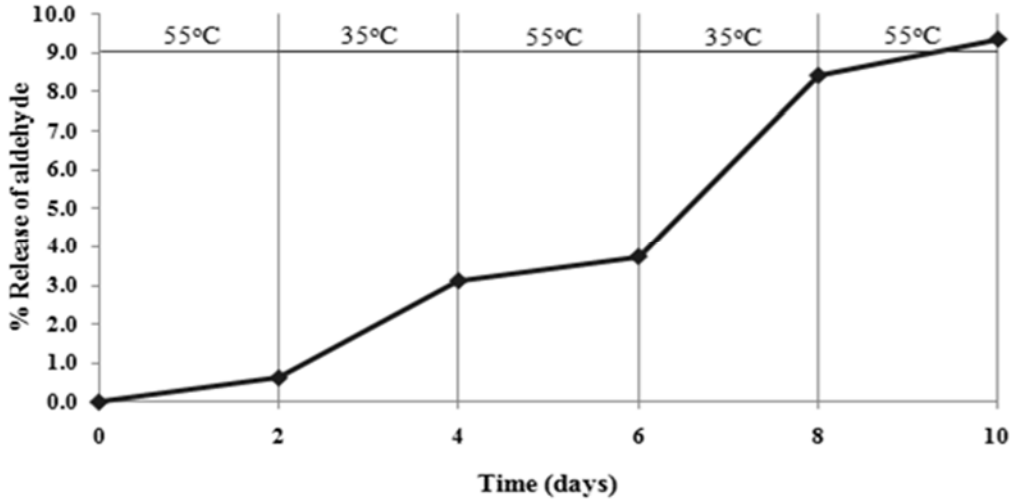

Figure 6 Thermally controlled release profile of vanillidene-mPEO-CS.

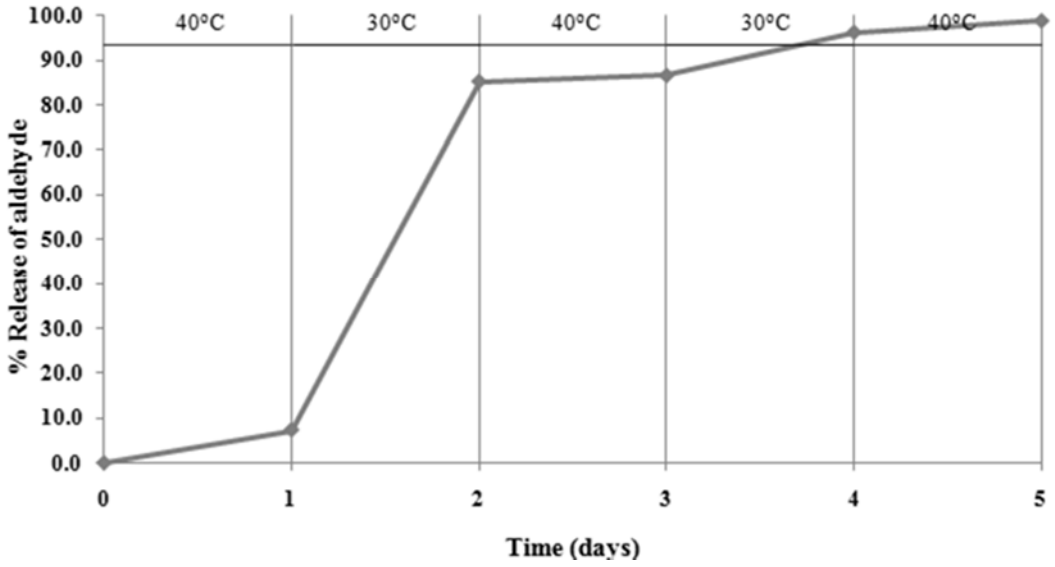

Figure 7 Thermally controlled release profile of citralidene-mPEO-CS.

3.5 Controlling the release of imine-mPEO-CS by adjusting salt concentration

Even at a constant temperature, the release of fragrant aldehyde could be controlled by adjusting salt concentration. This is because the LCST was dependent not only on temperature but also on the concentration of salt in the system. Presence of salt in the system draws the water molecules away from the PEO chains by forming into more stable hydrated ions in the system. This automatically lowers the LCST of the polymer in that system. In this report, $ZnSO_4.7H_2O$ was used for adjusting LCST. Therefore, the release of the aldehydes could be controlled by adjusting concentration of $ZnSO_4.7H_2O$. The results shown below illustrate the difference of perfumery aldehyde release rate between the conditions with and without $ZnSO_4$ at a constant temperature.

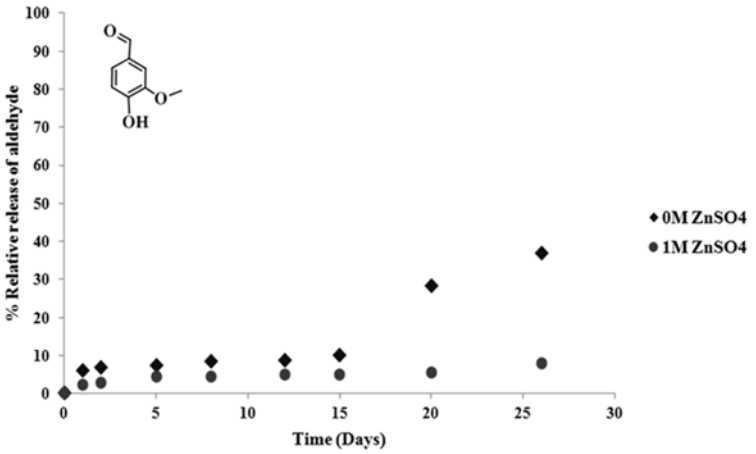

Figure 8 Release profile of vanillidene-mPEO-CS with and without 1 M $ZnSO_4$ at 40 ^oC.

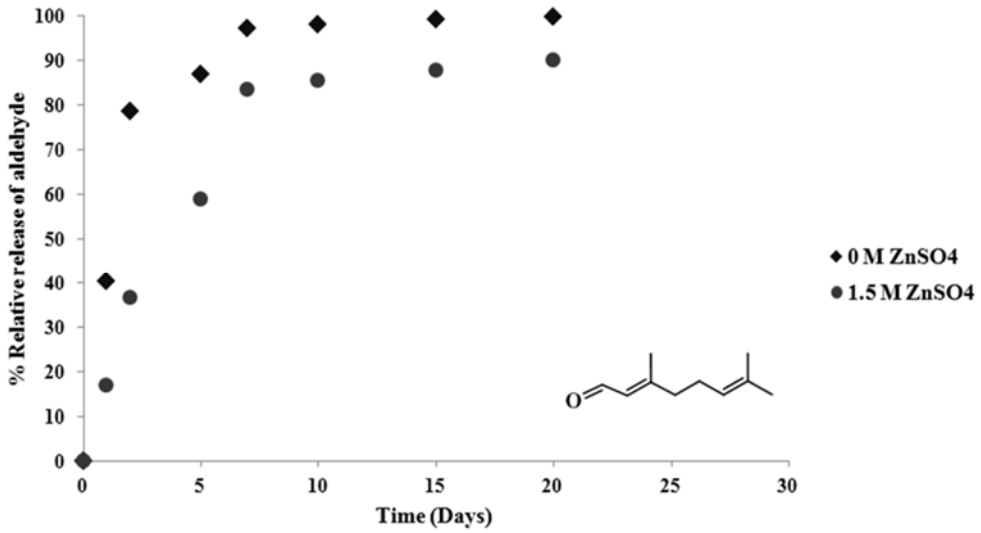

Figure 9 Release profile of citralidene-mPEO-CS with and without 1.5 M $ZnSO_4$ at 40 ^oC.

As seen in the Figures, the percent release of vanillin and citral from vanillidene-mPEO-CS and citralidene-mPEO-CS, respectively, with the addition of $ZnSO_4.7H_2O$ were more slowly comparing to the same system with no salt present. It is found that the molecular structure of the grafted fragrant aldehyde affected the rate of release. Vanillin possesses more hydrophobicity than citral, so vanillidene-mPEO-CS nanoparticles is more hydrophobic than citralidene-mPEO-CS. This means water molecule could penetrate difficultly into vanillidene-mPEO-CS nanospheres. Therefore, the release rate of vanillidene-mPEO-CS was more slowly than citralidene-mPEO-CS.

4. Conclusion

Thermoresponsive biopolymeric particle for controlled release of fragrances could be successfully fabricated. Vanillin and citral were grafted on the thermoresponsive copolymers, poly(ethylene oxide) grafted-chitosan (mPEO-CS, %DG = 16.8 %) with %DG for 15 and 12 %, respectively. The materials could self-assemble in aqueous media into particles with spherical shape. TEM photographs showed the estimated non-hydrated particle size of less than 1 μm for both vanillin and citral derivative. XPS high resolution spectral analysis confirmed that the position of grafted aldehydes were at the particles' core. The system showed thermally controlled release of the grafted fragrances in the presence of $ZnSO_4.7H_2O$; vanillidene-mPEO-chitosan with 0.8, 0.9, and 1 M $ZnSO_4$ showed the LCST at 55, 45 and 35 ^oC, respectively while citralidene-mPEO-chitosan with 1, 1.3 and 1.5 M $ZnSO_4$ showed the LCST at 65, 43 and 35 ^oC, respectively. The release of aldehydes could be thermally controlled in a switching manner. Release of vanillin with 0.9 M and citral with 1.5 M of $ZnSO_4$ was similar, minimal release could be obviously observed at the temperature above the LCST and significant release at the temperature below the LCST. Furthermore, the LCST of the system could be also selected by adjusting the salt concentration; an increase of salt concentration can reduce the LCST. Therefore, we successfully synthesized thermoresponsive chitosan polymer using poly(ethylene glycol) as a thermoresponsive moiety for the controlled release of fragrances. Moreover, we also successfully designed the thermo-switching controlled release system which is a completely biocompatible system for the release of fragrances.

References

1. Herrmann, A. *Angew. Chem. Int. Ed.* **2007**, *46*, 5836.

2. Berthier, D.; Trachsel, A.; Fehr, C.; Ouali, L.; Herrmann, A. *Helv. Chim. Acta.* **2005**, *88*, 3089.

3. Berthier, D. L.; Paret, N.; Trachsel, A.; Herrmann, A. *Bioconjugate Chem.* **2010**, *21*, 2000.

4. Yang, Y.; Wahler, D.; Reymond, J.-L. *Helv. Chim. Acta.* **2003**, *86*, 2928.

5. Morinaga, H.; Morikawa, H.; Wang, Y.; Sudo, A.; Endo, T. *Macromolecules* **2009**, *42*, 2229.

6. Kumar, M. N. V. R.; Muzzarelli, R. A. A.; Muzzarelli, C.; Sashiwa, H.; Domb, A. J. *Chem. Rev.* **2004**, *104*, 6017.

7. Fangkangwanwong, J.; Akashi, M.; Kida, T.; Chirachanchai, S. *Biopolymers* **2006**, *82*, 580.

8. Yoksan, R.; Chirachanchai, S. *Bioorg. Med. Chem.* **2008**, *16*, 2687.

9. Liu, R.; Fraylich, M.; Saunders, B. R. *Colloid Polym. Sci.* **2009**, *287*, 627.

10. Hua, D.; Jiang, J.; Kuang, L.; Jiang, J.; Zheng, W.; Liang, H. *Macromolecules* **2011**, *44*, 1298.

11. Santos, J. E.; Dockal, E. R.; Cavalheiro, É. T. G. *Carbohyd. Polym.* **2005**, *60*, 277.

12. Guinesi, L. S.; Cavalheiro, É. T. G. *Carbohyd. Polym.* **2006**, *65*, 557.

13. Jin, X.; Wang, J.; Bai, J. *Carbohyd. Res.* **2009**, *344*, 825.

14. Tree-udom, T.; Wanichwecharungruang, S. P.; Seemork, J. *Carbohyd. Polym.* **2011**, *86*, 1602.

15. Hann, R. M.; Jamieson, G. S.; Reid, E. E. *J. Am. Chem. Soc.* **1929**, *51*, 2586.

16. Yao, Z.; Zhang, C.; Ping, Q.; Yu, L. Carbohyd. Polym. **2007**, *68*, 781.

17. Jeong, Y.-I.; Kim, D.-G.; Jang, M.-K.; Nah, J.-W. *Carbohyd. Res.* **2008**, *343*, 282.

18. Choochottiros, C.; Yoksan, R.; Chirachanchai, S. *Polymer* **2009**, *50*, 1877.

19. Gumí, T.; Gascón, S.; Torras, C.; Garcia-Valls, R. *Desalination* **2009**, *245*, 769.

20. Sansukcharearnpon, A.; Wanichwecharungruang, S.; Leepipatpaiboon, N.; Kerdcharoen, T.; Arayachukeat, S. *Int. J. Pharm.* **2001**, *391*, 267.

21. Aiping, Z.; Tian, C.; Lanhua, Y.; Hao, W.; Ping, L. Carbohyd. Polym. **2006**, *66*, 274.

22. Opanasopit, P.; Ngawhirunpat, T.; Chaidedgumjorn, A.; Rojanarata, T.; Apirakaramwong, A.; Phongying, S.; Choochottiros, C.; Chirachanchai, S. *Eur. J. Pharm. Biopharm.* **2006**, *64*, 269.

23. Opanasopit, P.; Ngawhirunpat, T.; Rojanarata, T.; Choochottiros, C.; Chirachanchai, S. *Eur. J. Pharm. Sci.* **2007**, *30*, 424.

24. Anumansirikul, N.; Wittayasuporn, M.; Klinubol, P.; Tachaprutinun, A.; Wanichwecharungruang, S. P. *Nanotechnology* **2008**, *19*, 1.

25. Li, G.; Zhuang, Y.; Mu, Q.; Wang, M.; Fang, Y. *Carbohyd. Polym.* **2008**, *72*, 60.

Acknowledgements

First and foremost, I would like to express my deepest appreciation and gratitude to my supervisor, Professor Masayuki Yamaguchi, for his great supervision, helpful suggestion, thoughtful guidance and kind support to complete my doctoral study as well as my life in Japan. I would not have been able to complete my degree without his farsighted advice and professional encouragement. I also appreciate for his contributions of time, funding, knowledge and experience not only for the research thing but also for the daily life that I received from him. It is a great opportunity for me to be in Yamaguchi laboratory and complete my study under his supervision.

Secondly, I would like to give my best appreciation to the members of my committee: Associate Professor Kazuaki Matsumura, Associate Professor Ken-ichi Shinohara and Associate Professor Toshiaki Taniike of JAIST, and Associate Professor Kentaro Taki of Kanazawa University for their helpful reviews and comments. I also deeply appreciate Assistant Professor Shogo Nobukawa, who provided me a lot of valuable support and thoughtful suggestion.

I am profoundly grateful to Associate Professor Tatsuo Kaneko for his generous hospitality and support throughout my sub-theme research. Further, I would like to show my best gratitude to my supervisor in Chulalongkorn University, Associate Professor Supason Wanichwecharungruang, and also to Associate Professor Tsutomu Hamada of JAIST for their help and valuable advice during my completion sub-theme research. Without their kind

support, I would not have been able to achieve and complete my study. I am particularly very grateful to CU-JAIST Dual degree program for giving me the great opportunity to be a Ph.D. candidate through this program. Furthermore, I would like to thank Chulalongkorn University and JAIST for financial support throughout the Chulalongkorn University Dutsadiphiphat and JASSO Scholarship during my doctoral study.

I am indebted to my many colleagues who supported me throughout my study especially to Monchai Siriprumpoonthum, Tomoki Itoh and Chavakorn Samthong for their help and cooperation during my preparation of the experimental data. My great thanks also go out to all present and former members of Yamaguchi Laboratory especially to Kultida Songsurang, Suphat Korkiatithaweechai and Hikaru Shimada for their friendly help and emotional support during my stay in Japan. Furthermore, thank you all members of Thai student in JAIST and everyone else for their warm love and take part in a one of good memory in my life.

Finally, I would like to extend my deepest gratitude to my beloved family for their unconditional love and support, even during tough time in my Ph.D. life. Without their love, it is definitely hard to finish my Ph.D. degree.

Jiraporn Seemork

March, 2016

Ishikawa, Japan